ANL-7093

ANL-7093

Argonne National Laboratory

FLOW-REGIME TRANSITIONS AT ELEVATED PRESSURES IN VERTICAL TWO-PHASE FLOW

by

James L. L. Baker

Printed in USA. Price $4.00 . Available from the Clearinghouse for Federal Scientific and Technical Information, National Bureau of Standards, U. S. Department of Commerce, Springfield, Virginia 22151

ANL-7093
Engineering and
Equipment (TID-4500)
AEC Research and
Development Report

ARGONNE NATIONAL LABORATORY
9700 South Cass Avenue
Argonne, Illinois 60439

FLOW-REGIME TRANSITIONS AT ELEVATED PRESSURES IN VERTICAL TWO-PHASE FLOW

by

James L. L. Baker

Reactor Engineering Division, ANL
and
Associated Midwest Universities

Reproduced from a Thesis
Submitted in Partial Fulfillment of
the Requirements for the Degree of
Doctor of Philosophy in Mechanical Engineering
in the Graduate College of The University of Illinois

September 1965

Operated by The University of Chicago
under
Contract W-31-109-eng-38
with the
U. S. Atomic Energy Commission

FOREWORD

This report is one of a series that describes heat-transfer and fluid-flow studies performed at Argonne under a program sponsored jointly by the Associated Midwest Universities and the Argonne National Laboratory.

The earlier reports in this series are:

ANL-6625 Local Parameters in Cocurrent Mercury-Nitrogen Flow
L. G. Neal

ANL-6667 A Study of the Flow of Saturated Freon-11 through Apertures and Short Tubes
Hans K. Fauske and Tony C. Min

ANL-6674 Reduction of Vapor Carryunder in Simulated Boiling
P. L. Miller and C. P. Armstrong

ANL-6710 Transient Behavior of a Natural-circulation Loop Operating Near the Thermodynamic Critical Point
Darrel G. Harden

ANL-6734 Two-phase (Gas-liquid) System: Heat Transfer and Hydraulics. An Annotated Bibliography
Robert R. Kepple and Thomas V. Tung

ANL-6738 Development of an Electrical Resistivity Probe for Void-fraction Measurements in Air-Water Flow
George P. Nassos

ANL-6754 An Experimental Investigation of Two-phase, Two-component Flow in a Horizontal, Converging-diverging Nozzle
Joseph A. Vogrin, Jr.

ANL-6755 Two-component Two-phase Flow Parameters for Low Circulation Rates
Georges E. Smissaert

ANL-6779 Two-phase Critical Flow with Application to Liquid-Metal Systems (Mercury, Cesium, Rubidium, Potassium, Sodium, and Lithium)
Hans K. Fauske

ANL-6796 The Slug-annular Flow Regime Transition at Elevated Pressure
Peter Griffith

ANL-6854 Effect of a Transverse Magnetic Field on Vertical Two-phase Flow through a Rectangular Channel
Richard J. Thome

ANL-6862 Two-phase Heat Transfer with Gas Injection through a Porous Boundary Surface
A. A. Kudirka

ANL-6948 Condensation of Metal Vapors: Mercury and the Kinetic Theory of Condensation
Donald J. Wilhelm

ANL-7032 An Investigation of Instabilities Encountered during Heat Transfer to a Supercritical Fluid
Archie Junior Cornelius

ANL-7041 Frequency-response Analysis of Steam Voids to a Sinusoidal Power Modulation in a Thin-walled Boiling Water Coolant Channel
Carl C. St. Pierre

ANL-7053 Propagation of Density Disturbances in Air-Water Flow
George P. Nassos

ANL-7073 Self-sustained Hydrodynamic Oscillations in a Natural-circulation Two-phase-flow Boiling Loop
Kamal C. Jain

TABLE OF CONTENTS

TABLE OF CONTENTS

LIST OF FIGURES

LIST OF FIGURES

LIST OF FIGURES

LIST OF TABLES

NOMENCLATURE

A	Area, sq ft
A_p	Cross-sectional area of conduit, sq ft
b_{12}	Coefficient defined by Eq. (IV.1-8)
c	Wave speed, ft/sec
D	Diameter, ft
D_p	Diameter of conduit, ft
F_f	Orthobaric liquid property
F_g	Orthobaric vapor property
G	Mass flow per unit cross-sectional area, lb/hr-sq ft
G_0	Mass flow per unit cross-sectional area, lb/sec-sq ft
g	Gravitational acceleration, ft/(sec)^2
g_c	Gravitational constant
h	Thickness, ft
h^*	h/D_p
I	Intensity of radiation, R/hr
I_0	Initial intensity of radiation, R/hr
k	Wave number, ft^{-1}
L	Length, ft
L_s^*	Liquid slug length/pipe diameter
M	Molecular weight
$[P]$	Parachor
P	Pressure, psia
P_c	Critical pressure, psia
P_{sat}	Saturation pressure, psia
P_r	Reduced pressure, P_{sat}/P_c
Q	Volumetric flow rate, cu ft/sec
S	Slip ratio, $\left(\frac{x}{1-x}\right)\left(\frac{1-\alpha}{\alpha}\right)\beta$
s	Material thickness, ft
T	Temperature, °R
T_c	Critical temperature, °R
T_{sat}	Saturation temperature, °R
T_r	Reduced temperature, T_{sat}/T_c
t	Time, sec
U	Characteristic velocity, ft/sec
u	Absorption coefficient, ft^{-1}
u_a	Linear absorption coefficient, cm^{-1}
$\overline{V}$	Volume, cu ft
$\overline{V}_c$	Critical volume, cu ft
V	Velocity, ft/sec
V_*	Minimum vapor velocity for entrainment, ft/sec
V_f^*	Dimensionless superficial liquid velocity as defined by Eq. (II.2-6)
V_g^*	Dimensionless superficial vapor velocity as defined by Eq. (II.2-7)
V_f	Superficial liquid velocity, Q_f/A, ft/sec
V_g	Superficial vapor velocity, Q_g/A, ft/sec
V_{sg}	Average volumetric vapor flow rate per unit area, ft/sec
$V_{s\ell}$	Average volumetric liquid flow rate per unit area, ft/sec
v_E	Output voltage for vapor-filled channel, v
v_F	Output voltage for liquid-filled channel, v
x	Vapor mass fraction or quality
x_0	Channel spacing, ft
Y	Parameter as defined by Eq. (VI.3-6)

Dimensionless Groups

F	Froude number, U^2/gL
FR	Froude number as defined by Eq. (IV.2-9)
S^*	Dimensional group defined by Eq. (II.2-10), $\mu_f V/\sigma$
W	Weber number, $\rho L U^2/\sigma$
WE	Weber number as defined by Eq. (IV.2-10)

Greek Letters

α	Void fraction (A_g/A_p)
β	Orthobaric-density ratio, ρ_f/ρ_g
γ	T/T_c
δ	Liquid-film thickness, ft
λ	$\left[(\rho_g/0.075)(\rho_L/62.3)\right]^{1/2}$
λ_c	$\left[(\rho_g/0.075)/(\rho_L/62.3)\right]^{1/2}$
μ	Dynamic viscosity, lb/sec-ft
π	P/P_c
ρ	Saturation density, lb/cu ft
σ	Surface tension, dyn/cm
ϕ	$\overline{V}/\overline{V}_c$
ψ	$(73/\sigma)\left[(62.3/\rho_L)^2\mu_L\right]^{1/3}$

Subscripts

cr	Critical
g	Vapor or gas
ℓ, f, L	Liquid
i	Local value
0.03	Property evaluated at a reduced pressure of 0.03

FLOW-REGIME TRANSITIONS AT ELEVATED PRESSURES IN VERTICAL TWO-PHASE FLOW

by

James L. L. Baker

SUMMARY

Two-phase flow-regime transitions at elevated pressures for a single-component fluid, trichloromonofluoromethane (Refrigerant-11), were investigated for forced-circulation, upward flow in a vertical, rectangular conduit with internal dimensions of 0.380 by 1.050 in. The two-phase mixture was generated by an electrically-heated tube at a constant heat flux, which ranged from 4,000 to 74,000 Btu/hr-sq ft, mass flow rates from 0.20×10^6 to 2.0×10^6 lb/hr-sq ft. The orthobaric-density ratio ranged from 7 to 60. The mass qualities based upon thermodynamic equilibrium ranged to 90%; however, most of the data encompassed the segment from saturation to 50%.

The flow regimes were observed in the unheated rectangular section by employing an X-ray and television monitoring system. High-speed, color motion pictures were obtained which utilized a technique of directing blue light from above, and red light from below, the camera centerline to provide a method for distinguishing liquid from vapor due to inversion of the color pattern.

Three principal flow regimes were delineated: churn, annular, and wispy-annular flow. The latter is a distinctive flow regime in which liquid agglomerates or ligaments are transported in a vapor core. The plug-flow regime was not observed at elevated pressures.

For comparison of fluids as widely divergent in their physical properties as R-11 and water, identical orthobaric-density ratios were more suitable than reduced temperature or reduced pressure. With the fluorocarbon refrigerant group, the basis for comparison is arbitrary because of the adherence of the group to the principle of corresponding states. Expressions were developed to correlate surface tension and liquid dynamic viscosity for the refrigerants and water as a function of the reduced saturation pressure. Through an examination of these correlations of the orthobaric properties, a simplified modeling of the flow-regime transitions was possible. A comparison of the saturation properties of R-11 and water at constant orthobaric-density ratio revealed that the ratios of the various properties were relatively constant over the

range of test conditions. An examination of the Taylor-Helmholtz and Kelvin-Helmholtz stability criteria for flow-regime transitions yielded results that closely bounded the result from consideration of a purely intertial system.

Three flow-regime transitions were correlated in terms of the superficial liquid and vapor velocities in conjunction with the orthobaric-density ratio and an orthobaric-property group. The transition from churn to annular flow and from churn to wispy-annular flow contained an approximate dependency upon the square root of the orthobaric-density ratio; the transition from annular to wispy-annular flow contained a cube-root dependency. The additional orthobaric-property group was necessary to bring into alignment the transitions for the refrigerants and water.

Local void-fraction distributions were obtained for six orthobaric-density ratios by employing a gamma-ray traversing unit. The average void fractions were compared to available void data for water and a refrigerant, R-22, at identical orthobaric-density ratios. Agreement within the data was found. However, none of the existing correlations predicted the results over the entire range of quality and mass flow rate. An expression for the average void fraction was obtained for mass flow rates below 0.70×10^6 lb/hr-sq ft, which incorporated the mass-flow-rate effect. A comparison of this result with a fluorocarbon, R-22, and water over a wide range of saturation pressures yielded good agreement for systems with low subcooling at the entrance of the heated section.

I. INTRODUCTION

The study of two-phase flow with either single- or multi-component fluids has led in recent years to an accumulation of a vast literature because of the importance of two-phase flow in the nuclear, space, and chemical fields. Two of the more recent extensive compilations are due to Gouse[1] and Kepple and Tung.[2] A single-component fluid such as water has received wide attention in the literature. Under forced circulation and heat addition, various flow regimes have been encountered. For example, liquid water may appear as the continuous phase and the vapor as a dispersed phase, and the resulting flow regimes are classified as bubble or froth flow. Some regimes may appear to be approximately continuously variable in space and time, while other regimes may have widely varying space and time configurations, and the variation may also be random. Since many flow regimes can occur in a system, it is important to know where and how they occur with respect to system bulk variables such as flow rate, geometry, power input or removal, pressure losses, and fluid properties.

To simulate the effects of two-phase, single-component flow, the use of two-component systems, such as air-water, has been prevalent due to the ease of operation and construction of test equipment, and to the low cost of such units relative to some single-component structures. The extension of these types of experiments to systems in which the fluid is maintained at elevated pressures or temperatures has been based upon assumptions that the correct modeling parameters have been obtained. Systems that are investigated with air-water as the operating medium to simulate fluids, say water at elevated pressures, may grossly over- or under-estimate the effects of various fluid properties. The problem is especially pronounced when water is an operating fluid, since the normal atmosphere properties have very high values of liquid viscosity, surface tension, and liquid-vapor density ratio compared to the value of these quantities at high pressures and temperatures. These above properties undergo rapid decreases in value for relatively small temperature changes at near-atmospheric conditions. The thermodynamic properties do not change in the same functional relationship with pressure or temperature. The use of the results from the low-pressure studies for the application to high-pressure situations requires that the correct similarity parameters are known, or that the correct governing equations for the phenomena under consideration are obtainable.

Water, which has a critical pressure of 3206 psia and a critical temperature of 705°F, becomes a confinement problem, especially when visual observations of the flow regimes are desired. The flow regimes must be defined in terms of system parameters so that proper boundary conditions may be applied to any proposed analytical model. An analytical model. An analytical model predicting the transition from regime to regime with associated pressure-drop and heat-transfer characteristics is far from realization since the flow regimes themselves are not well-defined.

In general, the determination of velocity distributions, density profiles, the velocity difference between phases, and the effects of system geometry have been empirical. Critical heat fluxes and "burn-out" studies are facets of the two-phase flow problem that have been given considerable experimental study, and they will not be considered in the present investigation other than to note instances of their occurrence. Another facet of the problem is the stability studies that are encountered when a system is subjected to a mass-flow or power-input disturbance. This investigation is concerned with those flow phenomena that have a nearly time-independent inlet condition. Fluctuations in the flow patterns in the test system are entirely permissible under the foregoing condition.

This investigation studies forced-circulation flow of a fluid that enters an electrically heated vertical section under constant heat flux and then passes vertically upward through a rectangular test section. The effect of system-saturation pressure and a series of mass flow rates is determined for mass fractions of vapor and quality from zero to nearly complete vaporization. The flow patterns that occur in this system are studied by utilizing a television monitoring system that displays the absorption patterns of high-energy X rays passing through the test section and fluid, and by using high-speed, color motion pictures with preferentially directed beams of colored light for distinguishing vapor bubbles from liquid drops. The form of fluctuations in the local pressure drop is also considered since the form and magnitude of these results are indicative of some of the flow regimes.

The determination of the transverse vapor-volume-fraction distribution, or voidage, and the overall mean value are useful in determining the local velocity difference and the mean velocity difference of the vapor and liquid. Void-fraction distributions were obtained for the operating fluid selected for this investigation at the same time that the visual observations were made. The fluid selected for this investigation is trichloromonofluoromethane, a commonly used refrigerant, which is often designated as Freon-11, R-11, or F-11. Void-fraction determinations for the group of refrigerants, called Freons, is virtually nonexistent for operating conditions of elevated pressure. These void results should provide an additional parameter in the attempt to obtain a flow model among various fluids, in particular, in the comparison of various fluids with water.

Since the observation of van der Waals[3] concerning the Law of Corresponding States, various thermodynamic properties have been correlated on the basis of reduced properties, that is, on the basis of the ratio of a particular property to its value at the critical point. This thermodynamic modeling has its basis in the similarity of molecular structures. Under this form of premise, the fluid considered for this investigation is selected as one that has a low critical pressure and temperature so that a system may be employed in which the visual observations may be made. Hosler and Westwater[4] stated that a true test of any analysis of boiling-heat-transfer phenomena is the comparison of Freon-11 and water. Since Freon-11 possesses the requirements of a low critical-property state, it should provide the necessary range of pressures and temperatures, in addition to requiring lower heat fluxes to accomplish the desired qualities at the exit of the test section. Kestin[5] pointed out that the rendering of the viscosity dimensionless in the boundary-layer equations when a temperature profile exists tends to make modeling of the velocity profiles difficult. This observation may render certain regimes uncorrelatible by reduced physical properties or by the standard methods of dimensional analysis.

Recent investigations of two-phase, single-component flow in vertical test sections with visual observations at high pressures are few in number. The work of Tippets,[6] Martenson,[7] and Hosler[8] has added to the meager knowledge of flow regimes. In spite of these recent investigations, there is still little basic understanding of the fundamental mechanisms involved in two-phase, single-component, forced-convection flow with heat addition. A review of the literature by Collier[9] for 1935 to 1957 indicated a lack of knowledge of the flow regions. A series of investigations was conducted by the Atomic Energy Research Establishment, Harwell, England, in which steam and water were mixed and injected into various shapes of test sections. A series of AERE reports have since been published in which data have been collected to measure the effects of various regions of flow. This group also published various studies of air-water systems employed to simulate the regimes as shown in Fig. II.1. An example of this type of study is given by Hall-Taylor, Hewitt, and Lacey[10] concerning disturbance waves in annular flow of air-water mixtures.

The review work of Vohr[11] in 1960 on flow patterns in two-phase flow indicated that very limited visual observations have been made for vertical two-phase flow. At present, considerable effort is being made to alleviate the lack of visual studies. For fluids other than water, the current work of Staub and Zuber[12] utilizing Refrigerant-22 in electrically heated glass tubes is cited as an example of the increased interest in the problem.

The work of Tippets[6] was to a large extent exploratory in nature since no previous visual tests had been made on the high-pressure region for water. His photographs have been subject to controversy in the interpretation since they were taken for a single view and there was a lack of depth perception. In addition, the appearance of bubbles in the liquid that surrounded the inner observation window added to the problem. It was also difficult to ascertain whether the irregular shapes appearing in the test section were liquid or vapor. In the present study, a directed, two-color lighting system produced a positive distinction between the two phases.

Martenson[7] attempted to correlate the results of two high-speed motion-picture cameras operated simultaneously in two planes separated at right angles. Hosler[8] provided the best photographic record by employing a single heating strip with a prism mounted in an opposing wall and thus was able to obtain the two desired views. His conclusion was that the best observations could be obtained by utilizing a microscope for viewing the regimes. Vohr[13] conducted a high-speed motion-picture study of boiling-water flow in a vertical, rectangular channel at atmospheric pressure. He developed a technique for measuring two-phase flow velocities by superimposing two consecutive frames by an optical method. A flow-pattern scale was developed in which the characteristic size of the vapor and liquid volumes composing a flow pattern was measured. Vohr used a single heating strip and took photographs normal to the surface.

Analytical efforts to describe two-phase flow encountered extreme difficulties since a multiplicity of flow patterns has been observed which eludes simple descriptions. In comparison with single-phase flow, a simple laminar-turbulent transition is insufficient to describe the flow-pattern transition. In addition, in two-phase flow, dual equations of motion, energy, and continuity are to be handled with added interfacial expressions. Progress has been made in the description of annular flow in which the liquid appears as a film on the wall and the vapor in the core. The various theories for annular flow are generally derived by assuming that Prandtl and von Karman theories of turbulent flow apply to this situation. This form of analysis was employed by Calvert and Williams,[14] Hewitt,[15] and Anderson, Haselden, and Mantzouranis,[16] to cite some investigators following the same general format. The above form of analysis would not appear to be applicable where bubble formation occurred in the liquid film.

Changes in flow patterns have been suggested as being caused by hydrodynamic instabilities in the bounding regimes for annular flow. In particular, Ostrach and Koestel[17] reviewed the possible types of instabilities that may occur. These authors cited the caution that the application of external flow analysis to internal flow systems was not rigorously examined. That is, the applications of the four principal types of hydrodynamic-flow instabilities, a) Tollmien-Schlicting, b) Kelvin-Helmholtz, c) Rayleigh-Taylor, and d) Bernard, may not lead to the correct evaluation of the physical situation.

Other forms of analysis followed the dimensional analysis pattern, where either the governing parameters are assumed or the governing equations are rendered dimensionally invariant. The examination of a transition from one single-flow pattern to another has met with some success since the number of governing parameters may be reduced by considering the dominant factor in that particular transition. Haberstroh and Griffith[18] studied the transition from the annular to the slug-flow regime by employing a Froude-number analysis. This form of analysis implies that viscous and interface effects are secondary. Wallis[19] employed a modified Froude-number investigation of the annular-flow regime with entrainment. Some of his preliminary results indicated that the effect of viscosity and surface tension on this phenomena was not known and that the Froude-number analysis did not adequately cover these variables.

Hinze[20] developed equations for a flowing homogeneous suspension with slip between the phases, which could be applicable to the bubble or froth regime and to the liquid dispersed region. However, no solution of the equations is cited, and the difficulty in evaluating various terms may be nearly insurmountable. For example, the induced mass associated with an agglomeration of bubbles or drops in an accelerating system is unknown at present.

Bankoff[21] developed a variable-density model of a pseudosingle fluid for two-phase flow which employed a power form for the velocity and density (void) distribution. The unknown factors in his expressions are evaluated from experimental results. Extension of his results to other experimental data has met with varying degrees of success.

In a recent review of developments in vertical two-phase flow, Govier[22] summarized test results for the transition of various flow patterns. There is a lack of elevated pressure data evident in this review. The large literature for transitions at low pressures has not established a definite mode of transition in the various regimes.

In the review of past efforts in two-phase flow research, the emphasis has been confined in general to low-pressure systems, or to closed systems in which water has been the fluid. There is a general lack of information concerning flow regimes or patterns for single-component fluids at elevated pressures. Density, or void-fraction, distributions have been confined to water studies for the most part. To provide a better understanding of the governing parameters in two-phase flow, the examination of fluids other than water at elevated conditions is desirable. In the following section, the existing flow patterns in two-phase flow will be described.

II. DESCRIPTION OF TWO-PHASE FLOW

The term "two-phase flow" is considered to be representative of the simultaneous flow of liquid and vapor in a closed conduit. The two principal orientations of the major axis of the conduit that have been considered in the literature are horizontal and vertical flow. Upward flow in a vertical conduit is the configuration employed in this work. The flow configuration, or flow pattern, in horizontal systems will be considered for comparison purposes only. For very high flow rates, the direction of gravity may be expected to be of secondary importance in the arrangement of the liquid and vapor in the conduit, and horizontal and vertical systems may exhibit nearly the same flow-pattern orientations.

In two-phase flow studies, two general categories are presented: one in which the liquid and vapor are the same fluid (i.e., a single-component flow), and one in which the liquid and vapor are dissimilar fluids (i.e., a two-component flow). The majority of two-phase flow studies have involved water as the liquid, and for the latter case above, air has been the vapor or gas.

The results of a two-component flow study have been extended to predictions concerning single-component flows with varying degrees of success. In particular, the thermodynamic properties of a single-component fluid vary in a fixed manner as system pressure and temperature are changed. Furthermore, with the addition or removal of heat, the relative quantities of the liquid and vapor change. The advantage of a two-component system is that a particular thermodynamic property may be varied while the remaining properties are held at some fixed values. This form of variation will be satisfactory if the correct modeling parameters are known, and if there is no coupling of the controlling parameters in producing the various configurations.

The method of injection of the liquid and vapor (or gas) into a system can influence the development of flow patterns. This is analogous to the variation in velocity distribution in single-phase fluids due to the entrance configuration. Thus, some regimes in two-phase flow may not exist in very short test sections because of the time required for a particular regime to form. A difference in flow patterns may also be expected in systems where the two-phase mixture is produced by an energy input rather than by injection of the two phases separately.

The material that follows describes the possible flow regimes in both heated and adiabatic flow and the efforts made to present the various flow regimes in flow maps or plots.

A. Two-phase Flow Regimes

The survey of flow regimes for horizontal and vertical flow by Vohr[11] described the individual flow regimes that had been observed in the literature before 1960. The terminology employed by the various studies is widely varying in the description of the flow regimes. Seven basic horizontal flow regimes have been described:

1. Bubble flow. This regime is characterized by vapor or gas bubbles, which do not completely bridge the area normal to flow.

2. Plug flow. Long vapor or gas plugs are formed, usually by coalescence of bubbles from the first regime. The vapor plugs are separated by liquid plugs, which may or may not contain bubbles.

3. Stratified flow. The vapor or gas flows in a separated stream above the vapor-liquid interface, which remains relatively tranquil.

4. Wavy flow. This regime is a continuation of the previous one in which the interface develops waves of increasing amplitude.

5. Slug flow. This regime occurs with a complete bridging of the channel by slugs of liquid, which may contain bubbles. This liquid slug traverses the channel at a rapid rate.

6. Annular flow. This regime is characterized by an annulus of liquid on the channel walls with the vapor occupying the central region or core.

7. Spray flow. The liquid is dispersed in vapor, which becomes the continuous phase. In adiabatic flow, it may be expected that the liquid forms patches on the walls if wetting occurs.

This description of the horizontal flow patterns does not include some of the subdivisions of the flow regimes that have been described by some investigators. However, it should be sufficient to allow a comparison of the vertical flow regimes.

The listing of the primary, vertical flow regimes by Vohr included the following:

1. Bubble flow. Vapor bubbles aided by buoyancy effects move through the liquid stream, which is considered the continuous phase.

2. Piston flow. The vapor forms long plugs with a rounded leading surface. The liquid plugs that separate the vapor plugs may contain entrained bubbles.

3. Semiannular, dispersed plug flow, emulsion flow, turbulent flow, slug-annular flow. These various terms have been applied to the regime that separates the previous flow regime from the fully developed annular regime. This regime is probably the most difficult to describe. The flow structure is random in nature, with both phases alternately attempting to assume the continuous form.

4. Annular flow. This regime is characterized by an annulus of liquid on the channel walls, with the vapor occupying the central region or core.

5. Spray or dispersed flow. The liquid appears in droplet or ligament form and is dispersed in the continuous vapor phase.

By way of contrast, the classifications made by Nicklin and Davidson[23] for vertical flow in an air-water system are as follows:

1. Bubble flow. The bubbles are small in comparison with the flow area, and the shape is not greatly affected by the confining walls.

2. Slug flow. The bubbles appear as elongated forms, which have a rounded leading surface and a nearly flat bottom. The length varies by as much as several hundreds of tube diameters. These vapor slugs maintain their identity as they move up the conduit.

3. Semiannular flow. This regime has an appearance similar to the slug-flow regime in that alternate slugs of liquid and gas (or vapor) occur. However, the liquid regions alternately tend to build up and break down, which results in a churning motion. The gas slugs do not possess the characteristic rounded, or Taylor, nose.

4. Annular flow. The liquid is maintained on the walls, and the gas flows in the core. The interface is wavy, and the amplitude of the waves is not sufficient to form a liquid bridge.

5. Mist flow. The liquid is carried in the form of droplets swept from the walls by the gas flow.

There is an obvious similarity between the foregoing descriptions of the flow regimes. However, the descriptive terms for the regimes are slightly different.

To add to the descriptive forms mentioned above, the description by Collier[24] for the flow regimes occurring in vertical flow with heat addition is included. Figures II.1 and II.2 illustrate these regimes and their associated temperature effects.

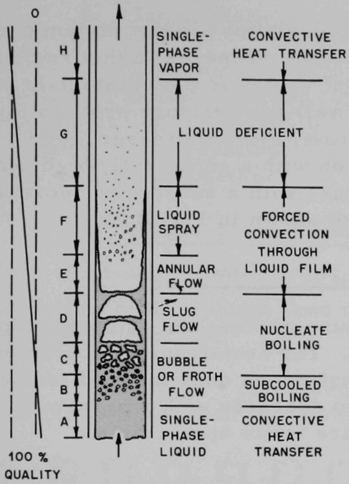

Fig. II.1. Flow Patterns in Vertical Flow during Heating

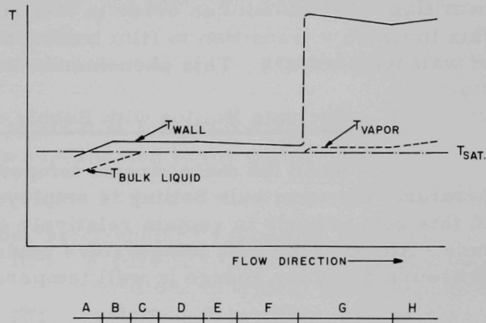

Fig. II.2. Temperatures Associated with Vertical Flow during Heating

The forced flow of a single-phase liquid upward through a vertical conduit with a uniform wall heat flux, its transition to various types of flow regimes, and the subsequent exit of a superheated vapor is shown in Fig. II.1. The associated wall and fluid temperatures are illustrated in Fig. II.2. In the diagrams, the transition from nucleate boiling to film boiling, i.e., a blanket of vapor on the walls, is not shown. This transition could occur at low qualities if sufficiently high heat flux is maintained.

The individual flow regimes as they may appear in vertical flow with heat addition are summarized as follows:

1. Single-phase Liquid

The forced-convection flow of single-phase liquid in a heated conduit has been investigated by many groups. The many correlations have been summarized by Knudsen and Katz.[25] The primary correlation has been based on three dimensionless groups; the Reynolds number, the Prandtl number, and the Nusselt number. Respectively, they signify the effect of velocity, system properties, and heat transfer. For a constant heat flux in this region, the wall temperature increased linearly.

2. Subcooled Boiling

As the liquid approaches the saturation temperature corresponding to the system pressure, bubbles form on the walls because the wall temperature is in excess of the saturation temperature. These bubbles are swept into the stream and generally collapse after a short distance in the subcooled stream. The heat-transfer coefficient increases in this region. The wall temperature tends toward a constant value for the constant-heat-flux situation. Jicha and Frank[26] presented wall-temperature profiles for subcooled boiling with a wide range of flow rate, system pressure, and heat flux. A burn-out can occur in this region with a sufficiently high heat flux in which a transition to film boiling occurs with a subsequent increase of wall temperature. This phenomenon is not shown in Fig. II.1.

3. Nucleate Boiling with Bubble or Froth Flow

When the main stream temperature reaches the saturation temperature, the term bulk boiling is employed. The heat-transfer coefficient in this region tends to remain relatively constant, as does the wall temperature. Although the bulk temperature tends to decrease with increasing pressure drop, the change in wall temperature is not appreciable.

4. Nucleate Boiling with Slug, Churn, or Froth Flow

This region is characterized by the coalescence of bubbles to form slugs of vapor interconnected with liquid containing bubbles. Froth or churn flow may appear dependent upon the surface-tension properties of the fluid. The slug-flow regime is unstable in the frequency of slugging and in the entrainment of small bubbles. The heat-transfer coefficient may increase in this region in accordance with the magnitude of the mass flow rate. The effect of high system pressures is not known for this region, nor is it known if slug flow exists for pressure approaching the critical pressure.

5. Annular Flow with Evaporization

At high velocities, the liquid tends to collect in a thin film on the wall and the vapor collects in the core. The heat-transfer mechanism in this region is the evaporation of the liquid and the forced convection between the vapor and liquid. The presence of bubbles in the liquid film has not been determined in this region although they may appear under certain system conditions. The heat-transfer coefficient rises very rapidly in this region, and the wall temperature remains substantially the same as in the previous cases.

6. Liquid-dispersed or Spray Region

The increase of the vapor velocity in this region entrains liquid drops from the thin, slow-moving liquid layer on the wall. The vapor constitutes the major portion of the fluid in this region and thus may be considered as the continuous phase. Liquid droplets continually impinge on, and are reentrained from, the liquid on the wall. The heat-transfer coefficient increases rapidly with increasing quality. For the heat-addition case, the actual flow pattern has not been clearly defined for this region.

7. Liquid-deficient Region

The region is characterized by a sudden drop in heat-transfer coefficient to that observed for dry steam, and the wall temperature increases rapidly. The liquid film tends to decrease in thickness and finally disrupt with the resultant appearance of dry patches. Finally, the liquid film vanishes altogether.

8. Single-phase Vapor

The vanishing of the liquid film from the wall results in the transition of the system fluid to a superheated vapor with a low heat-transfer coefficient.

Govier[22] classified the "semiannular" regime as listed by Nicklin and Davidson as "Froth" flow. Figure II.3 illustrates the flow distributions in typical two-component systems. It is difficult to portray the froth or semiannular regime in a single figure or photograph. High-speed motion pictures illustrate the random, turbulent character of this type of flow. The term "semiannular" or "churn" may be more descriptive of this regime.

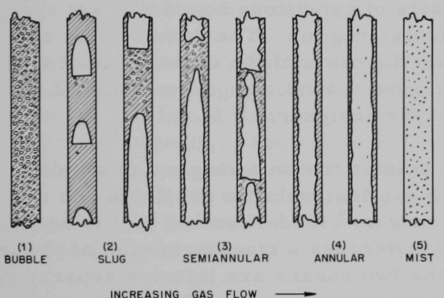

Fig. II.3. Two-phase Flow Patterns

The annular-flow regime, when viewed by means of motion pictures, ranges from a tranquil surface with low-amplitude waves to one in which the waves are of high amplitude with droplets separated from the peaks. A spectrum of frequencies may be seen in this regime, along with large-disturbance waves traveling at higher velocities than low-level waves, which are also present.[10]

A recent development in the description of flow regimes is that due to Bennett et al.,[27] in which a new flow regime entitled "wispy-annular" was determined by X-ray photographs and high-speed motion pictures. This regime has the usual characteristics of the annular flow regime in that liquid film moves slowly along the walls with an agglomerated, entrained, liquid phase in the vapor core. To quote directly from their report, the character of the new flow regime is such that "This (entrained) phase appeared to flow in large agglomerates somewhat resembling ectoplasm." The high-speed, color motion pictures obtained in this investigation revealed the same flow pattern as that obtained by Bennett et al. and are discussed in Section VI.

B. Two-phase Flow-regime Transitions

The conditions governing the existence of a particular flow regime are in part due to the thermodynamic and transport properties of the fluid, the orientation and configuration of the containment vessel, the turbulence of the fluid, the flow rate, and the rate of energy input into the system. To predict the probable phase distribution, some information concerning these aspects should be known. In general, the above quantities are known to some degree. However, the coupling of the forces acting within the system is not readily obtained. Since the pressure drop, heat transfer, and void-fraction distribution depend to a large extent on the flow regime, the transition between various regimes in terms of available parameters is an essential facet of the problems encountered in two-phase flow.

What is generally meant by a flow-regime transition is that a small set of conditions exists in which the distinction between two adjoining regimes is indeterminate, and that two sets of conditions bound this set such that each set is identifiable as a particular regime. The demarcation of a flow-regime transition may be made on the basis of the mean value of a transition set, the upper bound, or the lower bound. In general, any of the above values would be advantageous to the designer.

The expression of all possible transitions on a single plot or map in terms of two parameters would be most desirable for all fluids and operating conditions. The question that may be asked of such a plot is whether it holds for systems in which the fluid undergoes a transformation of phase by heating, and for systems in which the two phases are injected separately. Such a plot might exist if one of its parameters contains a transition time-scaling factor, since the formation of some regimes may not occur within the confines of an individual piece of equipment because of the length of the equipment and the time available. The initial orientation of the phases would also affect the developing flow pattern and should be included in the parameter.

A general map covering all possible situations in two-phase flow will probably not be developed until transitions between regimes are better understood. Some mechanisms for transitions will now be considered.

The transition from bubble to slug, or plug flow, occurs through the coalescence of a swarm of bubbles into an elongated bubble with a rounded or bullet-shaped head and a somewhat flat bottom nearly filling the conduit. The parameters that appear to affect the transition are the initial distribution of the bubbles, their sizes, the contact time, and the properties of the fluid. Coalescence is a function of the surface tension of the fluid and the density ratio.[28] The size of the bubbles is affected by the flow of fluid and the rate of energy input. Slug flow has been observed in subcooled boiling by Jeglic and Grace,[29] who found that the formation was a function of the heat flux.

The bubble-flow regime may transfer into the semiannular regime without the appearance of distinct vapor slugs of the previously described form. Kutateladze and Styrikovich[30] stated that slug flow does not appear in water systems above approximately 1500 psia. At sufficiently high flow rates, bubble flow undergoes a transition at increasing qualities to a dispersed type of system. The spray-annular type of regime would probably be encountered in adiabatic systems, since the liquid would wet the wall and form a film.

Nicklin and Davidson[23] indicated that two types of transition occur in slug flow. At low liquid velocities, in an air-water system, the transition to semiannular flow occurs due to a phenomenon similar to flooding of evaporators in which an instability of the liquid film produces a collapse of the gas slug. This transition was said to occur at a constant sum of the superficial velocities, or

$$V_{sg} + V_{s\ell} = \text{a constant,} \tag{II.B-1}$$

where the superficial velocity is the average volumetric flow per unit area, and the subscripts sg and sℓ represent the gas and liquid, respectively. Thus, at low liquid flow rates, an increase in liquid flow reduces the transition gas velocity. The cause of transition at high liquid flow rates was stated to be caused by a different instability. It was suggested that the nose of the slug underwent an instability, which produced the transition. At the higher liquid flow rates, the transition gas velocity increased with increasing liquid velocity.

A transition criterion from slug to homogeneous flows was developed by Moissis[31] by equating the relative velocity of the vapor slug and the liquid flow to the relative velocity at liquid-vapor interface obtained from a stability analysis of the Orr-Summerfeld equation. This analysis would imply that the transition is from slug flow to annular flow. However, since the length of the vapor slug enters into the solution, the analysis may be said to be applicable to the semiannular transition to annular flow. That is, for short vapor-slug lengths, the semiannular condition may be approximated.

An electrical-resistivity probe to determine whether a liquid bridge occurs in the flow field was employed by Haberstroh and Griffith[18] and by Suo et al.[32] to determine the transition from the bridging type of flow to annular or dispersed flow. This method would also appear to yield the transition from bubble to slug flow.

The transition from semiannular to annular flow was approached by Haberstroh and Griffith[18] in a Froude-number type of analysis in which there is no explicit dependency upon a Weber or Reynolds number.

Their experimental work provided two modes of transition expressions, which depended for a bound on a dimensionless, superficial liquid velocity. The transition expressions are

$$V_g^{*\prime} = 0.9 + 0.6V_f^{*\prime} \tag{II.B-2}$$

for

$$V_f^{*\prime} \leq 1.0, \tag{II.B-3}$$

and

$$V_{sg} = (7 + 0.06\beta)\, V_{sf} \tag{II.B-4}$$

for

$$V_f^{*\prime} \geq 1.5. \tag{II.B-5}$$

The dimensionless velocities employed above are modifications of expressions employed by Wallis et al.[33] in the forms

$$V_f^* = \frac{V_f}{[gD(1 - 1/\beta)]^{1/2}} \tag{II.B-6}$$

and

$$V_g^* = \frac{V_g}{[gD(\beta - 1)]^{1/2}}, \tag{II.B-7}$$

where β is the density ratio, ρ_f/ρ_g; and V_f and V_g are the superficial liquid and vapor velocities, respectively. Haberstroh and Griffith assumed that the density ratio was large and therefore replaced $1 - 1/\beta$ by unity in Eq. (II.B-6) and set $\beta - 1$ equal to β in Eq. (II.B-7). Wallis et al.[19] varied the bracket terms in the above expressions to incorporate the effect of entrainment on the vapor density. The implication of the above modeling parameters is that viscosity and surface-tension effects are of secondary importance. While two-phase flow cannot be regarded as a pure inertial system, the orthobaric-density ratio, β, for single-component fluids in some functional relationship may account for the effect of surface tension and viscosity in the correlations, since both thermodynamic properties can be expressed as a function of the density ratio. Both surface tension and liquid viscosity appear in the general flow-regime map produced by Baker.[34] However, the viscosity term is suppressed by the small value of the exponent on the term. In Section IV, the thermodynamic relationships are considered for orthobaric conditions.

The transition from annular flow to annular flow with droplet entrainment was examined by van Rossum[35] for horizontal flow in a rectangular duct with a variation of surface tension and viscosity of the fluids. Steen and Wallis[36] examined the transition for cocurrent, vertical, downward flow and compared experimental results of the former and the analysis of Zuber.[37] The results of van Rossum employed both a Weber number and Reynolds number based on the liquid-film thickness in the correlation of the entrainment study. Essentially, both van Rossum and Steen and Wallis found that the minimum gas velocity for entrainment was proportional to the surface tension and given by

$$V_* = C\sigma. \tag{II.B-8}$$

The value of C was 0.82 for the horizontal, and 1.25 for the vertical, downward flow, when V_* is expressed in ft/sec and σ in dyne/cm. Thus, the minimum gas velocity for entrainment would be higher for the vertical downward flow at a given surface tension. The inlet conditions require consideration in these studies, since entrainment may occur earlier than indicated by the above results.

J. van Rossum found that at sufficiently high velocities a critical Weber number becomes constant, and is

$$We_{cr} \geq \frac{\rho_g V^2 \delta}{\sigma}, \tag{II.B-9}$$

where δ is the liquid film thickness, and V is the mean gas velocity. A second parameter was defined as

$$S* = \frac{\mu_f V}{\sigma}, \tag{II.B-10}$$

where μ_f is the liquid dynamic viscosity. When S* is greater than 5, the critical Weber number becomes approximately 17. Recent experimental data for entrainment in vertical systems by Wallis <u>et al</u>.[19] would indicate a trend toward a constant Weber number. Zuber[37] analyzed the results of van Rossum and developed several bounding expressions for entrainment, which were subsequently compared by Steen and Wallis.[36] The latter did not obtain very good agreement except for a thick-liquid-film expression, which suggested that

$$\frac{V_* \mu_g}{\sigma \beta^{1/2}} = \text{a constant} = 2.46(10)^{-4}, \tag{II.B-11}$$

where μ_g is the gas dynamic viscosity. The onset of entrainment then appeared to be independent of the diameter of the system. Above a certain minimum liquid-flow rate, the onset of entrainment was independent of the liquid flow.

Continuing research at CISE, Milan, Italy, for flows in the annular-dispersed regime has not indicated any large effect of liquid or gas viscosity in this regime. Cravarolo and Hassid[38] indicated a dependency of the void fraction on surface tension and gas density. Little work has been done in this regime, and the factors involved remain somewhat in doubt. In an adiabatic system, some wetting of the walls should be expected in most situations. The transition from bubble flow to annular-dispersed flow may take place at high mass flow rates through the formation of liquid ligaments due to high shear forces, the liquid ligaments then breaking up into droplets.

Considerable literature concerning flow regimes in horizontal flow at relatively low pressures has been presented in the form of graphs or flow maps. Some investigators have considered the effect of the direction of the gravitational acceleration at very high flow rates to be a secondary effect and that some vertical flow patterns would be similar to the horizontal forms. The principal flow-regime map in horizontal flow is due to Baker[34] who utilized data from various investigations, principally air-water systems, to develop his flow map, which was employed in pipe-line flow of oil. Unfortunately, an examination of the calculated data presented in his paper for gas-oil flow does not agree with equations listed for the parameters. A recalculation of his parameters according to the given equations shifts the results from one flow regime to another in nearly one-third of the listed results. The flow map of Baker[34] is shown in Fig. II.4.

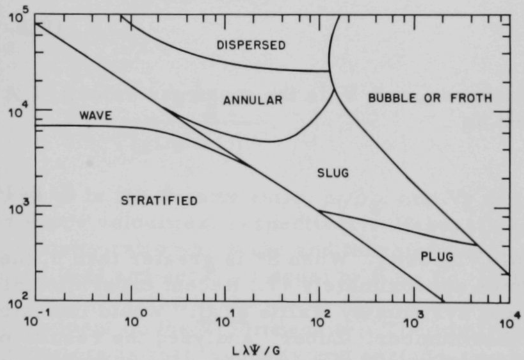

Fig. II.4

Generalized Flow-regime Transition Map

The coordinates for Baker's map are G/λ and $\lambda\psi L/G$ where

G = mass velocity of the gas phase, lb/hr-sq ft of total pipe area;

L = mass velocity of the liquid phase, lb/hr-sq ft of total pipe area;

$\lambda = [(\rho_g/0.075)(\rho_L/62.3)]^{1/2}$;

ρ_g = density of gas phase, lb/cu ft;

ρ_L = density of liquid phase, lb/cu ft;

$\psi = (73/\sigma)[(\mu_L/1)(62.3/\rho_L)^2]^{1/3}$;

σ = surface tension of liquid phase, dyne/cm;

and

μ_L = viscosity of liquid phase, cP.

The numerical factors in Baker's parameters are identified as:

0.075 = density of air at standard pressure and temperature, lb/cu ft;

62.3 = density of water at room temperature, lb/cu ft;

73 = surface tension of water at room temperature, dyn/cm;

and

1 = viscosity of water at room temperature, cP (this is implied in the abscissa of the Baker plot).

By rearranging the coordinates of the map, the parameters may be compared with other results. Employing the equations listed in Baker's text,

$$G/\lambda = C_1 V_{sg}/\beta^{1/2}, \tag{II.B-12}$$

where C_1 is a constant and the other terms are the superficial gas velocity and the density ratio as previously defined. Using the term for surface tension, σ, that has been previously employed,

$$\lambda\psi L/G = C_2 \frac{V_{sf}}{V_{sg}} \beta^{1/2} \frac{\rho_L}{\sigma} \left(\mu_L/\rho_L^2\right)^{1/3}, \tag{II.B-13}$$

where C_2 is a constant. Thus, for a single-component system under a given saturation pressure, the plot reduces to the superficial gas velocity as the ordinate, and the ratio of superficial velocities as the abscissa. The absence of an explicit diameter effect is particularly noticeable. In addition, the underlying assumption in any plot of this type is that the various regimes are dependent in the same manner on the fluid properties. The data evaluated in Table 1 of Baker's paper for the factor, λ, was erroneously calculated on the basis of

$$\lambda_c = [(\rho_g/0.075)/(\rho_L/62.3)]^{1/2}. \tag{II.B-14}$$

Thus, in the original equation the <u>product</u> of the two terms in parenthesis is taken, whereas the <u>ratio</u> of these terms is employed in the results presented in Table 1. The effect upon the coordinates may be examined by considering the proportion

$$\lambda_c/\lambda = 62.3/\rho_L, \qquad \text{(II.B-15)}$$

which provides only a slight modification in the coordinates if the liquid density is very nearly equal to that of water at room temperature. By way of comparison, the saturated-liquid density of water at 1000 psia (β = 20.6) is approximately 46.3 lb/cu ft, while R-11 at β = 20.6 has a saturated-liquid density of 75.3 lb/cu ft. In Section IV, the fluid properties are examined and the results indicate that the ratio of the fluid property group for water and R-11 in Eq. (II.B-13) is nearly a constant when determined at identical orthobaric-density ratios. The value of this constant is approximately 0.25. The evaluation of Eq. (II.B-15) for the above conditions results in factors of 0.828 for R-11, and 1.34 for water.

A fixed transition point in Baker's map does not modify the resultant superficial liquid velocity for either form of λ. However, the superficial vapor velocity was increased for water and was reduced for R-11 when Eq. (II.B-14) was employed. For the expressions in Baker's text, the superficial vapor velocities for R-11 and water would be identical, while the superficial liquid velocity of R-11 would be approximately 0.25 that of the water, at identical orthobaric-density ratios. For Eq. (II.B-14) to hold, the mass flow rates of the vapor must be equal for two fluids at a fixed transition point. The form of the Baker plot does not allow a single constant quality to be obtained as a condition for any transition line that purports to hold for fluids such as water and R-11 when examined at identical orthobaric-density ratios. Thus, the results of Haberstroh and Griffith[18] are incompatible with that of Baker[34] if extended to fluids such as R-11 and water at elevated saturation pressures.

Representation of the various transitions was shown by Griffith and Wallis[39] for the slug-flow regime in an air-water system. The coordinates employed in their representation were suggested by Kozlov[40] where the volumetric gas fraction, $Q_g/(Q_g + Q_f)$, is plotted as a function of the mixture volumetric Froude number,

$$N_{FR} = [(Q_g + Q_f)/A_p]^2/gD_p \qquad \text{(II.B-16)}$$

where Q_g and Q_f are the average volumetric flow rates of the gas and liquid, respectively; A_p is the cross-sectional area of the pipe; and D_p is the pipe diameter. The superficial velocities are thus the average volumetric flow rate divided by cross-sectional area. Govier[22] suggested that Kozlov's representation was not in accord with other investigations and should be discounted since the representation was based on insufficient data. Froude-number modeling implies that viscous and compressibility effects are negligible. The absence of a term with surface tension implies also a minor effect due to the interfacial conditions.

A graphical representation, somewhat similar to the above type, was due to Kosterin[41] in which the volumetric gas fraction was retained but the other coordinate was the mixture velocity that is the sum of the superficial velocities. Hoogendoorn and Buitelaar[42] employed the "Kosterin" diagram in the investigation of the effect of gas density and of gradual vaporization in horizontal gas-liquid flow. They employed a system in which superheated Freon-11 and water were the mixture, and with flashing Freon-11 at low pressures. The transition lines were shifted slightly due to change in gas density. The effect of the vaporizing Freon-11 was to inititae atomization at lower velocities and to shift the transition to froth flow to lower velocities. The range of pressures investigated was small, and the smallest density ratio was in the order to 100. The transition to spray-annular, or atomization, indicated by this investigation supports the approximation of Eq. (II.B-8) qualitatively.

Extensive research in vertical flow of two-component mixtures by the "Alberta" group[22] produced correlations of flow regimes in terms of pressure drop and superficial water velocity, and in terms of gas liquid-volume ratio. In particular, the plot of superficial water velocity and air-water volume ratio[43] is somewhat similar to the Baker plot when fluid property values are held constant. The difference appeared in the use of the superficial gas velocity by Baker instead of the liquid-velocity term. The correlations of the "Alberta" group do not contain any thermodynamic property relationships since there was little variation in these values. The Alberta group found no effect of diameter in the bubble-to-slug or -plug transition. In the transition from slug to froth flow, the diameter effect was to the one-third power; in the transition from froth to annular flow, there was an inversion of the diameter effect to the two-thirds power.

The application of the generalized plot of Baker[34] to steam and liquid water data at elevated pressures was made by Goldman, Firstenberg, and Lombardi,[44] where the coordinates for the map were the total mass flow rate and the mass quality. The presentation of flow patterns in this form confines the results to a single pressure. Thus, a family of transition curves would be necessary to display the effect of system pressure. This form of flow-regime map was modified by Suo et al.[32] for water at 1000 psia in which the transitions from bubble and slug flow to dispersed were estimated by combining the dispersed transition results of Baker,[34] Haberstroh and Griffith's semiannular transition,[18] and a constant-Weber-number representation due to Wallis.[45] The experimental transitions were obtained by utilizing a resistance probe. The transition that occurred from the semiannular-to-dispersed regime was at a lower quality than would be predicted by the square root of the orthobaric-density ratio representation of Griffith.[46]

The total mass flow rate and quality form of flow regime presentation were utilized by Bennett et al.[27] for water at 500 and 1000 psia wherein high-speed motion pictures and X-ray photographs were employed to determine the flow regime at the exit of a vertical heated tube. Their work contained a criticism of the resistance-probe method[18,32,46] for the determination of the annular transition. The wispy-annular regime described by this report would appear to be bounded by churn, or semiannular, flow at low qualities and high flow rates; the annular regime at low mass flow rates; and by the dispersed-annular flow regime at high qualities and high flow rates. The transition from annular to "wispy-annular" was indicated to have occurred at a nearly constant superficial liquid velocity. A statement that the transition occurred at increasing liquid velocities for increasing pressure is not compatible with the data presented in their report. A calculation of the superficial velocities from the quality and mass flow rate listed in their tables indicated an opposite effect. Their reported approximate values of transition from annular to wispy-annular are 4.5 ft/sec at 1000 psia and 3.5 ft/sec at 500 psia. Data available at present do not appear to be sufficient to make a definitive statement concerning the form of this transition. The results of this report and of Suo et al.[32] appear to invalidate a constant-quality transition as suggested by Griffith.[46]

Staub and Zuber[47] presented a transition map for Refrigerant-22 for reduced pressures of 0.12 and 0.22 for a limited range of total mass flow rates in the form of a superficial-velocity plot incorporating bubbly-slug, churn, churn-annular, and annular flow in their transition. In particular, their study revealed an absence of plug flow in the two-phase flow with heat addition. The transition to annular flow in their results is not predictable by the method of Haberstroh and Griffith.[18]

In summary, the information concerning the flow-regimes transitions of single-component fluids at elevated temperatures is not extensive. The effect of the change in fluid properties has not been well-defined, nor has the effect of the configuration, or diameter, met with any conclusive results. The use of a single plot to represent all regime transitions for a variety of fluids with large changes in properties does not seem feasible.

III. STATEMENT OF THE PROBLEM

The flow regimes produced by constant-heat-flux addition to a single-component fluid in forced-circulation, upward flow at elevated pressures were investigated. Visual observations of the flow regimes are made utilizing high-speed color motion pictures and a fluoroscope monitoring system. The similarity of flow patterns and transitions between a test fluid, trichloromonofluoromethane, and water is to be established. The basis for the modeling criterion will be shown in Section IV, where the orthobaric-density ratio is obtained as the preferred modeling parameter, rather than on a reduced-pressure or -temperature basis through consideration of the thermodynamic and transport properties, and the possible causes of transition between flow regimes.

The test fluid at near-saturation conditions is heated electrically through a series of qualities to the limit of the system. The pressure range selected for these tests, when modeled at identical orthobaric-density ratios, corresponds to a range of water saturation pressure from approximately 400 to 2000 psia. The orthobaric-density ratio involved ranged from 7 to 60. The mass flow rates based upon a rectangular channel with a flow cross section of 1.050 by 0.380 in. varied from 0.20×10^6 to 2.0×10^6 lb/hr-sq ft.

The observations are made in an unheated, rectangular channel above the heated section. Void-fraction traverses are made during each test run to provide information concerning the change in void distribution as the flow rate and quality are varied. Local pressure gradients are also obtained across the section of observation.

The goal of this investigation is to establish a correspondence in flow patterns and their transition between two widely different fluids (trichloromonofluoromethane and water). An immediate consequence of the existence of such correspondence is the possibility of ascertaining the flow regime for water at high pressure by conducting experiments on a single-component fluid at much lower temperatures and pressures.

IV. SIMILARITY METHODS

To provide a method of similarity modeling for two-phase flow systems, the thermodynamic and transport properties of various fluids must be considered. Since the observation of van der Waals[3] concerning the Law of Corresponding States, various thermodynamic and transport properties have been correlated on the basis of reduced properties, that is, on the basis of the ratio of a particular property to its value at some reference state. In general, the reference state has been the thermodynamic critical point. This thermodynamic modeling has its basis in the similarity of molecular structures. Under this form of premise, the fluid considered for this investigation was selected as one that has a low critical pressure and temperature so that a system could be employed in which visual observations could be made. Hosler and Westwater[4] stated that a true test of any analysis of boiling-heat-transfer phenomena is the comparison of water and Freon-11. The selection of trichloromonofluoromethane (Refrigerant-11 or Freon-11) for the operating fluid met the requirements of low pressures and temperatures; in addition, lower heat fluxes are required to accomplish the desired exit conditions.

The physical system itself must enter into consideration in any method of modeling. Hence, to circumvent the problem of adding an additional parameter to the investigation, the test unit was designed to fall within the realm of conduit sizes most frequently appearing in the literature for systems employing water as a working fluid. The primary question to be answered is that of what basis is to be employed for modeling various fluids. To answer this question, the physical properties of water and R-11 must be examined.

Guggenheim[48] pointed out that no substance can be completely described in its equation of state by a proposal that contains only two adjustable parameters. Many fluids are, however, relatable over certain regions by the Law of Corresponding States in terms of their critical properties. The literature contains many efforts to relate all substances in the reduced-property form with varying degrees of success. The Law of Corresponding States implies that a universal constant exists[49] such that

$$P_c\overline{V}_c/T_c = K, \tag{IV.1}$$

and that

$$P\overline{V}/T = K\frac{\pi\phi}{\gamma} = f_1(\pi,\phi,\gamma), \tag{IV.2}$$

where the reduced variables are $P = P_c\pi$, $\overline{V} = \overline{V}_c\phi$, and $T = T_c\gamma$. Certain classes of fluids fall into the above type of model. In general, correspondence has been found when the outer electron shell of a molecule shows similarity to another type of molecule. Two additional classes of fluids are the polar and nonpolar types of molecules. For example, it has been suggested that the decrease in viscosity at constant temperature of water as it approaches condensation (i.e., the saturated-vapor state) is due to preferred alignment of the polar molecules in "clusters," thereby allowing the "free" molecules a greater collision-path length. Further, surface phenomena are very different in polar and nonpolar fluids.[50] This point may be of importance in the study of two-phase systems. In polar fluids, the increased viscosity and a great elastic strength of the fluid at its surface, particularly near a solid interface, represent the prime differences. The most significant fluid in engineering applications is water, which is a polar fluid and is not correlatable with ordinary nonpolar fluids such as the simple straight chain organic fluids (for example, methane or ethane). The Freon group is, in general, polar.

For two-phase flow systems, the viscosity and surface tension of a fluid are generally required, in addition to the P-V-T data. It is often necessary to fit expressions to the available data in order to obtain the desired test condition. The modeling of viscosity has been approached by various methods in the absence of complete data. This aspect will be considered in the following sections.

The prime assumption in most fluid-flow studies is that the equilibrium-state properties are applicable to dynamic situations. This is definitely open to question in the appearance in flow systems of a dynamic surface tension that is significantly different from the static-surface-tension measurement.[51] It is also known that the relaxation time, or time to reach equilibrium, is not the same for the vibrational, rotational, and translational energies of a molecule. It will be assumed in this investigation that the equilibrium-state properties are sufficient for determining the fluid condition of the two-phase flow system.

Reduced properties have been used in previous heat-transfer work in boiling. Bankoff[52] presented the maximum heat flux in nucleate subcooled boiling as a function of reduced pressure in evaluating the difference between the fluid saturation temperature and the wall temperature. No one has pointed out a physical reason for the above correlation or that a maximum occurs at some reduced pressure. A recent correlation of peak and minimum heat flux for nucleate pool boiling by Lienhard and Schrock[53] utilized a reduced-pressure correlation. However, the scatter in their data about the "theoretical" curve is probably due, on the whole, to an inherent assumption in their dimensional analysis that the ratio of the Weber number to the drag coefficient is a constant. Some of the questions concerning correlations based on dimensionless groups that exhibit success in some instances and wide deviations in others will be shown in the following sections to be in part due to the various means of representing the physical properties.

A. Thermodynamic and Transport Properties

To establish a model for comparing water and the "Freon" group, we must examine the variation of thermodynamic and transport properties of these fluids as a function of the saturation conditions, that is, the variation of the properties as a function of either the saturation pressure or the saturation temperature, since the two parameters are not independent along the saturation line. An examination of the fluids may be initially considered in terms of the reduced pressure (the ratio of the saturation pressure to the critical pressure), and in terms of the reduced temperature (the ratio of the saturation temperature to the critical temperature). If P_r and T_r, respectively, represent the aforementioned ratios, a plot of the log P_r versus $1/T_r$ for a variety of substances will reveal that no two vapor-pressure curves overlap, as was shown by Martin.[54] Thus, there is no universal vapor-pressure plot in terms of the reduced pressure-reduced temperature parameters. Therefore, it can be concluded that any correlation that exhibits a single-parameter representation of many fluids in terms of the reduced saturation pressure will not have a single-parameter representation in terms of the reduced saturation temperature.

1. Saturation Properties

The saturation thermodynamic properties that are usually employed in flow-system calculations have been obtained originally by experiments in which thermal equilibrium has been attained. A series of static thermal equilibrium state points in which thermodynamic properties such as pressure, temperature, and specific volume (or density) are measured and connected as a continuous function represents the saturation line for the liquid or vapor. Other thermodynamic point functions, such as enthalpy and entropy, are obtained from indirect measurements since both are calculated quantities from other measurements. The variation of these equilibrium properties, as determined from these static equilibrium tests, is assumed to hold in most flow-system analyses.

Primarily, in modeling the "Freon" group with water, interest in the variation of the saturation properties as a function of either saturation pressure or temperature should be a first concern of an investigation. In this respect, the variation of the ratio of the saturation-liquid and saturation-vapor densities as functions of reduced saturation temperature or pressure is shown in Figs. IV.1 and IV.2, since this ratio exhibits the greatest variation over the normal operating range for most fluids.

The saturation-density ratio is defined as

$$\beta \equiv \rho_f/\rho_g, \qquad \text{(IV.A-1)}$$

where the saturation-liquid and saturation-vapor densities are indicated by the subscripts f and g, respectively. The saturation-reduced pressure ratio, which will be referred to as the reduced pressure in the following text, is given by

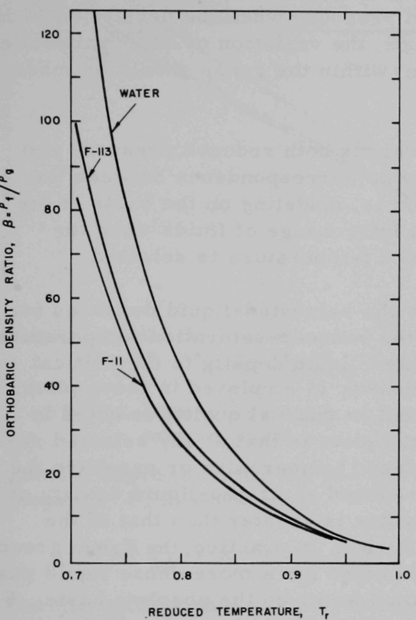

Fig. IV.1. Orthobaric-density Ratio as a Function of Saturation Temperature

$$P_r \equiv P_{sat}/P_c, \qquad \text{(IV.A-2)}$$

where the saturation pressure is represented by the subscript "sat," and the critical pressure given by the subscript "c." The critical pressure is defined as the pressure at which the saturation-liquid density is equal to the saturation vapor density. The saturation-reduced temperature ratio is given by

$$T_r \equiv T_{sat}/T_c, \qquad \text{(IV.A-3)}$$

where the saturation and critical temperatures are represented by the subscripts "sat" and "c," respectively. Any set of consistent absolute units may be employed with the above quantities.

Figure IV.1 indicates that separate curves are found for the various "Freon" fluids and water; in Fig. IV.2, the "Freon" group is represented by a single curve, which is separated from the water results. In Fig. IV.1, only the bounding curves

Fig. IV.2

Orthobaric-density Ratio as a Function of Saturation Pressure

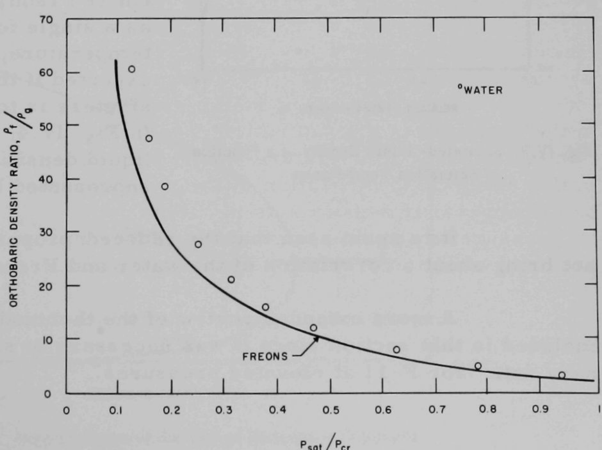

for the Freons are shown. Thus, an immediate conclusion as to the representation of various Freons within the group can be made. That is, experimental modeling that requires a correspondence within the Freon group should be made on the basis of reduced pressure when the density ratio is the prime factor. In subsequent sections, the variation of other properties will indicate that a model for the Freons within the group should be made on the basis of reduced pressure.

The plots of density ratio versus both reduced pressure and reduced temperature show that there is no correspondence between the water results and the Freon group. That is, modeling on the basis of the density ratio does not carry over in an interchange of fluids when the criterion of reduced pressure or reduced temperature is selected.

Figures IV.3 and IV.4 show the saturated-liquid densities for the Freon group and water in terms of the reduced-saturation temperatures and pressures. The ratio of the saturated-liquid density to the critical density is employed in these plots, and an unusual quality is noted in the plots in that at any selected reduced temperature or pressure the reduced saturated-liquid density of water is greater than that of the Freons. In practice, the Freon group is noted for a more dense liquid phase than water on the absolute basis. For example, R-11 has a liquid density of approximately 92 lb/cu ft at room temperature, compared to water with a value of 62.3.

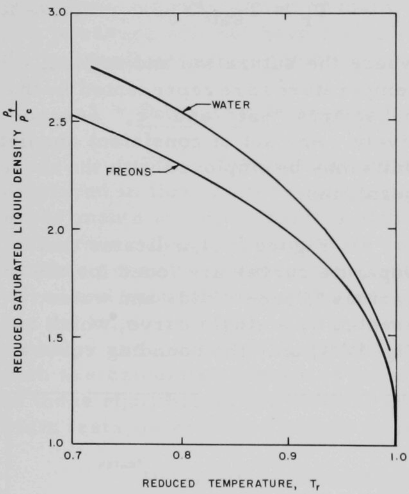

Fig. IV.3. Saturated-liquid Density as a Function of Saturation Temperature

Figure IV.3 indicates that the entire Freon group can be represented as a single function of the reduced temperature, which should have been expected if the law of rectilinear diameters is to hold for the Freon group. In Fig. IV.4, the reduced saturated-liquid densities for the Freons are represented by the bounding curves.

It is again seen that the reduced-property representation does not bring about a correlation of the water and Freon group.

A more extended review of the thermodynamic properties is included in this section since it was necessary to smooth some preliminary data[55] for F-11 at elevated pressures.

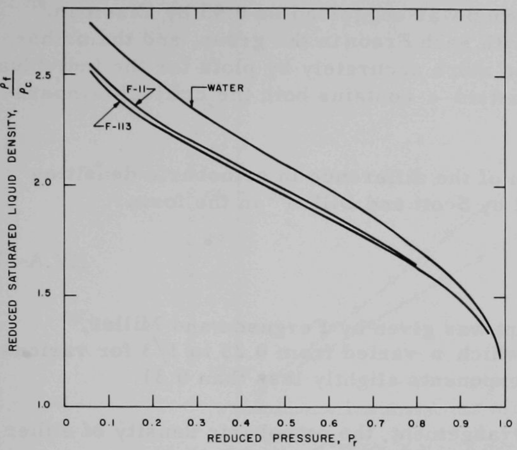

Fig. IV.4. Saturated-liquid Density as a Function of Saturation Pressure

The estimation of saturated-fluid densities has been the object of numerous publications over many decades, and identical formats are republished as new methods. Typical examples of this aspect are cited by Scott and Dillon[56] in a discussion on the use of reduced temperatures for the description of the orthobaric densities.

A typical representation of the law of rectilinear diameters is shown in Fig. IV.5 in which the orthobaric or saturation densities are represented and the mean density is indicated. The general expression for the law of rectilinear diameters for any orthobaric property, F, is given by

$$F_f + F_g = a - bT_r. \tag{IV.A-4}$$

For the saturation densities, the expression will be altered slightly by employing the definition that the saturated-liquid and vapor densities are identical at the critical point; then,

$$\frac{\rho_f + \rho_g}{2\rho_c} = 1 + c(1 - T_r). \tag{IV.A-5}$$

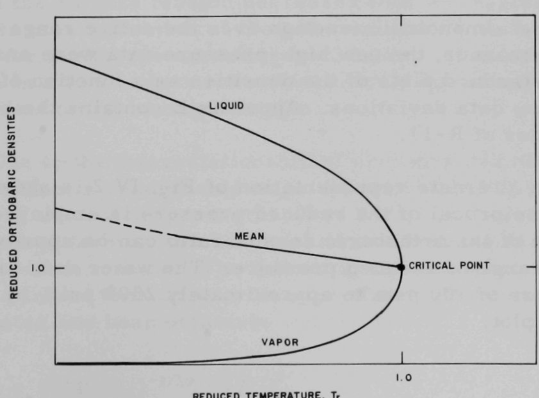

Fig. IV.5. Representation of the Law of Rectilinear Diameters

The value of c for the Freon group was suggested as 0.93 by Eiseman.[57] This constant varies slightly with each Freon in the group, and the orthobaric densities are represented more accurately by plots for the individual member in the group. The constant c contains both the critical temperature and the critical density.

The representation of the difference in orthobaric densities has a long history as indicated by Scott and Dillon[56] in the form

$$\rho_f - \rho_g = D_0(1 - T_r)^n. \quad \text{(IV.A-6)}$$

A value of 3/10 for the exponent was given by Ferguson and Miller.[58] Fishtine[59] provided a table in which n varied from 0.25 to 1/3 for various compounds. The Freons have exponents slightly less than 0.31.

After a slight rearrangement, the orthobaric density of either phase should be attainable from Eqs. (IV.A-5) and (IV.A-6) as

$$\rho/\rho_c = 1 + c(1 - T_r) \pm D_1(1 - T_r)^n, \quad \text{(IV.A-7)}$$

where the plus and minus signs represent the liquid and vapor densities, respectively, and D_1 is $D_0/2\rho_c$.

To check the consistency of the Freon orthobaric densities, the sum of the orthobaric densities at each temperature was formed and Eq. (IV.A-5) was employed to form the expression

$$b_{12} = \frac{(\rho_f + \rho_g)_1 - (\rho_f + \rho_g)_2}{T_2 - T_1}, \quad \text{(IV.A-8)}$$

which should be a monotonic function over the entire range of temperatures. In this manner, the new high-pressure data were analyzed in conjunction with standard plots of the densities as a function of temperature to ascertain any data deviations. Appendix B contains the original values of the properties of R-11.

An alternate representation of Fig. IV.2 is shown in Fig. IV.6 in which the reciprocal of the reduced pressure is employed. A linear representation of the orthobaric density ratio can be approximated over a considerable range of reduced pressure. The water data are represented, from a pressure of 100 psia to approximately 2500 psia, by the linear portion of the plot.

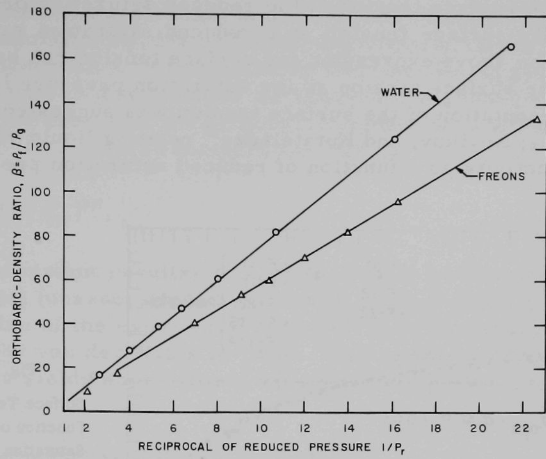

Fig. IV.6. Linearity Representation of the Orthobaric-density Ratio

2. Surface Tension

The surface tension exhibited in thermodynamic equilibrium may be considered to be the excess Gibb's free energy (the enthalpy minus the product of the absolute temperature and the entropy) between the free energy of a surface layer of molecules and that of a layer at some distance from the surface. The general trend has been to employ experimental data to derive expressions that relate the surface tension to the pressure, the temperature, the enthalpy, the density, or the parachor. The surface tension of a fluid has usually been considered independent of pressure for subcooled systems. However, if a gas at high pressure is maintained over a liquid, then the surface tension decreases with increasing gas pressure, and the decrease is a function of the gas employed.[60] A decrease of 50% was attained for pressures extending to 150 atm. At moderate pressures, gas pressure in a two-component mixture would not be expected to have a very large effect on the surface tension.

Due to the interrelationship of pressure and temperature along the saturation line, a relationship might be formulated for surface tension as a function of saturation pressure. This result is shown in Fig. IV.7 where the surface tension has been placed in a reduced form by employing a reference surface tension. The following approximate general expression for surface tension as a function of saturation pressure for the Freons and water has been obtained:

$$\frac{\sigma}{\sigma_{0.03}} = 0.749(P_r)^{-1/10}(1 - P_r)^2, \qquad \text{(IV.A-9)}$$

where σ is the surface tension at the reduced saturation pressure, P_r; and $\sigma_{0.03}$ is the surface tension at a reduced saturation pressure of $P_r = 0.03$. The above expression for surface tension can be successfully employed if the surface tension at any saturation pressure is known. This method of presentation of the surface tension was suggested by the work of Borishansky, Novikov, and Kutateladze[61] relating liquid viscosity and thermal conductivity as a function of reduced saturation pressure.

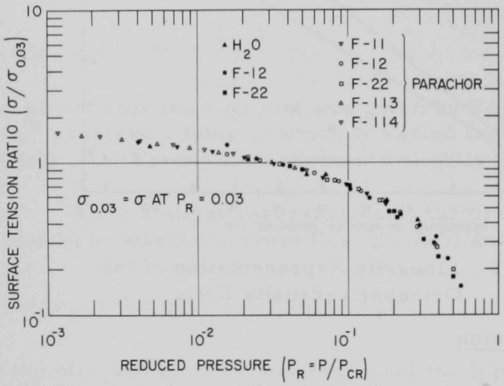

Fig. IV.7

Surface Tension as a Function of Reduced Saturation Pressure

The reference values for the surface tension at the standard reduced pressure are given in Table I. The experimental data for two of the Freons were obtained from a paper by Steinle.[62]

TABLE I. Physical Constants

	$\sigma_{0.03}$ (Exp.), dyn/cm	$\sigma_{0.03}$ (Parachor), dyn/cm	Critical Pressure, psia	Critical Temp, °F	Critical Density, cu ft/lb
Water	46	-	3206.2	705.4	19.88
R-11 (CCl_3F)	-	17.2	635	388.4	34.5
R-12 (CCl_2F_2)	13.7	15.8	596.6	233.6	34.84
R-22 ($CHClF_2$)	16.8	17.2	716	204.8	32.8
R-113 (CCl_2F-$CClF_2$)	-	15.8	498.9	417.4	35.96
R-114 ($CClF_2$-$CClF_2$)	-	14.7	474	294.3	36.3

Various formulations for the surface tension as a function of other thermodynamic variables could be considered at this point. Two representations of significance in the following text are the representation of the surface tension as a function of the reduced temperature and as a function of the difference of the orthobaric densities. The variation of surface tension with reduced temperature can be written as

$$\sigma = \sigma_0(1 - T_r)^m, \tag{IV.A-10}$$

where σ_0 is a constant peculiar to each fluid, and m is approximately a constant for all (unassociated) liquids with a value of about 1.2. In a study of the value of the exponent, Ferguson[63] indicated that the equation was presented by van der Waals in 1894. This exponent varies from fluid to fluid and only yields approximate values for the numerical value listed above.

The parachor, [P], is defined as

$$[P] \equiv \frac{M\sigma^{1/4}}{(\rho_f - \rho_g)} \tag{IV.A-11}$$

where M is the molecular weight. Sugden[64] devoted an entire book to the subject of calculating parachors for many fluids by utilizing additive contributions from the molecular structure of a fluid. The parachor permits a comparison of molecular volumes at constant surface tension. Thus, it makes some allowance for the effect upon molecular volumes of the large forces due to molecular attractions. Since the original book is not readily available, the term "parachor" is defined here as the combination of two Greek words ($\pi\alpha\rho\acute{\alpha}$ = set by the side of, and $\chi\acute{\omega}\rho\alpha$ = space). In the absence of any data on a particular fluid, the surface tension may be estimated if the orthobaric densities and the molecular weight are known, along with the molecular structure.

The surface tension, when expressed as a function of the difference of the orthobaric densities, was found by Macleod[65] to be of the form

$$\sigma = C(\rho_f - \rho_g)^p, \tag{IV.A-12}$$

where C is a constant independent of temperature, and p was taken by Macleod to be equal to 4. This expression led Sugden to the definition of the parachor. Ferguson[63] listed values of p for several fluids and indicated that the value of p varied from fluid to fluid. For most substances, the deviation from the value of 4 set by Macleod is not large. Therefore, a rule of thumb for the variation of surface tension with density may be taken as

$$\sigma \cong C(\rho_f - \rho_g)^4, \qquad \text{(IV.A-13)}$$

or, the parachor is a good approximation for surface tension.

An interesting result is obtained by equating Eqs. (IV.A-10) and (IV.A-12) and rearranging them to yield

$$\rho_f - \rho_g = (\sigma_0/C)^{1/p} (1 - T_r)^{m/p}. \qquad \text{(IV.A-14)}$$

If the general values of m and p are taken as 1.2 and 4, respectively, as suggested above, the resultant expression will be identical to the value listed for n in Eq. (IV.A-6).

In later sections, the above relationships for surface tension will be extended to the problem encountered in two-phase flow of evaluating the effect of various dimensionless groups.

3. Viscosity

The dynamic viscosity, which appears as a coefficient in the viscous stress-tensor in the equation of motion for both the vapor and the liquid, has been examined as a function of various thermodynamic properties, in particular as a function of temperature and density. In the literature, no completely satisfactory method has been cited that will predict the viscosity of a liquid from its molecular structure or from the physical properties. In general, experimental measurements have provided the desired viscosity data. Bondi[66] applied a simple molecular theory for non-associating liquids and produced some work over a limited range of temperature and pressure for fluids that have their liquid viscosity in the functional relationship of

$$\log \mu_f = A + B/T, \qquad \text{(IV.A-15)}$$

where μ_f is the dynamic liquid viscosity and A and B are constants.

Thodos et al. presented a series of correlations for the viscosity of pure substances over a considerable range of pressures and temperatures.[67,68,69] The fluids were separated into polar and nonpolar groups and further subdivided into classes of fluids. Both reduced temperature and reduced density were considered as variables. The viscosity term was expressed as the difference between the viscosity at elevated pressure and temperature, and the viscosity at atmospheric pressure and the same temperature. This difference was termed the residual viscosity.

In the dense gaseous and liquid regions, the residual viscosity was expressed as single-valued function of reduced density for polar substances. The Freons were included in this correlation.[69] It then should be expected that an extension of the limited viscosity data for the Freons can be made.

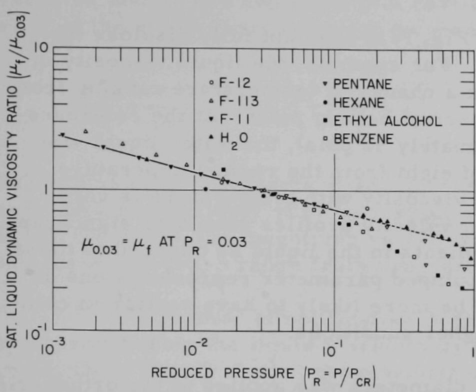

Fig. IV.8. Liquid Dynamic Viscosity as a Function of Reduced Saturation Pressure

A vast literature is available on two-phase flow studies carried out at low pressures and temperatures. Particularly numerous among these studies are those employing air-water systems. Extension of these results to systems at elevated pressures is difficult as in any extrapolation. Figure IV.8 is an expansion of the graph presented by Borishansky et al.[61] in which the liquid dynamic viscosity is plotted on a reduced basis (using the viscosity at a reduced pressure of 0.03 as a reference). The independent variable is the reduced pressure. Results for the Freons are added to the plot, as well as some additional water data. The curve drawn through the data in the original paper has been omitted and, in its place, a straight line is drawn through the water and Freon data. The resultant expression for the liquid viscosity is given by

$$\frac{\mu_f}{\mu_{0.03}} = 0.4(P_r)^{-0.261} \qquad \text{(IV. A-16)}$$

for

$P_r < 0.2$ for all fluids

and

$P_r < 0.9$ for water.

The reference viscosities at $P_r = 0.03$ for several Freons and water are as follows:

1. Water: $\mu_{0.03} = 11.45 \times 10^{-5}$ lb/sec-ft;

2. R-11: $\mu_{0.03} = 27.0 \times 10^{-5}$ lb/sec-ft;

3. R-12: $\mu_{0.03} = 24.8 \times 10^{-5}$ lb/sec-ft;

4. R-113: $\mu_{0.03} = 33.3 \times 10^{-5}$ lb/sec-ft.

The representation in Fig. IV.8 does not fully disclose the rapid decrease in liquid viscosity. For example, the liquid viscosity of water decreases nearly fourfold in a change of temperature ranging from normal room temperature to the normal boiling point. At the reference reduced pressure of 0.03 (approximately 96 psia), the water liquid viscosity has decreased by a factor of eight from the room-temperature value. In addition, the gradient of viscosity with temperature is very large for low temperatures. Thus, velocity profiles should be significantly affected by small temperature gradients in the liquid as opposed to those found at elevated temperatures. Lumped parameter representations at low temperatures would appear to be more likely to have scatter in comparison of results than those at higher conditions.

The law of rectilinear diameters was applied to the orthobaric or saturation viscosities by Starling et al.[70] Data for water were examined graphically. A linear portion occurs above 400 psia. A curvature near the critical point appears approximately at 2800 psia. Thus, the sum of the orthobaric dynamic viscosities may be written as

$$\mu_f + \mu_g = a_1 + b_1(1 - T_r), \tag{IV.A-17}$$

where a_1 and b_1 are constants. If the law of rectilinear diameters held exactly, then a_1 would be equal to twice the critical viscosity, or

$$\frac{\mu_f + \mu_g}{2\mu_c} = 1 + c_1(1 - T_r). \tag{IV.A-18}$$

The use of Eq. (IV.A-18) instead of Eq. (IV.A-17) would mean that unity has replaced a constant with a value of 1.15 for the water data in the first term on the right-hand side of Eq. (IV.A-18).

At this point, the reduced temperature may be replaced by the orthobaric-density difference as given by Eq. (IV.A-5), yielding

$$\frac{\mu_f + \mu_g}{2\mu_c} = 1 + (c_1/c)\left[\frac{\rho_f + \rho_g}{2\rho_c} - 1\right]. \tag{IV.A-19}$$

Or,

$$\mu_f + \mu_g = 2\mu_c(1 - c_1/c) + \frac{\mu_c}{\rho_c}\frac{c_1}{c}(\rho_f + \rho_g) \tag{IV.A-20}$$

$$\mu_f + \mu_g = A + B(\rho_f + \rho_g) \qquad \text{(IV.A-20a)}$$

where A and B are constants of a particular fluid. Further rearrangement of the above expression can be made as follows:

$$\frac{\mu_g}{\mu_f} = \frac{1}{\mu_f}[A + B\rho_f(1 + 1/\beta)] - 1. \qquad \text{(IV.A-21)}$$

The values of the constants c and c_1 for water are approximately 0.636 and 0.462, respectively, with c_1/c equal to 0.726. For the range of validity of Eq. (IV.A-21), the magnitude varies from 1/6 to 1/2, which covers a saturation pressure range from approximately 400 to 2800 psia for water.

A further simplification of the viscosity ratio can be obtained by approximating the liquid viscosity by Eq. (IV.A-16) and utilizing the result from Fig. IV.7, that the orthobaric density ratio is nearly proportional to the reciprocal of the reduced pressure, which then reduces Eq. (IV.A-21) to

$$\frac{\mu_g}{\mu_f} \cong D\beta^{0.261}[A + B\rho_f(1 + 1/\beta)] - 1. \qquad \text{(IV.A-22)}$$

The effect of the viscosities in the interpretation of single-component systems may be obscured by an empirical correlation in which the orthobaric-density ratio may satisfy the variation in some system condition by a complicated function without including explicitly the viscosities.

The ratio of the dynamic liquid viscosity to the surface tension can be expressed in terms of Eqs. (IV.A-9) and (IV.A-16) as

$$\frac{\mu_f}{\sigma} = \left[(\mu_f/\sigma)_{0.03}\right]\frac{(0.534)}{P_r^{0.161}(1 - P_r)^2}. \qquad \text{(IV.A-23)}$$

This ratio increases for increasing pressures. A comparison of the reference constant for water and F-11 indicates a ratio of approximately 6.30 for F-11 to water. Comparison of the results at identical density ratios indicates that the ratio is approximately 6.6.

The method of selection of the reference-reduced property for the liquid dynamic viscosity and the surface tension has no apparent theoretical basis from any classical thermodynamic considerations. The particular reduced pressure selected is a compromise in that the reference point provides agreement among the fluids in the neighborhood of that point. There is a deviation that grows as the data points extend further away from the reference value. Thus, the segment of the reduced-pressure coordinate that spans the region of greatest interest and provides the closest approximation to a single representative function is chosen. The reference point is then the value that yields the least deviation over the range of interest. This result is not unexpected since it was pointed out earlier in this section that no substance can be completely described in its equation of state by any proposal that contains only two adjustable parameters. Thus both methods of correlating the two fluid properties are at best only approximations of the true variations, and were developed to facilitate calculation of the effect of each property on the flow topology.

B. Dimensional Groups

The problem of determining the conditions whereby a particular flow regime can exist and the transition from that regime to another could in principle be determined if the equations of motion, continuity, and state, together with the appropriate initial and boundary conditions and the constitutive relationships are known, and a solution obtained. In practice, very few solutions are obtainable for even the simplest of systems. An appeal is then made to methods such as dimensional analysis where the governing parameters are assumed from physical requirements. Another method is that of inspectional analysis, which applies the principle that, if a set of mathematical equations is invariant under a group, then the same is true of all consequences of these equations.[71] Thus, a transformation is sought for the descriptive equations that will yield a similarity condition. Both of the aforementioned methods require experimental evidence for the confirmation of the analysis.

The transition between flow regimes can be considered as a hydrodynamic stability problem. The stability problem may be considered as follows: given a pressure field and a velocity distribution, which are an exact time-independent solution of the Navier-Stokes equations, the solution is given an initial disturbance. If the disturbance dies out as time becomes large, the flow is said to be stable, if not, it is unstable. Chandrasekhar,[72] among others, studied the linear-stability problem in unbounded flows. The linear-stability approach neglects quadratic terms in the disturbances. These terms give rise to nonlinearities, which produce difficulties in obtaining a solution. These quadratic terms also damp the system and prevent an unbounded increase in the amplitudes and allow another flow to be established. Two methods of solution, which are standard in the approach to the linear-stability problem, are the Laplace transform in time with a study of the disturbances at large times; and the normal-mode type of analysis in which variables are separated to produce a time-dependent function and a spatial-dependent function. The latter form is more prevalent in the literature. The normal-mode analysis was applied by Tippets[6] in a study concerning the liquid film stability for conditions approaching burn-out in forced convection. Moissis[31] utilized the method in a study of the transition from slug flow to homogeneous flow.

The basic difficulty involved in applying the unbounded-flow-stability results is that the effect of the enclosure, such as in conduit flow, is generally neglected because of the complexity of the situation. An example in which the analysis for an essentially unbounded situation proved effective in a small confinement is the analysis of Taylor[73] for the instability of liquid surfaces accelerated in a direction perpendicular to their planes. The subsequent experimental investigation of Lewis[74] in a vertical channel, whose cross section was $2\frac{1}{2}$ by 1/2 in. provided ample confirmation of the analysis. The effect of the channel walls was to develop the instability at a faster rate for the more viscous fluid. The velocity of propagation of gas columns upward through a liquid layer, initially given a downward acceleration, was proportional to the square root of the product of the radius of the gas tip and the sum of the gravitational acceleration and the initial acceleration. Taylor had initially shown that the rate of development of the instability was proportional to

$$\sqrt{\frac{\beta - 1}{\beta + 1}},$$

where β is the orthobaric-density ratio. The transition from the slug-flow regime to the semiannular may be related to this form of instability. Thus, as the system pressure increases, the rate tends to decrease.

The transition from annular flow to the froth or semiannular flow may be characterized as an instability in the vapor-liquid interface that leads to bridging of the channel. This problem was treated by Moissis[31] who assumed an infinite thickness of the vapor layer. The solution to the standard velocity-propagation equation (see, for example, Milne-Thomson[75]) for waves at an interface of two fluids bounded above and below by rigid horizontal planes is sought for a wave of small amplitude, which has a sinusoidal variation. The general expression may be written as

$$k\rho(V - c)^2 \coth(kh) + k\rho'(V' - c)^2 \coth(kh') = g(\rho - \rho') + \sigma k^2, \tag{IV.B-1}$$

where k is the wave number; c is the wave speed; σ is the interfacial tension; ρ, V, and h are the density, velocity parallel to the interface, and depth of the lower fluid, respectively; the primed quantities represent the upper fluid; and g is the gravitational acceleration. This expression represents a combined Taylor-Helmholz instability for a constant velocity parallel to, and an acceleration normal to, the interface.

The following quantities are defined:

$$W = \text{Weber Number} = \rho L U^2/\sigma, \tag{IV.B-2}$$

and

$$F = \text{Froude Number} = U^2/gL, \tag{IV.B-3}$$

where U is a characteristic velocity, and L is a characteristic length. Thus, on substitution and rearrangement, Eq. (IV.B-1) becomes

$$W^{-1} + F^{-1}(1 - \rho'/\rho)/(kL)^2 = (kL)\left[\frac{V - c}{U}\right]^2 \coth(kh) + (kL)(\rho'/\rho)\left[\frac{V' - c}{U}\right]^2 \coth(kh'). \tag{IV.B-4}$$

The above equation has been rendered dimensionally invariant, and the dimensional groups are a Weber number, a Froude number, and the density ratio. In Moissis' analysis for a vertical wall, the second term on the left-hand side does not appear, and as a consequence of taking the thickness of the vapor layer to be very large, coth (kh') is set equal to unity. The result is Eq. (10) in Moissis' paper, which is

$$\rho_f(-V_f - c)^2 \coth(kh) + \rho_g(V_g - c)^2 = k\sigma, \tag{IV.B-5}$$

where the subscripts f and g refer to the liquid and vapor, respectively. At this point, the above expression could be made dimensionally invariant and yield a Weber number and the density ratio. However, Moissis considered the linearized stability solution and obtained

$$(V_f + V_g)^2 \leq \frac{\sigma k[\rho_f \coth(kh) + \rho_g]}{\rho_g \rho_f \coth(kh)}. \tag{IV.B-6}$$

The analysis continued with the assumptions that it was possible to neglect the interfacial shear, momentum changes, and pressure forces. The liquid-film thickness was then obtained by a balance of the gravity and wall shear forces. The bubble rise velocity was considered proportional to the square root of the piper diameter. A further assumption was made that the most unstable wave length could be expressed as ten times the film thickness. The solution still remained indeterminate, since the length of the liquid slug entered the expressions and no single value could be assigned to it. The length of the bubble was also a variable. Therefore the analysis was made on the basis of various possible bubble lengths. The limiting stability criterion was finally obtained as

$$WE(0.2FR^{1/2}+C)^2 = (32\pi/10)(1-h^*)^2 h^*, \quad \text{(IV.B-7)}$$

where

$$C = 0.35 + 2.8 \exp(-1.06L_s^*), \quad \text{(IV.B-8)}$$

$$FR = [(Q_f+Q_g)/A_p]^2/gD_p, \quad \text{(IV.B-9)}$$

and

$$WE = \rho_f \frac{gD_p^2}{\sigma} \frac{\coth(kh)}{\beta \coth(kh)+1}, \quad \text{(IV.B-10)}$$

where h^* is h/D_p, D_p is the pipe diameter, A_p is the cross-sectional area of the pipe, Q/A is the superficial velocity, and L_s^* is the liquid slug length divided by the pipe diameter. The author then compared his results with air-water data with the number of equivalent pipe diameters for the bubble length as a parameter. From the graphical representation, it appeared that a bubble length in excess of ten diameters was required to produce the transition from slug to froth flow in comparing the calculation with visual observations. No limiting criterion was set in the work that would permit a bound to be made on the transition from slug flow to froth or annular flow. In reviewing the method of analysis, it appeared that Moissis was examining the transition from annular to slug flow, not as was stated in the conclusions that the transition was from the nonhomogeneous slug flow to a homogeneous fog or froth-flow region.

The most significant portion of the preceding discussion of the linearized stability problem is that a Weber number, Froude number, and the density ratio appear when the equations are rendered dimensionally invariant. Since the effect of density ratio may be obscured in Eq. (IV.B-10), a further reduction may be made. For a thin liquid layer, the term coth (th) can be approximated by $1/kh$ and the following simplification made:

$$WE \sim \rho_f \frac{gD_p^2}{\sigma} \frac{1}{\beta + kh}. \quad \text{(IV.B-11)}$$

The wave length, given by $2\pi/k$, is further reduced by the assumption that the critical wave length is approximately 10h. This yields

$$WE \sim \rho_f \frac{gD_p^2}{\sigma} \frac{1}{\beta + \pi/5}. \quad \text{(IV.B-12)}$$

Thus, for $\beta \gg \pi/5$,

$$WE \sim \rho_f \frac{gD_p^2}{\beta\sigma} = \rho_g \frac{gD_p^2}{\sigma}. \tag{IV.B-13}$$

To illustrate the effect of increasing the saturation pressure, the surface tension can be approximated by the difference in saturation densities to yield the Weber number in Moissis' analysis as

$$WE \sim \frac{gD_p^2}{C\beta\rho_f^3(1 - 1/\beta)^4} \tag{IV.B-14}$$

which indicates the rapid rise in the limiting-stability Weber number as the system pressure is increased.

The Froude number, FR, based upon the volumetric flow rate, can be written as in Eq. (IV.B-9) in the following form:

$$FR = (Q_g/A_p)^2 (1 + Q_f/Q_g)^2/gD_p$$

$$= (xG_0/\rho_g)^2 \left[\frac{x\beta}{1-x} + 1\right]^2/gD_p \tag{IV.B-15}$$

where x is the mass quality, and G_0 is the total mass flow rate per unit area. For a fixed flow rate and quality, the volumetric Froude number decreases with increasing system pressure. The volumetric Froude number does not appear to be a large factor in Eq. (IV.B-7) since it appears in the square-root form, and the magnitude of the Froude number in the air-water systems was in the order of 100. Therefore, its contribution is of the order of a factor of two added to the expression for C in Eq. (IV.B-8). Since bubbles do not appear to affect the rise of another bubble when the separation distance is more than approximately five diameters, the limiting stability criterion should be encountered when the liquid-slug thickness approaches zero. Thus, the value of C approaches 3.15. The effect of the Froude number on this transition is then small for rather substantial changes in its value.

A further estimate of the variation of the film thickness, h, for the limiting stability criteria is seen for the case in which the thickness is much less than the pipe diameter. From Eqs. (IV.B-7) and (IV.B-14), the film thickness is approximately proportional to the cube of the pipe diameter, inversely proportional to the density ratio, and inversely proportional to the cube of the liquid density.

The question of the effect of viscosity on the analysis initiated from Eq. (IV.B-1) was in part answered by Bankoff,[76] when he expressed the result of equating the rate of viscous work to the rate of dissipation of energy in the wave in the form

$$\exp[-2k^2 t(\mu + \mu')/(\rho + \rho')]. \qquad \text{(IV.B-16)}$$

Reference to Milne-Thomson[75] is indicated for the above expression. The instability criterion then becomes

$$k < [-g(\rho^2 - \rho'^2)/4(\mu + \mu')^2]^{1/3}, \qquad \text{(IV.B-17)}$$

where μ and μ' are the viscosities. At low system pressures, the liquid viscosity would dominate the above expression. The use of Eq. (IV.A-20a) reduces Eq. (IV.B-17) to

$$k < \left[\frac{-g(\rho^2 - \rho'^2)}{4[A + B(\rho + \rho')]^2}\right]^{1/3}. \qquad \text{(IV.B-18)}$$

The effect of viscosity would appear to be reduced at elevated pressures. Single-component fluids will suffer from the functional relationships that connect the various physical properties. Thus, empirical expressions which employ only several of the many possible parameters can describe processes if the functional relationship is made sufficiently complicated. The effects of surface tension and viscosity on the Taylor instability were investigated by Bellman and Pennington,[77] and they concluded that surface tension has a damping effect on the instability but entered only to the one-fourth power in the results. The effect of viscosity was shown to reduce the rate of growth of the amplitude of the disturbance at any particular frequency. Hunt[78] showed that Taylor instability is most affected by viscosity differences in the fluid when the density difference is large. When the ratio of density difference to the sum of the densities is large, the mode of maximum instability resembled the Taylor inviscid solution.[73] For small values of the ratio, the solutions resembled the result of Chandrasekhar[72] for equal kinematic viscosities. In these linearized analyses, the density ratio appears to play a prominent part. Thus, in flow-regime transitions, the density ratio apparently is the proper modeling parameter to initiate an examination of the effect of elevated pressures and temperatures. Of course, other properties must come into the control parameters to provide a precise distinction.

The transition from slug flow to semiannular flow may be described as a form of Kelvin-Helmholtz instability in the liquid bounded above by the base of a vapor bubble and below by the nose of a rising bubble. The flow of liquid may be idealized as flowing from the wall along the upper portion of the liquid and toward the wall in the lower portion. Instability of the liquid portion may result when the outflow of liquid tends to exceed the inflow from above (that is, as the vapor bubbles tend to merge). This could occur as a spike of vapor rising along one side of the channel. If only the effect of surface tension is included, and the interfaces considered nearly parallel, the Kelvin-Helmholz instability is supressed when the velocity difference, expressed by Chandrasekhar,[72] is

$$(U_1 - U_2)^2 < 2\,\frac{\beta + 1}{\beta}\,[(\beta - 1)g\sigma/\rho_1]^{1/2}, \qquad \text{(IV.B-18a)}$$

where U_1 and U_2 are the velocities parallel to the surface. These velocities are not directly known as a function of input flow rates or the superficial velocities. The above expression shows that the velocity difference varies approximately as the square root of the density ratio, and the fourth root of the surface tension. From Eq. (IV.A-13),

$$(U_1 - U_2)^2 < C(\beta + 1)(\rho_1)^{3/2}\left(\frac{\beta - 1}{\beta}\right)^{5/2}, \qquad \text{(IV.B-19)}$$

where C is a combination of the constants. Or, employing the absolute value of the velocity difference, one obtains for an equality

$$\left|U_1 - U_2\right| < C_2(\beta + 1)^{1/2}\,(\rho_1)^{3/4}\left[\frac{\beta - 1}{\beta}\right]^{5/4}, \qquad \text{(IV.B-20)}$$

where for large values of the density ratio, $(\beta + 1)^{1/2}$ may be replaced by $\beta^{1/2}$, and the last factor can be replaced by unity. Griffith[46] suggested that the transition to annular flow from slug flow (more probably, semiannular) varied in the steam-water system in his investigation as approximately the square root of the density ratio for various saturation pressures. The form of the surface-tension relationship for water does not follow precisely the relationship given in Eq. (IV.B-13). However, the above result is only approximate since the interface has some curvature and there is a viscous effect due to the flow near the walls. The velocity of the liquid flowing out of the space between the two vapor interfaces is a function of the height of the liquid space and the relative velocity of the approach of the two vapor spaces.

The instabilities described in the preceding paragraphs do not take into account the interfacial work or any vaporization from the interface. It is also tacitly assumed that disturbances that predominate in the linear analysis would also predominate in the nonlinear formulation. Thus, the results should be taken as a possible guide to the fluid parameters that may govern the transitions in flow regimes.

C. Proposed Similarity Method

The thermodynamic properties of the Freons and water indicate that no single index of two independent properties can be selected to establish a one-to-one correspondence between the fluids. Employing a reduced-pressure or reduced-temperature criterion does not bring the fluids into a single universal relationship. An inner examination of the refrigerants as a group could be made on either of the above parameters, but the inclusion of water as a fluid of interest alters the problem. As an example of the breadth of the problem, Van der Walle and Lamein[79] determined that 15 similarity parameters governed the general flow equations for an axi-symmetric vertical boiler under natural circulation. The problem at hand can be simplified to some extent by considering the conditions surrounding the present range of interest.

In two-phase flow at elevated pressures, the question of what flow regimes exist is to be answered, as well as what the transitions are. Since the problem must be concerned with interfaces and their orientations, the surface tension and viscosity must be considered in addition to the densities of the phases. The liquid dynamic viscosity has been shown as a function of saturation pressure, and it undergoes its greatest decrease near standard atmospheric conditions. Thus, large gradients should not be expected again until the fluid approaches the critical region. The dynamic viscosity of the saturated vapor undergoes a relatively slow increase. For example, there is an approximate 30% increase for water vapor in the pressure range from 200 to 1000 psia, while it is only 11% in the range from 500 to 1000 psia. Thus, for the most part, the viscosity of the saturated vapor is relatively constant. The appearance of the ratio of dynamic viscosities of liquid and vapor in previous studies relative to void-fraction and pressure-drop correlations has found the ratio appearing to some fractional power. As was previously stated in an earlier section, the viscosity ratio ranges from 6 to 2 for water over a pressure range from 400 to 2800 psia. The initiation of entrainment in annular flow as indicated in Section II-B would be affected by the liquid viscosity and the surface tension. Further, if the stability analyses of the preceding section are qualitatively correct, then the orthobaric-density ratio would become a major factor in the flow patterns in the elevated pressure region. Since surface tension may not play the major role in governing the phase distributions, it would be more advantageous to fix the orthobaric-density ratio and examine the ensuing flow patterns. Thus, the test parameters are formulated on the basis of a series of experiments at orthobaric-density ratios that are in accord with existing information concerning water-flow patterns at high pressures. The variables within each set will be the mass flow rate and the thermodynamic quality.

V. EXPERIMENTAL APPARATUS AND OPERATIONAL PROCEDURE

A closed forced-circulation loop was designed and constructed with provision for the inclusion of a three-unit, interchangeable test facility composed of a heated test section, a transition section, and an unheated test section. The loop was designed for operation with trichloromonofluoromethane, Refrigerant-11, as the fluid. Auxiliary systems for the void-fraction determination, the X-ray monitoring of the flow patterns, and the photographic tests were developed. The principal items will be considered individually.

A. The Forced-circulation Loop

The closed forced-circulation loop was constructed of welded stainless-steel components with the exception of several flanged connections, which were included for interchanging various elements of the equipment. A flow diagram of the loop is shown in Fig. V.1.

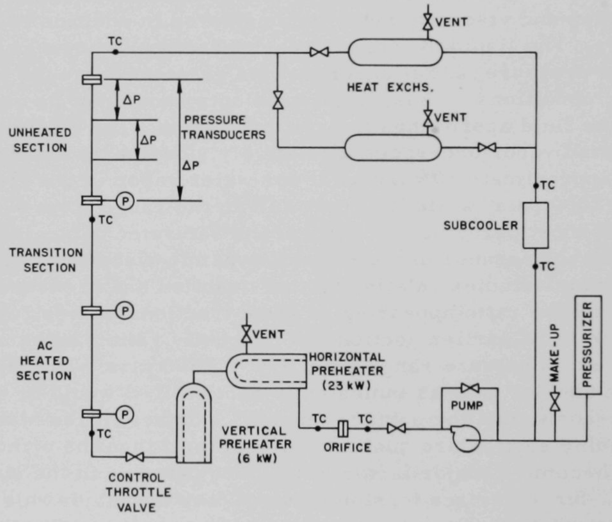

Fig. V.1. Schematic Diagram of Forced-circulation Loop

A Westinghouse, Model 30-A, totally enclosed, centrifugal pump was employed in the loop. It was originally designed for operation with water as a fluid with an inlet pressure of 2000 psi and water temperature of 600°F, and its rated head of 35 psi at 20 gal/min was attainable by water at 600°F. In operation with R-11 as the fluid, the pump delivered a head in excess of 50 psi for the major portion of the test runs.

The flow proceeded from the pump through a 1-in., Schedule-40 line and passed through a three-valve manifold, through a sharp-edged orifice, and into a horizontal preheater. From the horizontal preheater, the flow entered a vertical preheater and then passed through the main throttling valve into the vertical test unit. Flow exited from the test unit into a 2-in., Schedule-40 line, where it could be directed into one or both of the horizontal condensers by control valves in the line. Condensate flowed through a horizontal subcooler and into a downcomer connected to the suction of the pump. A by-pass line was included in the system around the pump. The loop was supported by constant-support hangers located on each condenser at the vertical test unit. The loop was insulated by a combination of 1-in.-thick, molded-magnesite pipe insulation and bats of $1\frac{1}{2}$-in.-thick, spun fiber glass with an aluminum-foil backing.

The horizontal heater was a 6-in. pipe, 5 ft long, containing three Calrod heaters each rated at $7\frac{1}{2}$ kW. Two of the heaters were wired for on-off operation; the third was connected to a variable transformer. The horizontal heater contained a vent line in which a rupture disc assembly with a pressure rating of 1000 psi was inserted. These heaters were only employed in the higher-pressure test series to eliminate excessive subcooling of the fluid.

The vertical preheater consisted of a 3-in. pipe, 2 ft long, containing three Calrod heaters, each rated at 2 kW. Two of the heaters were wired for on-off operation; the third was connected to a variable transformer for fine control of the inlet-fluid temperature.

The two horizontal condensers are identical in design and consisting of four 3/8-in.-diam U-tube units mounted in a 6-in., Schedule-40 pipe. Cooling water was directed into the tubes through a sharp-edged orifice for flow measurement. Control valves were located in the cooling-water line before and after the condenser. Thus, a condenser could be effectively removed from the system by excluding cooling water from it. The control valve at the cooling-water exit permitted operation of the condenser at conditions where pressurization of the cooling water was necessary to suppress boiling in the cooling-water tubes. A vent line from each condenser contained connections for a vacuum line and a rupture disc assembly. Each cooling-water supply line contained a check valve upstream of each unit as a safety precaution against a tube rupture.

A horizontal subcooler was constructed of 6-in., Schedule-40 pipe, 2 ft long, and contained two 3/8-in.-diam U-tubes. The cooling-water system for the subcooler was designed in a similar manner to the cooling-water system for the condensers.

Flow rates in the loop were determined from the pressure-drop measurements obtained from a sharp-edged orifice connected through flange pressure taps to a differential-pressure transducer. Lengthy horizontal lines were run from the orifice location to the transducer to eliminate variable-density effects in pressure-drop measurements. Standard ASME orifice flanges were employed in the system, and three sizes of orifice plates were constructed. The orifice pressure gradient was transmitted by the differential-pressure transducer to a chart recorder, and the output was monitored on a Wheatstone-bridge potentiometer. The orifice flow was calibrated by an in-place, weigh-tank test. Three temperature-compensated, differential-pressure transducers were employed with ranges of 0 to 1 psid, 0 to 2 psid, and 0 to 5 psid. Each transducer was calibrated in a separate known-pressure facility.

The cooling-water flow rate for each unit was determined by employing a standard orifice plate connected across a 60-in. manometer. Each orifice was calibrated by the use of the standard weigh-tank test.

To reduce flow oscillations induced by the pump and preheater system, the major pressure drop in the system was taken across a throttling valve approximately 5 ft from the inlet to the test section. The high pressure developed by the pump was isolated by the throttle valve and provided a means of suppressing boiling in the preheaters located between these two components of the system. The flow rate to the test section was also controlled by the throttle valve. The amount of fluid in the system and the conditions in the condensers set the pressure level in the loop.

The loop had a capacity of slightly less than 5 cu ft, which represented a charge weight of 450 lb of R-11 at room temperature. To operate at the various test conditions, an accumulator system was installed so that the fluid could be charged into, or withdrawn from, the system on the suction side of the pump. The accumulator was of the shell-and-bag type construction with nitrogen as an operating gas for pressurization. A separate tubing network permitted the charging of the accumulator from a tank of R-11. The accumulator could be by-passed and the loop charged directly from the R-11 tank.

A separate installation was employed for distillation of the R-11 before charging the loop. The R-11 took on a yellowish cast when heated without prior distillation. This was due to an inclusion of a foreign substance in the commercial grade of the fluid. Distillation prevented a recurrence of the yellow cast to the fluid and is recommended for experiments in which the common, commercial refrigerants are employed. The source of R-11 for these tests was the E. I. DuPont Company, whose trade name for the refrigerant is Freon-11. Thus, it is more consistent to employ the term F-11 rather than R-11 for the fluid in these tests.

The thermocouple locations are indicated in Fig. V.1. and represent the fluid and cooling-water temperatures. The thermocouples were shielded iron-constantan, 24-gauge units and were calibrated in a hipsometer-type unit. Output from these thermocouple units were connected through a selector switch-box assembly and an ice-bath cold junction to a Wheatstone-bridge potentiometer. The accuracy of the thermocouples was within one degree over the temperature range employed.

Figure V.2 shows the instrumentation equipment and controls in an isolation location from the flow loop, which was shielded from the laboratory area by aluminum sheeting.

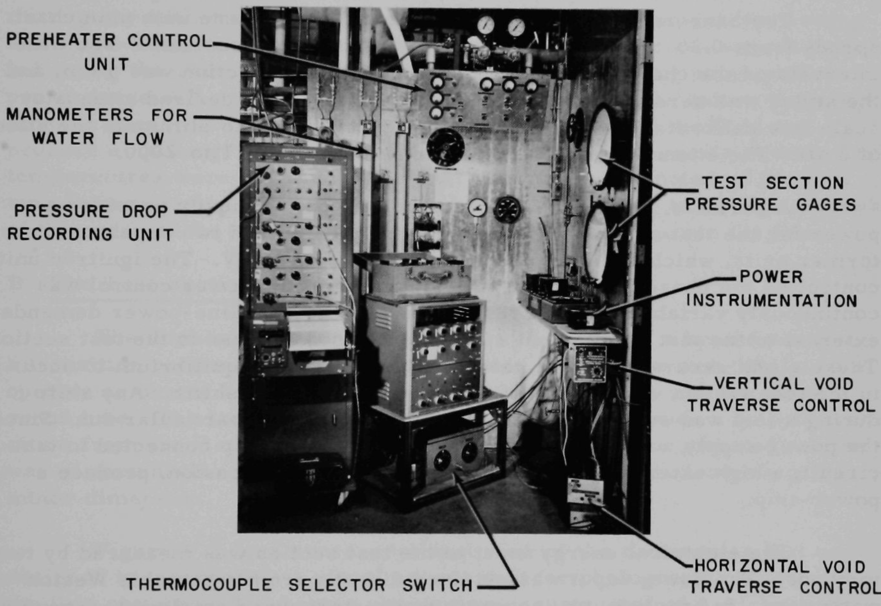

Fig. V.2. Instrumentation and Control Location

The local pressure drops in the vertical test section were obtained from the output of temperature-compensated pressure transducers and recorded on a Sanborn Model 150 recorder. These transducers were of the differential-pressure type and varied in range from ±1 to ±15 psid. The range of the system pressure, flow rate, and distance between the taps determined the transducer unit employed. The transducers were calibrated for a range of output from 0 to 10 mV to cover the full-scale pressure rating of each unit. Each transducer was calibrated by applying a known differential pressure and reading the output of the transducer on a Wheatstone-bridge potentiometer for a fixed excitation voltage.

The Sanborn recorder consisted of a four-channel unit with three stabilized d.c. preamplifiers capable of reproducing the waveform of an input signal from 0 to 10,000 cps with a sensitivity of 0.1 mV per division. The performance data with driver amplifier and recorder indicated a frequency response of 0 to 100 cps, a recording system drift of approximately 0.1 division per hour, and a recording system sensitivity from 0.1 to 0.2 mV per division. A low-level preamplifier with zero suppression was employed periodically to examine the output of the pressure transducer across the flow orifice.

The Sanborn recorder had a horizontal chart plane with nine chart speeds from 0.25 to 100 mm/sec. A stylus marker recorded 1-sec time intervals on the chart. The width of each recording section was 5 cm, and the stylus was zeroed at the center of each strip. The desired attenuator scale was calibrated at intervals during a set of tests to eliminate the effect of drift. The attenuator had 11 selector settings from 1 to 2000.

A portable, Sciaky ignitron-controlled, power supply provided a.c. power for the test section. The power supply contained two separate transformer units, which had an input voltage supply of 440 V. The ignitron units controlled the phase shift in the power cycle, and the power control was continuously variable over the test range. Occasional line-power demands external to the test unit caused a slight drift in the power to the test section. These slight excursions were noted, and the time for equilibrium to occur in the test system was extended to compensate for the shifts. Any shift during a test was sufficient cause for eliminating that particular run. Since the power supply was water-cooled and an interlock trip connected to that circuit, a high external demand for water would, on occasion, produce a power-trip.

The electrical energy input to the test section was measured by two methods. The power input was obtained directly from a portable Weston wattmeter. In practice, two separate wattmeters were employed, depending upon the power level. The power input was also obtained by utilizing an a.c. Weston voltmeter and an a.c. Weston ammeter. These units were typical portable units with 1/4% precision of full scale. These units were calibrated by comparison with units of standard known outputs. The current across the test section was reduced by a step-down transformer so that standard-range instruments could be used.

Three Heise bourdon-tube pressure gauges were incorporated into the loop for the determination of the static pressure at the inlet of the heated section, at the inlet of the unheated section, and in the horizontal preheater. Calibration curves were obtained for these gauges by means of a deadweight test. A maximum deviation of 3/4 psi was noted in the up-and-down calibration tests for these units over the test range of pressures. A comparison of the indicated pressure with the corresponding temperature in the test section, when it was occupied by a saturated vapor, indicated a negligible deviation from the saturation temperature corresponding to the pressure.

Iron-constantan thermocouples were attached to the heated section with glass tape. One thermocouple was approximately 6 in. below the exit from the heated section, and another was approximately 6 in. above the inlet. The output of the couples were connected to Brown Pyr-O-Vane temperature-indicating units with scales from 0 to 600°C. A variable-temperature selection trip was connected to the power-supply interlock, thereby permitting any wall-trip temperature to be selected. In general, the setting was made at approximately 400°C. Normally, a rise in wall temperature, indicating the overheating of the test section, was readily noted, and the power decreased or the flow increased. Operation of the unit at temperatures in excess of 600°F would result in a breakdown of the fluid and produce a "coking" in the heated section if prolonged periods at these high temperatures were sustained. Several instances were noted of the wall temperature rising to a high value and then diminishing to a value somewhat of the order of the setting before a change in the power or in the flow.

B. The Test-section Assembly

The vertical test-section assembly consisted of a heated section, a transition section, and an unheated section. Two units were designed to operate as heated sections: one, a rectangular section, and the other, a round tube. The transition section was designed to provide a smooth transition from the circular to the rectangular conduit. The unheated section was of rectangular cross section, with pressure-tap locations along the minor dimension.

Figure V.3 is a cross-sectional view of the rectangular test unit designed to incorporate a visual access port for photographic studies of the flow patterns. The heater element was constructed of A-nickel with outside dimensions of 1.250 by 0.625 in. and a wall thickness of 0.125 in. This element was electrically insulated from the containment shell by Durabla insulation strips. Thermocouples were inserted through the Durabla into the area at the outer surface of the heater element and electrically insulated from the heater by thin sheets of mica. The pressure jacket and cover plates were machined from Type 304 stainless steel. The total length of the unit after assembly, was $44\frac{1}{2}$ in. The visual access windows were 35 in. long and were located on the minor dimension of the heater element. Single sections of optical glass were employed with nominal dimensions of $1\frac{1}{4}$ by 3/4 in. by 36 in. long. The pressure-jacket assembly is shown in Fig. V.4.

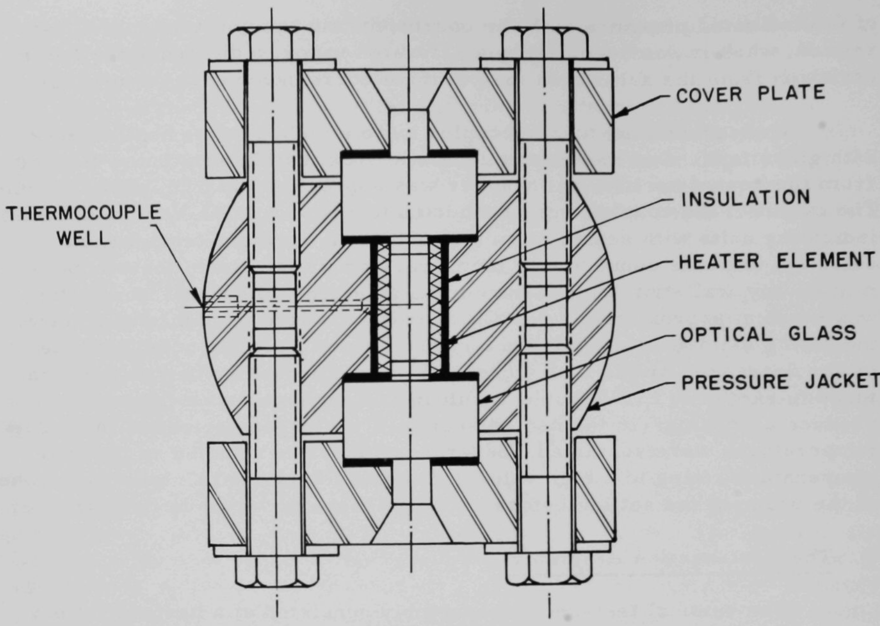

Fig. V.3. Cross Section of Visual Test Section

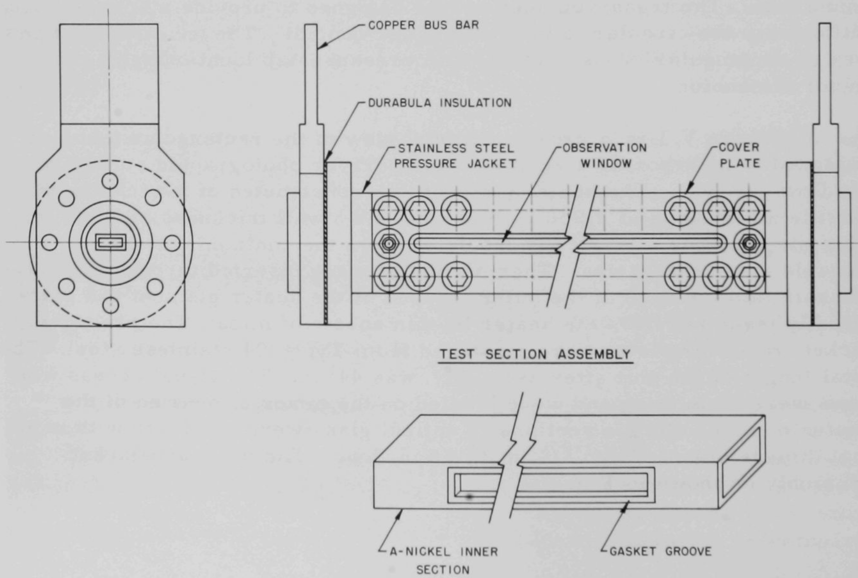

Fig. V.4. Pressure Jacket and Inner-section Assembly

Several problems were encountered in providing a leak-free assembly of the rectangular heating unit. The assembly of the components of this unit required that a single copper bus bar be soldered to the A-nickel element; then this unit was inserted into the pressure jacket in which the thermocouples and Durabla insulation had been placed on one side. The Durabla insulation for the other portions were then inserted, and the unit clamped at the bus bar end. Heater strips were then placed in the inner section, and dry ice was applied to the outer jacket. The purpose of this procedure was to provide the maximum expansion possible in the inner element. The final, terminal copper bus bar was then attached to the assembly. Slight cracks developed initially in the nickel element, which produced substantial leakage under pressure. This problem was somewhat masked by the failure of several glass sections during assembly and testing. In addition, the glass sections required extensive assembly trials, since many failures resulted from improper loading procedures. Appendix D contains the loading procedure developed by trial and error for the assembly of long, glass units. Continued modifications of the nickel rectangular section were required. A narrow groove was machined around the periphery of the nickel section to provide a better sealing surface for the gasket between the glass and the metal section. Since sealing the rectangular section presented a lengthy delay in the tests, a Type 304 stainless-steel tube of the same length as the rectangular section was assembled with copper bus-bar attachments and included in the loop. The electrically heated tube had a heated length of $34\frac{1}{2}$ in. and an ID of $1\frac{1}{8}$ in. The use of this unit reduced the upper limit on the qualities obtainable without undergoing a burn-out.

The transition-section assembly, shown in Fig. V.5 consisted of a rectangular insert with a circular-to-rectangular transition cone, and a 2-in., Schedule-40, stainless-steel pipe, which added rigidity to the system and provided a standard flange connection to facilitate interchangeability of components. The rectangular transition piece was drawn from Type 304 stainless-steel tubing with a resultant internal section 1.050 by 0.380 in., with a tolerance of ±0.005 in. and an overall tolerance of ±0.003 in. The wall was 1/16 in. thick, and the total length was 36 in. The insert was

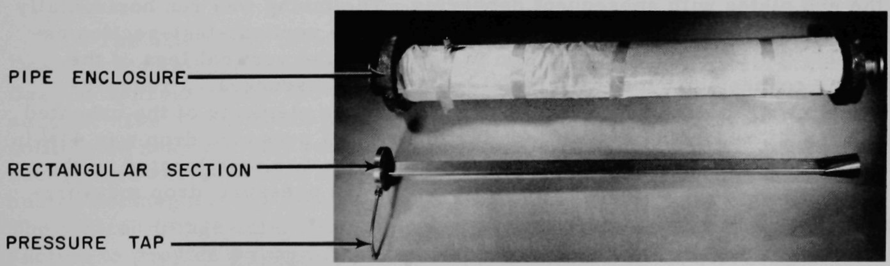

Fig. V.5. Transition-section Components

welded into an end piece, and a pressure-tap hole was drilled and deburred. The pressure-tap fitting was 1/8-in. tubing, welded into a countersunk hole. A thermocouple fitting was welded to the wall of the pipe, and a shielded thermocouple was inserted so that it butted against the insert. The location was approximately 4 in. from the exit.

Figure V.6 is an assembled view of the rectangular, unheated, test section. The rectangular-flow channel was formed of the same material as the transition piece, and identical tolerances were maintained. The overall length of the section was $45\frac{3}{8}$ in. after Heliarc welding of the end plates. Backup plates added rigidity to the unit and were insulated from the inner section by Durabla gaskets. Between the cover plates, metal spacers constrained the section in the minor dimension. The void traverses were made at locations between these spacers. Several spacers were removed at the location of the fluoroscope centerline to provide an uninterrupted path for the X-ray beam. A slot was milled in the two cover plates to provide an access port for void traverses normal to the major dimension.

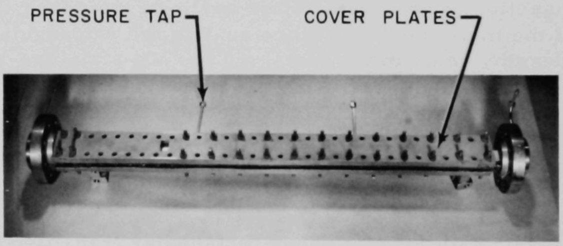

Fig V.6. Unheated, Rectangular, Test-section Assembly

Local pressure-drop measurements were made in the unheated section. The four pressure-tap holes were constructed by welding 1/8-in. tubing into countersunk holes, which were drilled through the section and the end plates with subsequent deburring. The tubing was run horizontally to the exterior of the enclosure surrounding the vertical-test-section assembly to eliminate any variation in density in the vertical legs of the tubing connected to the differential-pressure transducers. Pressure-gradient measurements were made across three elements of the unheated section. The length between taps for the overall pressure drop was $44\frac{29}{32}$ in. The intermediate length was $14\frac{15}{16}$ in. between the two taps located on the unheated section; the length was $14\frac{27}{32}$ in. for the pressure-drop measurement at the exit end of the unheated section.

The rectangular sections were aligned by inserting a rectangular block with a connecting rod into the space between the sections, and by tightening the flange bolts. The spacing block was then removed from the units. Durabla gaskets were employed between all flanges and formed an effective seal after the system had been heated. Movement between the sections was greatly inhibited. This became apparent when attempts to disassemble the sections were made. Thermal insulation of the sections was effected by layers of spun fiber-glass insulation. The outer wrapping was covered with bonded aluminum foil to reduce the radiation loss.

C. The Fluoroscope Monitoring System

Flow patterns in high-pressure systems were observed by Johanns[80] through the combination in a fluoroscopic system of an X-ray tube, collimator, image-intensifier tube, and a television monitoring network. The investigation by Johanns into the feasibility of employing standard X-ray equipment for the delineation of flow patterns encompassed an examination of the absorption characteristics of various containment materials which could be utilized with high-pressure water systems. The use of single photographic plates with X-ray sources is commonplace in many industrial fields and has been employed in two-phase flow investigations, as for example in the work of Bennett, et al.[27] However, the primary question of whether sufficient detail could be obtained from a continuous observation of moving-flow configurations was in doubt. The principal problem was whether sufficient high-energy photons from the X-ray source could penetrate the conduit walls and still be of low enough energy to meet the absorption requirement in the fluid.

The examination of the absorption characteristics of X-ray photons of various energy levels in water, steel, titanium, and aluminum by Johanns provided the information required for the use of a similar installation in this investigation. Both titanium and aluminum are better conduit materials than steel for the X-ray system. However, the problem of the strength of the materials under high pressures mitigated a compromise in the high-pressure water studies. Such a problem is reduced in severity for systems incorporating the common refrigerants as a working fluid. Thin-wall stainless steel was sufficient for the present study.

The schematic layout of the fluoroscope system is shown in Fig. V.7. Due to the shielding requirements, the X-ray and fluoroscope location was fixed at approximately 150 equivalent diameters from the exit of the heated section. The X-ray beam was collimated at the X-ray source and was also collimated near the test section by movable lead panels, which reduced the background radiation to a safe level. The X-ray beam traversed the unheated rectangular test section in a path normal to the minor dimension. The vidicon image-intensifier unit was adjusted at a distance from the test section to provide a magnification of approximately four to one when the image was transmitted through the television camera unit to the monitor screen. The lead shielding employed as a collimator also prevented any

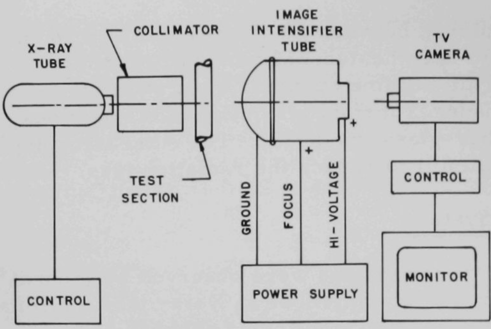

Fig. V.7. Schematic Diagram of Fluoroscope System

high-intensity sources from becoming incident upon the fluoroscope screen. High contrast in the intensities incident upon the unit would either "burn" the fluoroscope screen or, in the minimum, prevent a sharp contrast in the image desired. An optical mirror arrangement incorporated into the fluoroscope unit permitted the observation of the fluoroscope-screen output. The image viewed at this position was not magnified to any degree and presented a sharper picture of the flow pattern. As a safety precaution, the mirror arrangement was not continuously employed.

The operating conditions for the X-ray unit were determined by balancing the level of sharpness obtained by increasing the current level at fixed voltage with the increase of image persistence at increasing current levels. The operating conditions for the television viewing for the present investigation were a voltage of 120 kV and a current of approximately 3 mA. At high fluid flow rates, the image would tend to persist for higher currents. Therefore, the precise setting of the unit was dependent upon the flow conditions.

As with most visual observations, the viewer develops a discriminating eye, which tends to render the observations subjective rather than objective. This is unfortunately true of both single photographs and motion pictures. Thus, the description of an event can at most be consistent with another event, only if the observer asserts the same criteria for the designation of similarity. To remove some element of observer prejudice, the randomized block type of factorial test program is ideally the best form of test selection. The major problem of the time required for the present system to reach equilibrium was a counterbalancing factor in deciding the form of the actual test program. To provide operating experience in the observing of flow patterns, the system was maintained in natural circulation, and the developing flow patterns were observed. A significant aid in the initial observations of plug flow was obtained by observing the void traverse chart recorder at fixed position some distance below the X-ray equipment. The rapid response of the chart pen to both bubbles and vapor slugs yielded an indication that the pattern was nearing the monitor field. The interfaces were in sharp outline with the liquid appearing as the darker element. The churn patterns were quite clear in the alternating downflow of the liquid. In annular flow with large-amplitude waves, the walls of the section appeared to oscillate, since the liquid film was the darker element. The obvious uncertainty of whether a liquid bridge or a liquid annulus passed could not be rectified from the television monitor alone. The simultaneous recording of the local pressure drop and its corresponding oscillations was a secondary method of rectifying the uncertainty, although a band of flow conditions could be ascribed to one flow regime or another. The use of the high-speed, color motion pictures added another dimension to the determination of the flow patterns.

The determination of what is seen in the television monitor becomes less distinct as the liquid and vapor velocities are increased. The perception of high-velocity droplets in an annular core would appear at best as streaks for high concentrations. As the system saturation pressure is raised, the difference in vapor and liquid velocities decreases and the perception improves for a given quality and flow rate. However, as the densities become more nearly of the same magnitude, the difficulty again arises in distinguishing between the phases. The range of usefulness of the fluoroscope system is thus confined to moderate velocities for high-pressure systems when direct viewing is employed. It is possible, however, to record the program on video tape for repeated viewing, which should provide a better background for judgment. The photographs taken by Johanns were not of sufficient quality to employ as single frame reproductions. Therefore, this study did not attempt to produce any of these films.

D. Photographic Equipment and Techniques

The use of still photographs and high-speed motion pictures to record the various flow regimes in two-phase flow has been prompted in part by the variance in visual interpretations of flow patterns. Unfortunately, even high-speed motion pictures have not clearly dissipated the personal interpretation of the events recorded in the film. One difficulty has been the inability of an observer to interpret an oddly-shaped region as being either liquid or vapor. With the advent of higher-speed, color film, the delineation of bubbles and droplets in two-phase flow has been greatly improved. A two-color lighting system was described by Cooper, Hewitt, and Pinchin.[81] A single-color light source (say blue) is directed from above the plane of vision at a narrow angle to the normal, and a second light source (say red) is directed from below in a symmetrical position. With the lighting arranged in the above manner, a vapor bubble will be seen as possessing a blue upper surface and a red lower surface. A liquid droplet, on the other hand, will have a red upper surface and a blue lower surface. The arrangement shown in Fig. V.8 was employed in the present photographic study in which a Fastex camera with framing speeds up to 8000 frames per second was utilized. The camera was tilted at a slight downward angle.

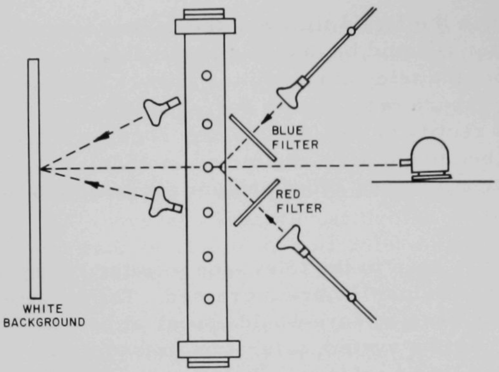

Fig. V.8. Schematic Diagram of High-speed, Color, Motion-picture Arrangement

The Fastex camera was equipped with a Wollensak 2-in., 50-mm lens with a 1/2-in. extension tube. The camera lens was located approximately 1 ft from the outer edge of the glass section. The illumination was obtained by arranging four 300-W photographic lamps as shown in Fig. V.8. The film employed in the tests was Eastman Kodak ERB color film.

Lighting arrangements are normally set by the particular phenomenon to be studied. For example, an annular liquid film on the wall and liquid droplets in the core would require a lighting arrangement similar to the one described above when large-amplitude waves may be present on the liquid surface. For the above lighting sequence, the high-amplitude waves would have a red surface, whereas low-amplitude waves would lose the predominant red color and appear as dark lines in the liquid surface. Since the liquid film and the wave move at rather low speeds, the subsequent camera speed need not be very fast. The liquid droplets in the core may have velocities in the order of 100 ft/sec and require very high camera speeds to slow down the action.

The effects of various types of lighting arrangements and the results obtained from these methods should be mentioned. The two general methods for illumination are incident and transmitted light. Incident light is transmitted in the same general direction as the point of viewing. The back reflectance is the source for photographic viewing, although the majority of the light is transmitted through the test section. This method is somewhat insensitive to the many high lights and configurations when a narrow angle of incidence is involved. With obliquely-lit surfaces, such as described above, the sharp outline of waveforms such as appear in annular flow are given large degrees of contrast.

Transmitted light produces refraction effects and thus allows a survey of small refraction effects. Bubbles appear in profile and are more sharply defined. Three types of transmitted light are employed:
1) collimated or focused systems, 2) diffuse systems, and 3) dark-ground systems.

The first system is employed to examine dimensionally-small effects. The light must travel through the liquid in the rear of the test section before passing out of the section, and thus variations in intensity are sometimes incorrectly interpreted. The use of a mirror or prism can reduce the observer error.

The second system avoids the variation of intensity as described above but also reduces the amount of information that is conveyed. The third system depends on reflection and refraction at interfaces that yield sharp contrasts, but the evaluation of the results is again in doubt.

In the present system, a light background was used to raise the general intensity during the high-speed, motion-picture study. The general effect was the transmission of a background through the liquid. During the presence of bubbles, there was very little transmission of background light.

E. Void Distribution by Gamma-ray Attenuation Method

The volumetric vapor void fraction is determined through a technique described by Hooker and Popper.[82] Its principle is based on the absorption of photons as gamma rays pass through the material, with the intensity decreasing exponentially with the distance traversed. The amount of absorption is proportional to the intensity of the radiation and to the thickness of the material at a given point. Thus,

$$dI = -u_a I\, ds, \tag{V.E-1}$$

where

I = intensity of radiation (R/hr),

u_a = linear absorption coefficient of the material traversed (cm^{-1}),

and

ds = thickness of the material traversed (cm).

For a collimated beam of monoenergetic gamma rays of initial intensity I_0, integration of the above equation yields

$$I = I_0 \exp(-u_a s), \tag{V.E-2}$$

when s is the material thickness.

Three assumptions are inherent in this method: 1) the gamma radiation is monoenergetic, 2) the vapor mixture can be represented by layers of vapor and liquid perpendicular to the incident radiation, and 3) the radiation received by the scintillation crystal passes only through the vapor-liquid mixture.

Deviations from the second assumption were considered by Hooker and Popper.[82]

The physical arrangement of the gamma-ray unit is shown in Fig. V.9. A thulium-170 source, which decays to ytterbium-170 by beta emission, is contained in a lead shield, and the emission beam is directed through the test section onto a scintillation crystal mounted on the face of a photomultiplier tube. This assembly is shielded from extraneous light and is cooled by a water jacket to maintain the unit at constant temperature. The light output of the fluorescent crystal is proportional to the incident radiation. Thus, the current output of the photomultiplier reflects the amount of absorption of photons. The current output of the photomultiplier is amplified and recorded by an inking pen on a continuous recorder. The system is calibrated by taking readings for the test section filled with liquid and then with vapor at the same test pressure. This form of calibration is not always readily obtainable, and a correction chart may be obtained for correction factors obtained at normal pressures and temperatures. (See Appendix B for correction factors.)

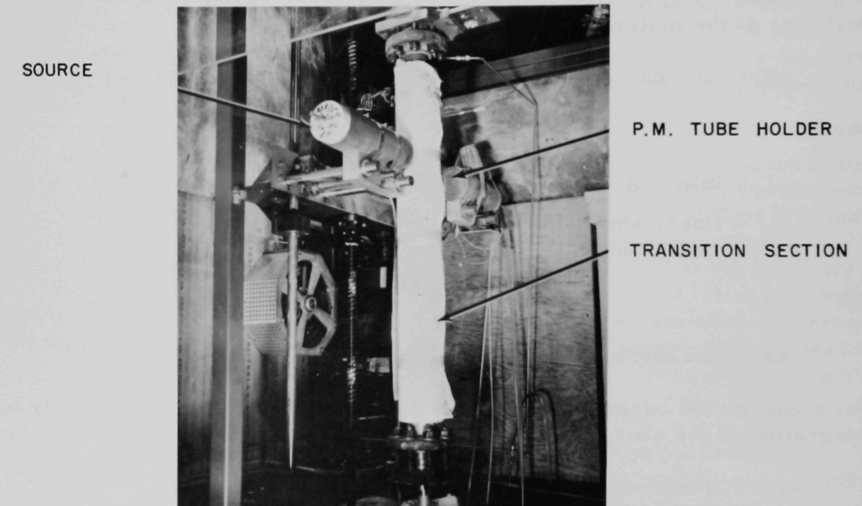

Fig. V.9. Void-traverse Equipment

The source employed in these tests was a 23-R unit at 2 in. The vertical slit at the photomultiplier-tube receptacle was 1/32 in. wide. The horizontal traversing length was set at approximately 1/2 in. so that the test-section wall would also be traversed. The output from the photomultiplier-tube unit was recorded on a 0-10-mV strip recorder with a chart speed of 3 in./min . The traversing speed was set so that a complete traverse of the section across the narrow dimension required 4 to 5 min, which corresponded to a trace of approximately 13 in.

The void-traversing unit is shown in Fig. V.9 in a position along the transition section. The vertical-traversing system was designed for variable speed so that a camera could be mounted on the assembly and photographs taken along the vertical direction. In the void-traverse application, a rapid vertical movement was not required. The horizontal-traverse mechanism was designed to incorporate a constant-speed motor drive with an interchangeable worm-gear drive for maintaining low translational speeds. To maintain alignment, both the source and photomultiplier assemblies were driven from the same shaft. The location of the wall on the void trace was easily obtained since the passage of the traverse across the wall produced a minimum in the void trace as the traverse passed out across the Durabla gasket between the rectangular test section and the cover plates.

The constancy of the traversing speed was examined by measuring the distance along the void trace at a given level near the point of entry into the wall. As the void profile passed into the wall, a straight line could be passed through the trace on both sides of the profile, which permitted a check on the repeatability of the spacing. The major error involved in these void measurements occurred at the location near the wall where a large gradient existed in the trace. The areas involved represented one-sixth of the total area.

The local void fraction can be obtained from the output signal of the photomultiplier tube, which is recorded on the strip recorder when the output signals for the full (liquid) and empty (vapor) conditions in the channel are known, since the relationship for local void fraction[82] is given by

$$\alpha_i = \frac{\ln (v_i/v_F)}{\ln (v_E/v_F)}, \qquad \text{(V.E-3)}$$

where v is the output signal, and the subscripts E and F represent the empty and full signals, respectively. The cross section was subdivided into 12 segments and the mean value recorded for each segment. Empty and full readings at the same locations were also recorded several times during each test period. These values were then reduced to local void fractions by a digital-computer program. The average of these local void fractions yielded the mean value of void fraction for the test section.

The vertical placement of the void traverse was readily controlled through the instrumentation. All void measurements were taken at a level slightly above the lower pressure tap for the intermediate pressure drop. Several runs were made at various positions along the unheated section, but the results showed no significant variance. Thus the tests were conducted at a position approximately 120 equivalent diameters from the exit of the heated section.

The basic assumption made in these results is that the time of traverse was long enough, and the local cross section small enough, that the time average and the space average were identical. The sensitivity of the unit was sufficient to respond to a vapor plug, at no liquid flow, with rapid sweep from full to empty when the traverse was stationed at some channel position.

From the results of previous test programs, it was estimated that a maximum error of 10% in void determinations is to be expected. Very little drift was noted in the empty-full readings taken over a 4-hr period.

F. Test Procedure and Data Analysis

The procedures for charging, operating, and cleaning the loop are included here. The physical burn-out of several preheater elements and test sections occurred during the testing period. The possible causes and techniques for prevention of recurrences of these failures are described.

In operation, the loop was stable for the most part. However, several instances of flow instabilities within the loop were observed in which flow fluctuations were so large and expanding in amplitude that the power supply and pump were dropped from service. These high instabilities resulted when a rapid, large change in either flow or power was attempted. The operational procedure was modified to prevent recurrences of these excursions.

The destruction of several preheaters was due to a combination of factors. In the initial design of the horizontal preheater, a baffle ring was placed over the heaters where the fluid entered the heater. This baffle prevented fluid circulation near the point at which the heater elements entered the horizontal section. This situation resulted in a failure of a heater during the initial shakedown of the loop. During the initial operation of the loop, a vertical heater was also destroyed due to a faulty heater element. Destruction of the heaters produced deposits in the system, which were removed by filling the loop with alcohol, heating, pressuring with nitrogen, and then circulating. The system was then flushed with R-11 and drained.

Two test sections were destroyed during the test program. The first burn-out occurred when the air-supply pressure to the remote-control valve in the exit line from the test section was reduced through a supply-line failure and the valve closed during the operation at a high heat flux. The burn-out detector, which at the time consisted of a thermocouple attached near the exit of the heated section, failed to operate. Upon removal of the insulation, the tube was observed to have failed at the inlet end of the test section. A substantial amount of "coking" had occurred in the region of the failure. The deposit of the substance, which was due to the breakdown of the R-11, appeared as rings inside the test section. Exposure to the atmosphere had produced subsequent flaking of the test section even though the section was cleaned with a wire brush. This flaking tendency was also noted in a separate facility employing Freon-114 as a test fluid after a burn-out had occurred. In both instances, the test sections were of the same stainless-steel composition.

In the second burn-out of a heated section, the failure occurred after the system had been rapidly depressurized due to a gasket failure. A pinhole opening developed in the section upon repressurizing the system. The area of this failure was bulged out from the section, and its location was intermediate between the copper bus bars. Subsequent examination of the damaged section over a period of time revealed continual scale formation. This scale was not soluble in R-11 or in the alcohol. Spectrochemical analysis of the residue indicated the presence of iron and nickel as the major constituents. However, the particular compounds that may have formed were not ascertained.

The final burn-out in the system occurred when two preheaters failed nearly simultaneously during the warm-up of the loop for some of the photographic work. This failure was believed to be due to a flow stoppage, but the actual cause was not determined.

The loop was initially pressurized with nitrogen and a slight amount of refrigerant to facilitate a leak test utilizing a standard halogen leak-detector unit. Other than minor leaks in the valve packings, the system was secure from leakage through any of the elements through pressures to 1000 psia.

The system was purged with nitrogen, and the Heise pressure gauges and differential pressure transducers were isolated from the system. A vacuum pump with a knock-out trap using acetone and dry ice was employed to draw down the system. The vacuum was maintained overnight and the loop checked for leakage. The refrigerant, which had been previously distilled in a separate system, was vented into the evacuated loop. The condenser and the subcooler water were used to maintain a low pressure in the system. To complete the charging of the system, an auxiliary refrigerant-holding tank was pressurized with nitrogen and the charging completed.

The accumulator for pressurizing the loop was charged with refrigerant to approximately one-half its capacity. To attain the proper operating pressure, the loop was slowly heated and fluid either added or removed to reach the test condition. The system was vented under pressure to remove any noncondensibles that may have been in the charging fluid. All of the pressure-tap lines were vented to the atmosphere. The venting procedure was employed at intervals throughout the testing period. Since the possibility of a breakdown of the fluid was evident for the high-temperature operations, the loop was recharged at intervals during the series of tests.

Operating procedures varied in accordance with the pressure level of the test series. For the low-level pressure tests, the system could be brought up to a stable operating condition within 3 or 4 hr from a start-up at room temperature. Thus, a normal start-up and shut-down could be attained on a day-to-day arrangement. This method could not be employed effectively at the elevated pressures because of the prolonged warm-up period. Therefore, the loop was operated continuously for periods of 5 or 6 days.

The operation of the loop with the glass test-section unit installed was made continuous since the failure of the glass during a cool-down would have resulted in considerable downtime for replacement. Only one failure of a glass section occurred during operation, and this was attributed to a faulty glass section.

The instrumentation units were calibrated periodically throughout the testing sequences. In particular, the Sanborn recorder for the differential pressures was recalibrated after each run in order to minimize drift. The circuitry for the differential-flow pressure drop was checked for drift during the operating sequence, and periodic comparisons with a portable potentiometer reading were made.

The time required to reach equilibrium was minimized when the flow rate was changed while a constant heat flux was maintained, as opposed to a change in heat flux at constant flow rate. Basic test sequences were set as constant heat flux-variable flow rate sets.

The information obtained for each set of the daily tests was refined to yield the mass flow rate, the qualities, and the superficial velocities based upon inlet conditions to the unheated section. The data were subsequently recorded on punch cards for further computer calculations. Appendix C contains a summary of the flow data and the void-fraction determinations.

An energy balance for the loop components was obtained by circulating pressurized, preheated liquid through the loop at several temperature levels.

From these tests, the heat loss from the system was made a linear function of the saturation temperature of the fluid over the test range of temperatures. The energy losses on the suction side of the pump were not minimized since the pump operation was most stable when the fluid was subcooled. The preheaters were of sufficient size to bring the fluid to the desired inlet test condition. Some uncertainty entered into the condenser heat balance during some operational conditions when the auxiliary condenser was employed as a surge tank to dampen any system oscillations. It thereby produced some unaccountable loss in the balance. Primarily, the energy balance for the three-unit test section was more critical for R-11 determinations than it would have been for water, since there is an order-of-magnitude difference in the latent heat of vaporization. The temperature level of the system was relatively low, and the maximum fluid-saturation temperature for the test series was 325°F. The heat loss for the test-section assembly was approximately 0.2 Btu/sec at 180°F, and it was considered constant at a particular saturation pressure, although the heater-wall temperature rose as a function of the increase in power level.

VI. EXPERIMENTAL RESULTS

This section examines the results of the test program for the effects of the orthobaric-density ratio and mass flow rate on the flow patterns produced by a constant heat-flux addition in the upward, vertical flow of F-11. The X-ray monitor observations of the flow patterns in an unheated, rectangular channel located above the electrically-heated test section are compared with the color motion pictures taken with a Fastex camera. The local void fractions and the average void fractions obtained during the series of tests are presented, and these results are compared with water data at identical orthobaric-density ratios.

Six sets of tests were made at constant orthobaric-density ratios, which varied from 7 to 60. This density-ratio range spans an equivalent water-saturation-pressure range from approximately 400 to 2000 psia. The mass flow rate based upon the cross-sectional area of the unheated rectangular test section ranged from 0.2×10^6 to 2.0×10^6 lb/hr-sq ft. The mass qualities based upon thermodynamic equilibrium ranged to 90%; however, the majority of the data encompassed the range from saturation to 50%. The subcooled boiling region was not included in the study. In general, the test conditions were limited by the departure of the wall temperature to values above 600°F where continued operation would have resulted in a breakdown of the fluid with resultant deposits in the system.

The local pressure gradient in the unheated section and its characteristic oscillations were obtained. The form of the oscillations is somewhat indicative of the various flow regimes encountered in this study.

The flow regimes observed at small values of the orthobaric-density ratio are described, and the approximate regions of occurrence are presented graphically.

A. Description of Flow Patterns

The X-ray generator and fluoroscope monitor were arranged to yield a magnification of approximately four to one on the television screen. The mirror-optical system produced a nearly one-to-one image, which yielded sharper details than the magnified image. Flow patterns observed in the unheated test section normal to the smaller dimension were recorded along with the associated local pressure gradients and local void fractions. After the test series employing the X-ray unit, the rectangular test section unit was replaced by the test section containing the optical glass windows that were normal to the smaller channel dimension. Inlet-fluid conditions were fixed in an approximation of previous test conditions, and a series of high-speed, color motion pictures was obtained. The flow patterns observed by the two methods were compared.

Ideally, if a mass flow rate were to be fixed, the expected flow patterns would proceed with increasing mass quality through all-liquid, bubble, plug, semiannular, and annular, to dispersed flow. The actual flow patterns encountered are dependent upon the magnitude of the mass flow rate and the initial fluid conditions for a fixed geometry. Since this study did not include the subcooled boiling region, the initiation of bubble flow was not observed.

The flow patterns observed with the fluoroscope monitoring system and the high-speed, color motion pictures were compared. The results are described in the following paragraphs.

1. Bubble Flow

Only a few isolated tests indicated bubble flow in the net quality region at very low qualities and high flow rates. Bubble flow was not observed in these tests for superficial liquid velocities below approximately 3 ft/sec. The quality range over which bubble flow may exist at small orthobaric-density ratios would appear to be very narrow for refrigerants that possess small latent heats of vaporization.

2. Plug Flow

Plug flow with the characteristic bullet-shaped vapor heads that maintain their identity as they move up the channel did not appear in the forced-flow system at elevated pressures. This type of flow could only be generated at the lower pressures in nonforced circulation flow. For forced-convection, saturated flow, the churn-type flow pattern was developed for the lowest flow rates and qualities. It is to be concluded that the plug-flow regime is not attained in a boiling system at net qualities at elevated pressures.

3. Slug Flow

Slug flow, in which vapor slugs nearly filling the channel are interspersed with smaller vapor bubbles, occurred but had a tendency to collapse or agglomerate into a churning flow. This churn-slug type of flow has been included into a single regime along with what some investigators call the churn-annular regime, since a sharp distinction could not be made between the two flows.

4. Semiannular or Churn Flow

In the terminology employed in the fluoroscope study, the term "churn" denoted the regime at low liquid and vapor superficial velocities where the downflow of liquid was evident for collapsing liquid bridges. At higher flow rates, the "churning" motion was not as evident on the television monitor and the flow had an appearance of alternating liquid and vapor slugs. The high-speed motion pictures revealed a retardation of the upward flow of bubbles near the walls due to a downflow of liquid. The liquid slugs were transporting bubbles. Bubbles near the walls would hesitate and then elongate as they accelerated upward. Patches, which suggested an attempt to form an annular liquid film, appeared with cross-sectioned patterns upon the passage of the agglomerated slug. At low flow rates, this regime had a transition into the annular regime. At the higher flow rates, the transition was to the wispy-annular regime. This regime was characterized by high local-pressure-drop oscillation, which possessed a form somewhat different from the bounding regimes at higher qualities.

A distinction in regime definition is now made in which the region formerly identified as semiannular is separated into the churn flow (alternately called semiannular henceforth) and the separate regime, which is termed wispy-annular flow.

5. Annular Flow

The usual connotation for annular flow is employed in these results wherein the walls of the conduit are covered by a film of liquid while the central core contains vapor and possibly some entrained liquid drops. The character of the liquid film may vary from a slow-moving tranquil liquid, with small-disturbance waves on the interface, to a highly disturbed surface on which both small-disturbance waves and faster-moving, high-amplitude, roll waves exist simultaneously. Liquid droplets are entrained in the vapor core from the high-amplitude waves. These droplets may return to the liquid film at various downstream points. The annular region may be characterized as quiet-annular or unsteady-annular, depending upon the magnitude of the local pressure-drop oscillations. The region with the high-amplitude roll waves has the greater amplitude in pressure-drop oscillations.

The high-speed, color motion pictures revealed the high-amplitude roll waves as bright red bands moving upward in the direction of flow, while the low-amplitude disturbance waves appeared as dark narrow lines. The liquid film had a neutral, or gray, appearance in the undisturbed regions of the interface. Before the abrupt rise in heater-wall temperature, the liquid film had only small-disturbance waves on the interface and substantial droplet entrainment in the core for low total mass flow rates. The appearance of this "normal" annular flow occurred only at low liquid superficial velocities of the order of 2 ft/sec. Since the photographs were taken in the unheated section, a liquid film would persist, so that an annular-spray regime would be found at the limit of this region of flow.

No bubbles were seen in the liquid film in any of the motion pictures of the annular-flow tests that provided a distinction from the bounding semiannular flow regime.

A comparison of the fluoroscope observations with the motion-picture results indicated that the limit of the television-monitor delineations was in the region of the high-amplitude roll-wave region of the annular flow, since the region near the wall gave the impression of an expansion and contraction during this type of flow, whereas the very thin liquid film associated with the low-amplitude disturbance waves was not discernible. Due to the high velocities and small droplet sizes, it was not possible to distinguish liquid droplets in the vapor core by the fluoroscope method.

6. Wispy-Annular or Ligament Flow

A separate classification of one type of annular flow, which is distinct from the usual connotation, was made by Bennett et al[27] in which the term "wispy-annular" was coined. The appearance of the usual liquid film on the walls of the conduit is supplemented by a different form of flow in the core. The vapor in the core appeared to transport agglomerates of liquid, which take on the appearance of billowy clouds of liquid rising in a similar manner to a wispy, turbulent stream of cigarette smoke. The inner flow is not continuous and is probably due to sheets or ligaments of liquid being torn from the highly-disturbed liquid film. A major problem in viewing this inner core is the difficulty imposed by the liquid film on the surface of the section. In the fluoroscopic observations, the flow was described as streaming with intermittent segments of vapor slugs. The fluoroscope method was not encumbered by the wall liquid film but did suffer from the fact that the flow in the core was very rapid. The color motion pictures had the lighting arranged so that the color-pattern arrangement was abruptly disturbed when the wispy core was present. From the disarrayed nature of the inner flow pattern, it seemed likely that vapor bubbles were entrained in the agglomerate. The distinguishing feature of this flow regime is that the agglomerate appeared to flow upward through the core while there was a liquid film on the wall, whereas in semiannular flow the liquid film would alternately form and disappear as a mixture of liquid and vapor passed the observer.

This flow regime was characterized by high pressure-drop oscillations. The nature of these oscillations appeared to be different from the form developed in the semiannular, or churn, regime.

The streaming nature of this flow would appear to give rise to the shearing of ligaments of liquid, which would subsequently break up into liquid droplets as the mass flow rate is increased. Since the liquid ligaments are in contact with the liquid film on the wall during some portion of their existence, an electrical-resistance probe would probably indicate a bridging of the conduit and thus lead to an erroneous conclusion as to the condition of the flow regime. The results of Suo et al.[32] for water at 1000 psia revealed that the transition to annular, or dispersed, flow occurred at a substantially lower quality than predicted by the proposed correlation of Haberstroh and Griffith.[18] These differences are large enough to question the quantitative results of the electrical-resistance-probe method.

A film containing brief segments from some of the high-speed, color motion pictures obtained during the test series has been compiled. The churn, annular, and wispy-annular regimes are included. The film segments were taken at either 3000 or 6000 frames per second. Since the period of each section is approximately one minute, the film does not represent the entire range of configurations that occur but rather represents some of the more pertinent features. The film is available and may be borrowed from the Argonne National Laboratory. The original films and data of the tests are on file at the Argonne National Laboratory.

B. Flow-regime Transitions

The flow regimes that are most prominent in the net quality, forced-circulation flow at low orthobaric-density ratios in vertical flow are bubble, churn, annular, and wispy-annular. Plug flow is absent in the two-phase flows produced by heat input at these conditions. Bubble flow occurred only at very low qualities and high flow rates in the net equilibrium-saturation region. Numerical results of the various series of tests are tabulated in Appendix C. In Fig. VI.1, the test results are plotted in terms of the superficial liquid and vapor velocities for a series of fixed inlet pressures to the unheated, rectangular test section. Consequently, the plot represents a parameter of orthobaric-density ratios that were selected to correspond to the density ratio for which a set of flow-regime information was available. In three of the cases, flow-regime data for water were known for saturation pressures of 415, 615, and 1000 psia. The data for water at 1000 psia were obtained by the electrical-resistance-probe method,[32] and by X-ray photographs and high-speed motion pictures.[27] In both cases, the flow was upward in a vertical tube with inside diameters of 0.4 and 0.497 in., respectively. Data for water at 500 psia was also available from the above investigations. A limited amount of data for Refrigerant-22 was available for reduced pressures of 0.12 and 0.22 in a 0.4-in. tube.[47] The orthobaric-density ratio is identical for R-22 and R-11 at the same reduced pressure; therefore the higher reduced pressure corresponded to a limited series of test runs in this R-22 data.

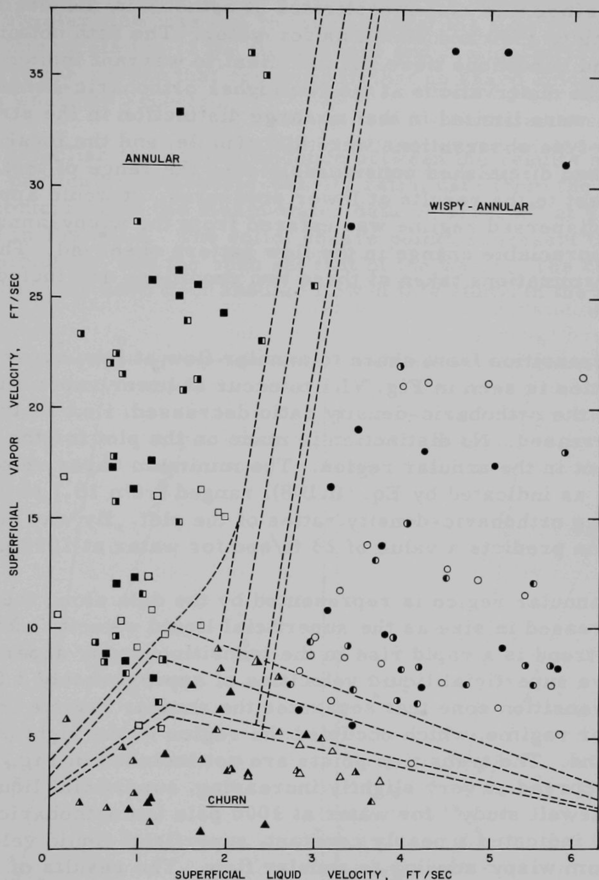

Fig. VI.1. Churn, Wispy-annular, and Annular Flow Transitions for Four Orthobaric-density Ratios

The transitions for churn, annular, and wispy-annular flow are shown in composite in Fig. VI.1 for orthobaric-density ratios of 58.0, 37.7, 20.6, and 24.4. The last density ratio cited represented the value corresponding to a reduced pressure of 0.22, which was identical to an R-22 fluid test pressure employed by Staub and Zuber.[47] The three preceding values are representative of the orthobaric-density ratios of water at 415, 615, and 1000 psia, respectively. The steam-water results of the electrical-resistance-probe study by Griffith[46] for 215, 415, and 615 psia were available for comparison with the present study. The effect of elevated pressure was also investigated at orthobaric-density ratios corresponding to 1500 and 2000 psia for water. The data obtained at these elevated conditions were not sufficient to warrant inclusion in Fig. VI.1. The observations at the two higher orthobaric-density ratios, 11.8 and 7.5, were limited in that no large distinction in the streaming to annular flow-type observations were discernible, and the local pressure oscillations had diminished considerably over the range of test data that was in contrast to the results at lower pressures. It would appear that the annular-dispersed regime was entered from the wispy-annular regime without an appreciable change in the flow pattern observed. The void-fraction determinations taken at these two conditions are included in a later section.

The transition from churn to annular flow at low, superficial liquid velocities is seen in Fig. VI.1 to occur at lower vapor superficial velocities as the orthobaric-density ratio decreased, i.e., as the system pressure increased. No distinction is made on the plot for the inception of entrainment in the annular region. The minimum vapor velocity for entrainment, as indicated by Eq. (II.B-8), ranged from 15.7 to 9.3 ft/sec for decreasing orthobaric-density ratios of the plot. By way of contrast, the expression predicts a value of 23 ft/sec for water at 1000 psia.

The annular region is represented by the data along the vertical axis and increased in size as the superficial liquid velocity increased. The general trend is a rapid rise in the transition-vapor superficial velocity above superficial liquid velocities of approximately 2 ft/sec. There is a transition zone that separates the annular regime from the wispy-annular regime, which occupied the region to the right of the transition band. The transition points are not included in Fig. VI.1. This transition occurred at very slightly increasing, superficial liquid velocities. The Harwell study[27] for water at 1000 psia (an orthobaric-density ratio of 20.6) indicated a nearly constant, superficial liquid velocity in the transition from wispy-annular to annular flow. The results of Haberstroh and Griffith[18] indicated a constant quality-line transition to annular flow above a liquid superficial liquid velocity of approximately 2 ft/sec, for which the value of 0.291 is obtained from Eq. (II.B-4). The result was indicated as nearly independent of diameter.

The lower bounds for the annular and wispy-annular regimes are indicated for the churn-flow regime that incorporated the various subdivisions of this regime. The transition line <u>increased</u> in the superficial vapor velocity bound with <u>increasing</u> orthobaric-density ratio (i.e., <u>decreasing</u> pressure). The transition from churn to wispy-annular occurred at decreasing vapor superficial velocity for increasing superficial liquid velocity at constant orthobaric-density ratio. Thus, the churn-flow regime reached a maximum in a narrow range from 1 to 3 ft/sec for the superficial liquid velocity, and had a range of maximum superficial vapor velocities from 5 to 10 ft/sec.

The partial uncertainty in establishing the transition from wispy-annular to annular flow was due to the nature of the flow regimes and the subjective interpretation of the fluoroscope and motion-picture results. This added to the spread that occurred in that no sharp deviation, or change, in patterns would be expected.

To establish the correspondence between the results of this investigation at a particular orthobaric-density ratio, data from the two sets of runs that coincide with the steam-water data of Griffith[46] at 415 and 616 psia are plotted in Fig. VI.2. The solid, square points represent the annular flow points of this study, and the open set that of the water. The circles represent data that may have been annular flow in this study; in the resistance-probe

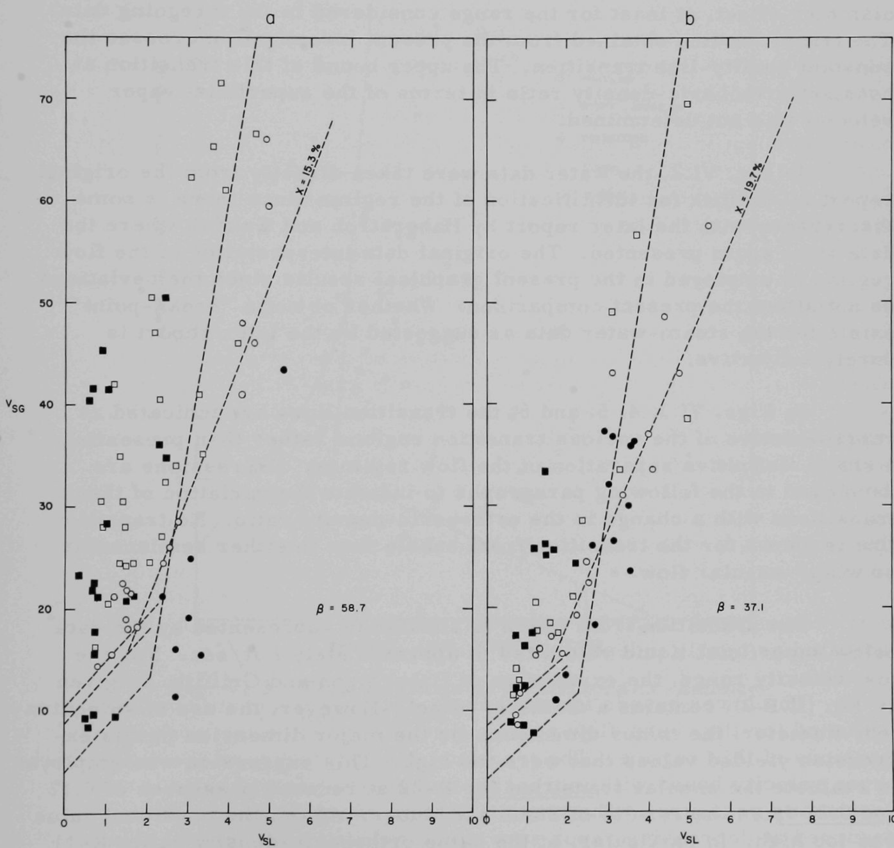

Fig. VI.2. Annular Flow Comparison of R-11 and Water
a) Orthobaric-density Ratio: 58.7
b) Orthobaric-density Ratio: 37.1

method, the circles represent annular flow with occasional, thin, liquid bridges. The water data were comprised of the results from tests in three tubes with diameters of 0.375, 0.625, and 0.875 in. The annular-flow points for the R-11 data occur at lower, superficial vapor velocities. The transition line predicted by Haberstroh and Griffith, as listed in Eq. (II.B-4), is shown as a dashed constant-quality line (0.153 and 0.197, respectively). The data for the steam-water tend to turn toward higher qualities at large values of the superficial vapor velocity. The trend toward a transition line of nearly constant, superficial liquid velocity was suggested by the steam-water data of Harwell[27] for pressures of 500 and 1000 psia, where the X-ray and motion pictures were employed. The transition from wispy-annular to annular flow has no apparent diameter effect, at least for the range considered in the foregoing data. The transition line obtained from the present investigation crosses the constant quality-line transition. The upper bound of this transition at constant orthobaric-density ratio in terms of the superficial vapor velocity was not determined.

In Fig. VI.2, the water data were taken directly from the original report by Griffith for identification of the regime since there is some discrepancy with the later report by Haberstroh and Griffith where the data were again presented. The original data interpretation of the flow regime is employed in the present graphical results since the deviations do not affect the present comparison. Whether or not a "break-point" exists for the steam-water data as suggested by the later report is purely subjective.

In Figs. VI.3, 4, 5, and 6, the transition lines are indicated as representative of the various transition regions rather than presenting a sharp, definitive separation of the flow regimes. Expressions are developed in the following paragraphs to indicate the variation of these transitions with a change in the orthobaric-density ratio. No transition line is shown for the transition from bubble flow to either semiannular or wispy-annular flow.

The transition from churn to annular is represented by the data below superficial liquid velocities of approximately 2 ft/sec. For the low-velocity range, the expression of Haberstroh and Griffith, as given by Eq. (II.B-2), contains a diameter effect. However, the use of an equivalent diameter, the minor dimension, or the major dimension in this expression yielded values that were too high. This expression was employed to evaluate the annular transition for R-22 at reduced pressures of 0.12 and 0.22 from the results of Staub and Zuber. Again, the predicted value was too high. In particular, at the same orthobaric-density ratio, R-11 and R-22 have higher vapor densities (and thus, higher liquid densities) than water. The surface tensions are lower than that for water, with approximately the same values at identical reduced pressures, as can be

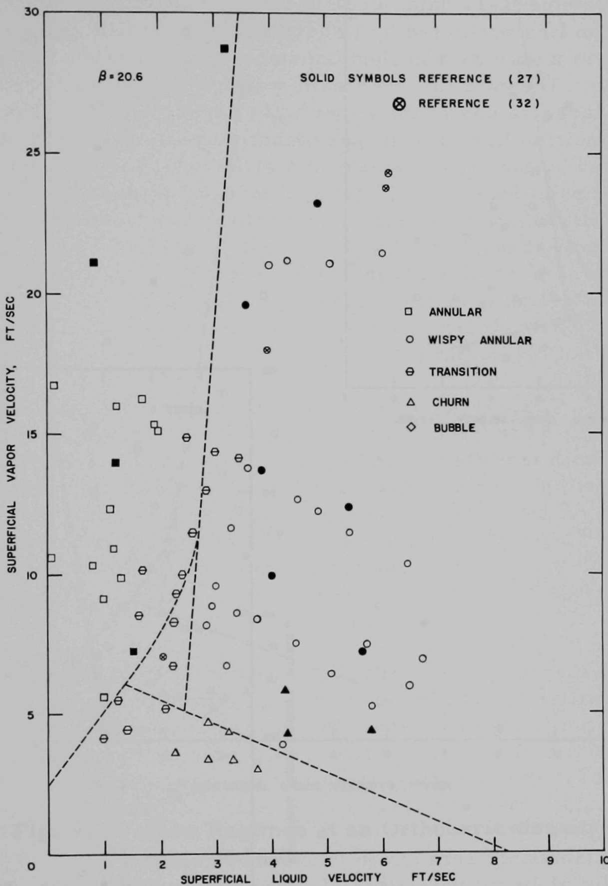

Fig. VI.3. Flow Regimes at an Orthobaric-density Ratio of 20.6

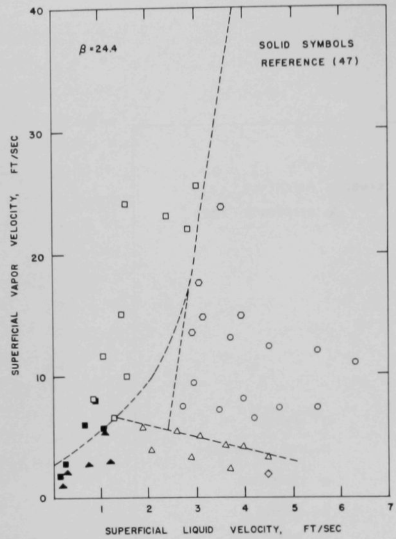

Fig. VI.4

Flow Regimes at an Orthobaric-density Ratio of 24.4

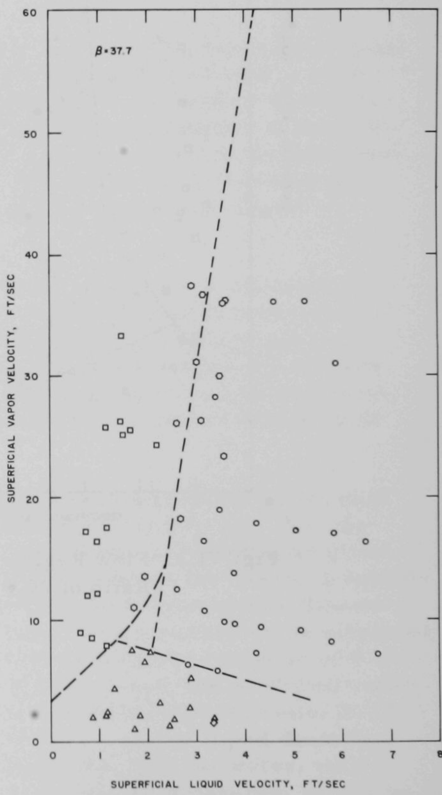

Fig. VI.5

Flow Regimes at an Orthobaric-density Ratio of 37.7

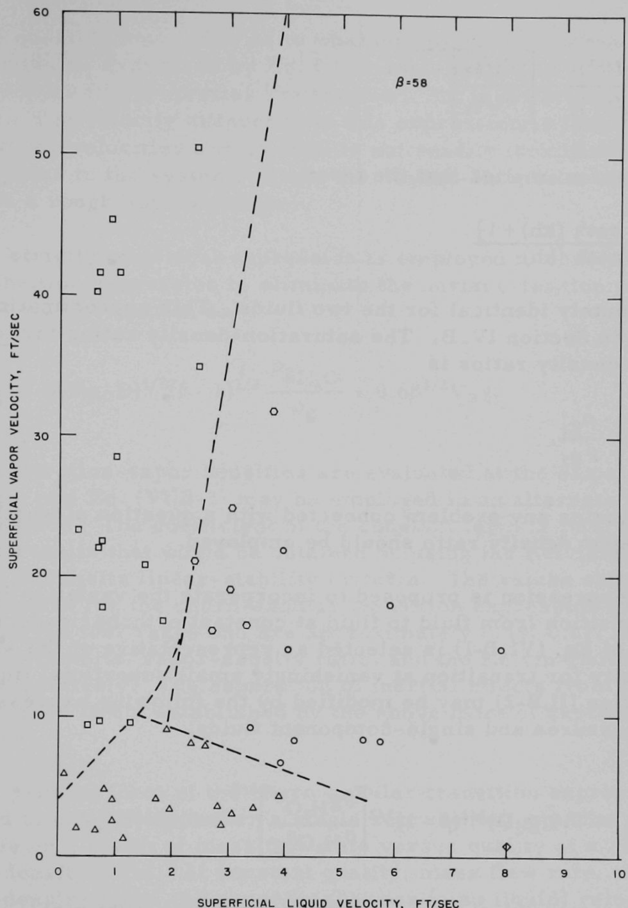

Fig. VI.6. Flow Regimes at an Orthobaric-density Ratio of 58.0

seen from Eq. (IV.B-9). The linear stability analysis of Section IV.B for a combined Taylor-Helmholz instability indicated a dependency of the velocity on the surface tension, the density, and the density ratio. At superficial liquid velocities approaching zero, it will be assumed that the Weber number is dominant, compared to the Froude number. For two fluids, the equality in Eq. (IV.B-6) is then assumed to hold, and the transition superficial-vapor-velocity ratio is given approximately as

$$\frac{V_{sg}(0^+)_1}{V_{sg}(0^+)_2} = \left[\frac{\sigma_1 \rho_{f_2}}{\sigma_2 \rho_{f_1}}\right]^{1/2} . \qquad \text{(VI.B-1)}$$

This expression implies that the term

$$\frac{k[\beta \coth(kh) + 1]}{\coth(kh)}$$

is approximately identical for the two fluids. This approximation was considered in Section IV. B. The saturation-density ratios for identical orthobaric-density ratios is

$$\frac{\rho_{f_1}}{\rho_{f_2}} = \frac{\rho_{g_1}}{\rho_{g_2}}, \qquad \text{(VI.B-2)}$$

which eliminates any problem connected with a question of whether the liquid or vapor density ratio should be employed.

An expression is proposed to incorporate the variation in the churn-annular transition from fluid to fluid at constant orthobaric-density ratio. The result of Eq. (VI.B-1) is selected as representative of the superficial vapor velocity for transition at vanishingly small superficial liquid velocities. Equation (II.B-2) may be modified by the following expression for elevated pressures and single-component fluids:

$$V_{sg} = 0.9(g_c D)^{1/2}(\beta - 1)^{1/2}\left[\frac{\rho_{g_{H_2O}} \sigma}{\sigma_{H_2O} \rho_g}\right]^{1/2} + 0.6\beta^{1/2} V_{s\ell}, \qquad \text{(VI.B-3)}$$

where the operational definitions of Eqs. (II.B-6) and (II.B-7) are employed, and the above expression reduces to the result of Haberstroh and Griffith when employed with water as a fluid and at large orthobaric-density ratios. The interchangeability of the liquid-saturation-density ratio with that of the vapor is assured by Eq. (VI.B-2). The surface tension-density term in the above expression is nearly constant for the range of orthobaric-density ratios considered, which reduces the coefficient by approximately a factor of one-half.

Better agreement is obtained by employing the expression developed above with the lower-surface-tension fluids. However, for fluids with nearly identical surface tensions, the effect of the variation of vapor density would appear in the results at identical orthobaric-density ratios.

The question may arise as to whether the Kelvin-Helmholtz instability criterion, as expressed by Eq. (IV.B-18a), should be employed. The same thermodynamic properties are involved, but in different degrees of importance. The velocity difference in this expression is that of the local liquid and vapor velocities and as such is not readily identifiable with the known velocities in the system. Thus, the Taylor-Helmholtz expression is employed as a rough approximation.

If a strictly empirical expression is employed to correct the churn-annular transition expression to eliminate the surface-tension property, Eq. (VI.B-3) may be written as

$$V_{sg} = 0.9(g_c D)^{1/2}(\beta - 1)^{1/2} \frac{\rho_{g_{H_2O}}}{\rho_g} + 0.6\beta^{1/2} V_{s\ell}, \qquad \text{(VI.B-4)}$$

where the saturation-vapor densities are evaluated at the same orthobaric-density ratio, and Eq. (VI.B-2) may be employed in an alternate form of the above expression. The coefficient of the constant term is intermediate between the results that would be obtained by using the Kelvin-Helmholtz and Taylor-Helmholtz linear-stability criteria. The values obtained for the modifying factors for the churn-annular transition expression are relatively constant over the test range and are approximately 0.49, 0.61, and 0.70 for the Taylor-Helmholtz, vapor-density ratio, and the Kelvin-Helmholtz methods, respectively. The separation of inertial effects from the effects of surface forces is not established by the above form of expression for the transition.

The general form of the churn-annular transition expression may be examined to establish whether a single representation of the transition may be made on a graph of mass flow rate versus quality at a set orthobaric-density ratio. At constant quality, mass flow rate, and orthobaric-density ratio, the superficial vapor (also liquid) velocities are inversely proportional to the liquid (or vapor)-density ratios for two fluids. Or,

$$\frac{V_{sg_1}}{V_{sg_2}} = \frac{\rho_{f_2}}{\rho_{f_1}}, \qquad \text{(VI.B-5)}$$

which is obtained from the definition of the superficial velocity. The churn-annular transition expression may be written in the form,

$$V_{sg} - CV_{s\ell} = D, \qquad \text{(VI.B-6)}$$

where the coefficients C and D contain any geometry and fluid-property effect. The expression may be rewritten as

$$\beta x(G/\rho_f) - C(1-x)(G/\rho_f) = D. \qquad \text{(VI.B-7)}$$

If the expression holds for two fluids such that $C_1 = C_2$, $x_1 = x_2$, and $\beta_1 = \beta_2$, where the subscripts 1 and 2 represent the two fluids, the following may be obtained:

$$\beta x[(G/\rho_f)_1 - (G/\rho_f)_2] - C(1-x)[(G/\rho_f)_1 - (G/\rho_f)_2] = D_1 - D_2. \qquad \text{(VI.B-8)}$$

Upon rearrangement,

$$1 - \frac{\rho_{f_1}}{\rho_{f_2}}\frac{G_2}{G_1} = \frac{\rho_{f_1}}{G_1}\frac{(D_1 - D_2)}{[\beta x - C(1-x)]} = \frac{D_1 - D_2}{D_1} = 1 - \frac{D_2}{D_1}. \qquad \text{(VI.B-9)}$$

Then,

$$\frac{D_2}{D_1} = \frac{\rho_{f_1}}{\rho_{f_2}}\frac{G_2}{G_1}. \qquad \text{(VI.B-10)}$$

At identical mass flow rates (i.e., $G_1 = G_2$),

$$D_2 = D_1\frac{\rho_{f_1}}{\rho_{f_2}}. \qquad \text{(VI.B-11)}$$

Thus, the approximation given by Eq. (VI.B-4) would provide a transition line on the mass-flow-rate-versus-quality type of plot, which would be identical for two fluids if the coefficients C and D are correctly chosen to represent the geometry effect and the fluid-property effect. The transition lines have been plotted in Fig. VI.7 for an orthobaric-density ratio of 20.6 (equivalent to a saturation-water pressure of 1000 psia) for the expressions given for the transitions.

The churn flow to wispy-annular transition does appear to be directly represented by the preceding analysis. However, Fig. VI.1 showed that the transition could be represented by a linear transition form. In Fig. VI.8, the churn flow and wispy-annular points are plotted with a reducing parameter of the square root of the orthobaric-density ratio operating on the superficial vapor velocity. The results are somewhat satisfactorily handled in this reduction. Reference is made to Fig. VI.3, where the results of the water data are plotted as solid symbols for the Harwell results and as circles with crosses for the transition points of Suo et al.[32] The transition from churn to wispy-annular flow occurred at higher values of the superficial vapor velocity for water than for the R-11. The transition line may be brought into agreement by the addition of the effect of the liquid (or vapor) density to the one-half power to the linear expression such that

$$\frac{V_{sg}}{\beta^{1/2}} + C_0 V_{s\ell} = \frac{D_0}{\rho_g^{1/2}} \quad \text{(ft/sec)}, \qquad \text{(VI.B-12)}$$

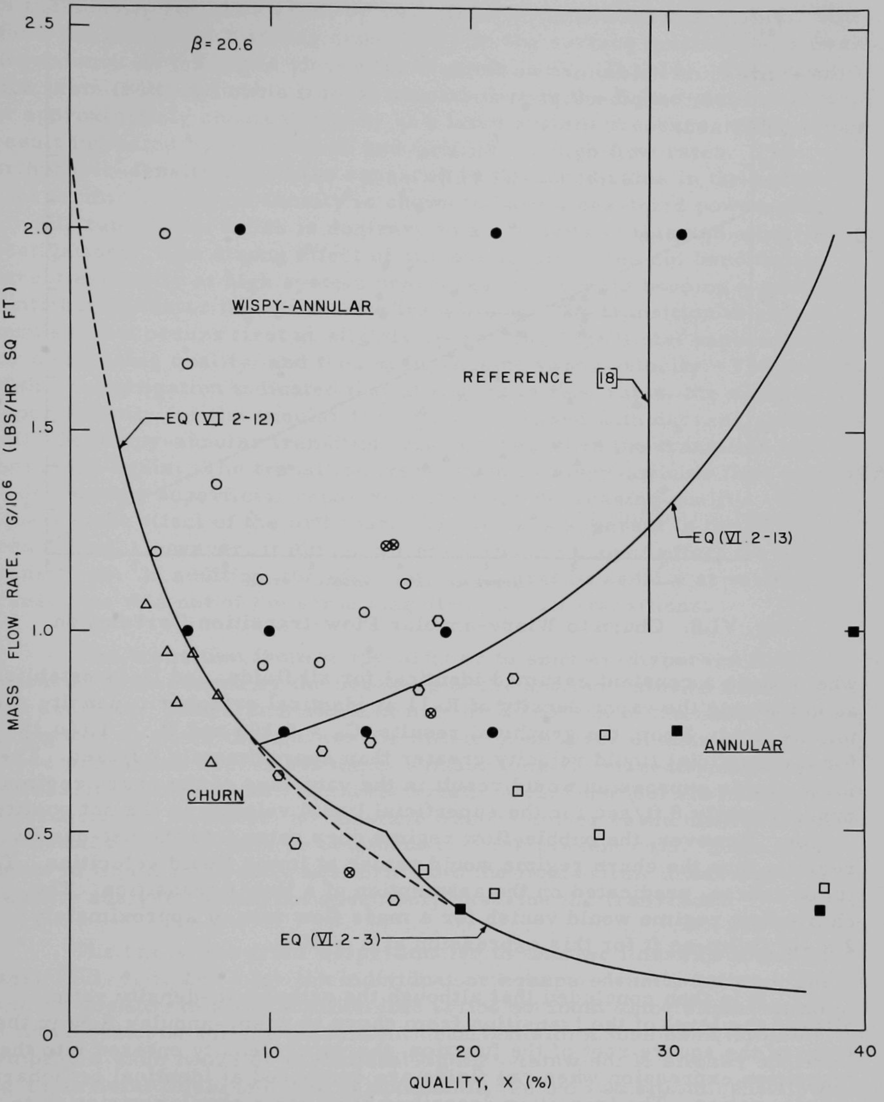

Fig. VI.7. Mass Flow Rate and Quality Representation of the Transitions at an Orthobaric-density Ratio of 20.6

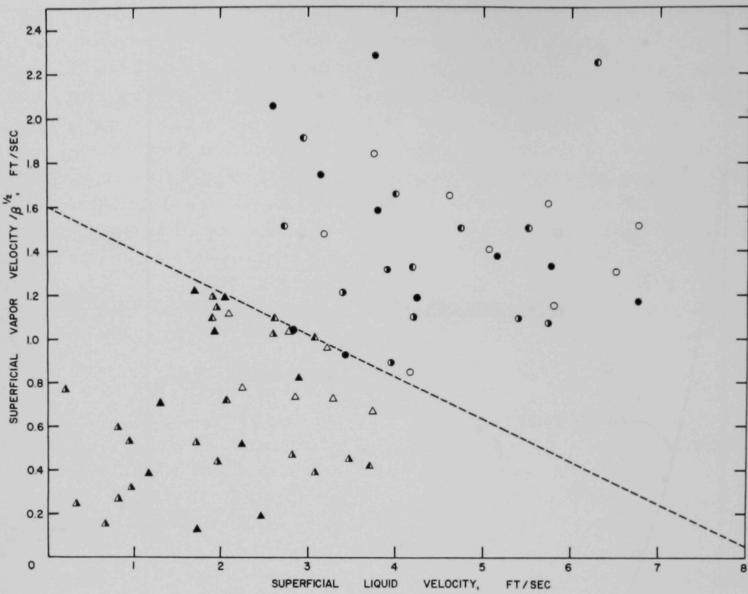

Fig. VI.8. Churn to Wispy-annular Flow-transition Correlation

where C_0 is a constant assumed identical for all fluids, and D_0 is established as containing the vapor density of R-11 at identical orthobaric-density ratio for the fluid. From the graphical results, $C_0 = 0.194$ and $D_0 = 1.6(\rho_g)^{1/2}_{R\text{-}11}$ for a superficial liquid velocity greater than approximately 2 ft/sec. The form of this expression would result in the vanishing of the churn regime at approximately 8 ft/sec for the superficial liquid velocity in the net quality region. However, the bubble-flow regime does enter into the net-quality regime; thus the churn regime would vanish at lower liquid velocities. This is, of course, predicated on the assumption of a linear transition. The churn-flow regime would vanish for a mass flow rate of approximately 2×10^6 lb/hr-sq ft for this expression at $\beta = 20.6$.

It is then concluded that although the orthobaric-density ratio altered the level of the transition from churn to wispy-annular flow in the form of the square root of the function, the vapor density entered into the transition expression when two fluids are compared at identical orthobaric-density ratios. The transition described here has a similar variation to the effect of gas phase density observed in the air-water study of Brown, Sullivan, and Govier.[43]

The original, generalized, flow-regime map as presented by Baker[34] had as its ordinate the superficial vapor velocity divided by the square root of the density ratio, as given by Eq. (II.B-13) and shown in Fig. II.4. The abscissa contained a strong dependency on the surface tension and a weak dependency on the liquid viscosity, as given in Eq. (II.B-14). The transition from froth or bubble flow to annular flow in the Baker plot occurred at approximately constant quality at a fixed system pressure, which is the result indicated by Haberstroh and Griffith for high flow rates. The orthobaric-density ratio also appeared in the coordinates in the square root form. The liquid density is shown to have a one-third power effect for all transitions, which is contrary to the results in this and other investigations. The strong effect of surface tension does not become apparent explicitly at high system pressures, and should become a minor contributing factor in some of the transitions. The transition in slug to annular flow occurs first at slightly decreasing superficial vapor velocity for decreasing quality, and then at increasing vapor velocity. The results of this investigation indicated that at low mass flow rates, the superficial vapor velocity for the annular transition increased with decreasing quality until the wispy-annular transition was reached; then the transition quality increased again. The transition from churn to wispy-annular flow occurred at decreasing superficial vapor velocities for decreasing quality. The square-root effect of the orthobaric density was apparent in the churn transitions. However, it did not appear to be the proper effect for all transitions. In addition, the effect of the saturation density at various transitions was not of the same magnitude for all transitions.

The transition from wispy-annular to annular-dispersed flow appeared to be caused by the break-up of the agglomerates in the core into droplets. This transition then may be a function of the same fluid properties as those that govern the initiation of spray in annular flow. These properties are, in the main, surface tension, viscosity, and the orthobaric-density ratio. A characteristic Weber number may exist for the transition. However, no constant Weber number based upon a single geometrical length could be obtained from the present data. Since ligaments of liquid apparently are torn from the liquid film, linearized stability analyses would not adequately describe the transition.

The transition from wispy-annular to annular flow was shown in Figs. VI.3, 4, 5, and 6 for the individual orthobaric-density ratios. The precise position of the transition line is not obtained since a band would be more realistic for the transition. The transition zone does not encompass a wide range of superficial liquid velocities. A slightly increasing superficial liquid velocity is obtainable for the transition. Within the spectrum of the points of uncertainty, the transition line could be set as linear with a separation between orthobaric-density ratios in terms of the superficial liquid velocity varying as the cube root of the orthobaric-density ratio. However, there is no justification for such a setting of the transition due to the spread in the transition zone. In comparison with the water data of Bennett et al., the transition occurred at lower superficial liquid velocities for identical vapor velocities; or conversely, for a fixed liquid velocity, the R-11 had a higher vapor velocity. The transition in the G-x plane would be identical for R-11 and water if the ratio of superficial vapor velocities along a constant-quality line in the superficial-velocity plane were inversely proportional to the liquid-density ratio. The ratio is in the order of 0.61 for R-11 to water. This would imply that the superficial liquid velocities are separated by the same ratio. Identical plots of the transition lines would then be obtained. The transition line appeared to occur at higher mass flow rates for the R-11 when compared to the water data. Again, the band of transition cannot be made clear-cut, as observation of the motion pictures of the flow regimes results in subjective conclusions.

The proposed transition from slug to annular flow as given by Haberstroh and Griffith contained two inflection points for their air-water data. The final inflection point led to a constant-quality line, which was extrapolated to estimate the transition at elevated pressures. If the cube root of the orthobaric-density ratio suggested as a rough estimate of the transition from wispy-annular to annular flow in the preceding paragraph is employed to extend the air-water data to elevated pressures, the transition line would be between 3.2 and 3.8 ft/sec at 500 psia for the range of the transition superficial liquid velocities, and between 4.2 and 4.8 ft/sec for water at 1000 psia. This would be in agreement with the Harwell statement[27] as to the constant superficial-liquid-velocity magnitudes, but not with their listed data. The discrepancies involved in the second transition-inflection point will now be considered.

The electrical-resistance-probe method of determining the transition to annular flow at high mass velocities[18,32,46] was employed by Haberstroh and Griffith[18] to develop an expression for the transition in terms of a constant quality, dependent only upon the orthobaric-density ratio. The range of validity of the constant-quality transition is given by Eq. (II.B-5) in terms of the superficial liquid velocity. The predicted values of the transition quality are 17.5 and 29.1% for water at 500 and 1000 psia, respectively. The result is included in Fig. VI.7 for comparison with the transition points obtained by Suo et al.[32] Excluding the higher mass-velocity transition points, the measured values obtained for 1000 psia are qualities of 0.14, 0.181, 0.158, and 0.161 for mass flow rates of 0.4, 0.8, 1.22, and 1.22 x 10^6 lb/hr-sq ft, respectively. These values are much less than the predicted value of 29.1%, which casts some doubt as to the effectiveness of the electrical-resistance probe for quantitative measurements, particularly for the wispy-annular transition to annular flow. Only two points were available for the 500-psia water data. The transition qualities there were 0.167 and 0.105, respectively, at 0.41 and 1.22 x 10^6 lb/hr-sq ft. The probe measurements for 500- and 1000-psia water did not agree with the transitions obtained from the X-ray and motion-picture results of the Harwell study. Either the extrapolated prediction of the constant-quality transition is incorrect, or the resistance-probe method is open to question as a tool for quantitative measurements. The physical properties of R-11 were not amenable for the use of a probe of this design; thus the observed flow patterns could not be compared by this method.

The approximate expression for the transition from wispy-annular to annular flow may be written as

$$V_{sg} = 25V_{sf} - 150D_1/\beta^{1/3}, \quad V_{sg} > 0, \tag{VI.B-13}$$

where D_1 is unity for R-11. The difference in the transition results for R-11 and water differed by some factor that could be expressed in terms of either the liquid or vapor density at identical orthobaric-density ratios for the previous transitions. In addition, the effects of viscosity and surface tension could not be separated. The factor D_1 is apparently independent of diameter effects. It also could be expressed as

$$D_1 \sim \rho_{f_{R-11}}/\rho_{f_{H_2O}} \tag{VI.B-14}$$

at identical orthobaric-density ratios. The discussion of Baker's flow-regime map in Section II.B led to a difference in transition superficial liquid velocity such that the R-11 value was 0.25 that of the water at identical orthobaric-density ratios. This transition is approximately correlated by the above expressions. However, no upper limit can be given.

The transition expressions obtained in this investigation are compared in Fig. VI.7 with the test results at an orthobaric-density ratio of 20.6. Included in the plot are the electrical-resistance-probe results of Suo et al.[32] and the Harwell data[27] for water at 1000 psia. Only some representative points for the R-11 results have been shown. If Eq. (VI.B-14) is employed to relate the water data with the R-11 result, then the single line shown in the figure as Eq. (VI.B-13) represents both fluids. A transition band for the wispy-annular to annular flow would extend downwards toward the intersection of Eqs. (VI.B-3) and (VI.B-12) and would include the uncertain data points. The constant-quality transition suggested by Haberstroh and Griffith is shown with the lower limit extending to the criterion stated by their work. Their result disagrees with the electrical-resistance-probe transition points.

Ultimately, as the system pressure approaches the critical pressure, it might be expected that bubble flow would have a transition to wispy-annular in a direct manner with a further transition to annular-dispersed. The test results for orthobaric-density ratios comparable to water at 1500 and 2000 psia did not indicate any substantial pressure oscillations, nor were distinct flow patterns observed by the fluoroscope method. The general appearance of the flow at very small orthobaric-density ratios was that of streaming flow. For the limited flow rates involved at elevated pressures, no distinction could be made for a transition from wispy-annular to annular flow.

The local pressure gradients obtained during the series of tests are illustrated by examples from the test set for an orthobaric-density ratio of 20.6. Three differential pressures were determined. Sequentially, the overall, intermediate, and exit lengths of the unheated rectangular section are displayed for transducer differential-pressure ratings of 15, 5, and 5 psid, respectively. The zero for each chart is centered and was calibrated before each run. A timing mark along the edge of the strip indicated an interval of 1 sec. The chart settings were adjusted to represent either 1 or 2 mV/cm. The transducers were calibrated for a 10-mV range for the differential-pressure rating. For the annular flow runs, 1 mV/cm was employed for the intermediate pressure-drop recording; the overall pressure-drop recording was set at 1 mV for these figures; the exit pressure drop remained at 2 mV/cm. The output of the recorder carried an electrical noise, which was not removed by any damping capacitor and remained in evidence, particularly in the overall pressure-drop reading. Figures VI.9, 10, 11, 12, 13, and 14 illustrate the effect of flow regime on the local pressure drops. Churn, wispy-annular, and annular flows are represented, and the effect of flow rate is illustrated in Figs. VI.9 and 10, where the quality is approximately 0.11 and the mass flow rates are 0.46 and 1.04 x 10^6 lb/hr-sq ft, respectively. The former set illustrates the churn-annular transition region; the latter is in the wispy-annular region. (There is a scale change for the intermediate pressure-drop recording in these two graphs.)

Figure VI.11 represents the churn-flow oscillations in which the quality was 0.07 and the mass flow rate was 0.67 x 10^6. The character of the fluctuations in this figure tended toward periodic bands of oscillations, which moved at intervals along with the occasional damping of the pressure drop. In Fig. VI.12, the wispy-annular region is represented at a quality of 0.15 and at a flow rate of 0.72 x 10^6. The band of oscillations is not seen in this figure as compared to the former. This run was near the transition to annular flow. Annular flow is shown in Fig. VI.13, in which the intermediate recorder setting was changed to 1 mV/cm to magnify the oscillations. The value of the quality was 0.39, and the mass flow rate was 0.54 x 10^6. The oscillations have been damped considerably. The occasional oscillations are probably due to the high-amplitude waves that were evident in the high-speed motion pictures. The final figure is an indication of the system pressure drop before an excursion in the wall temperature. Figure VI.14 indicates annular flow at a quality of 0.38 and a mass flow rate of 0.36 x 10^6.

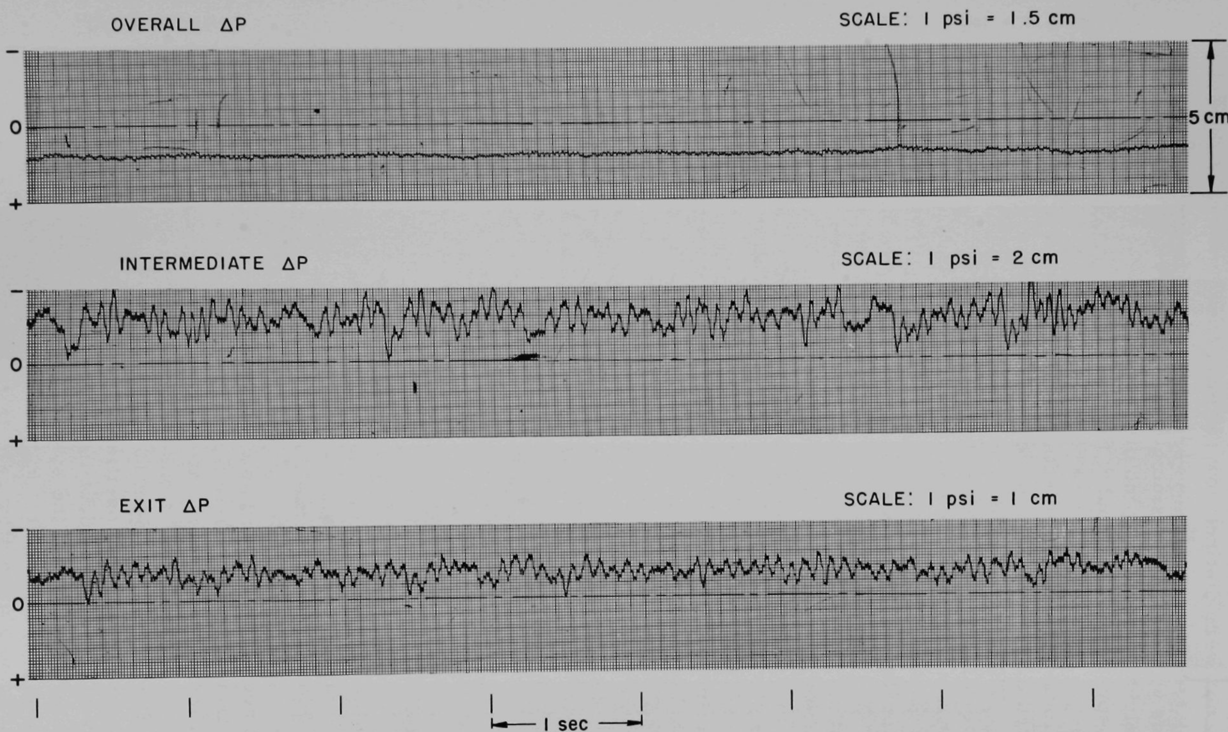

Fig. VI.9. Local Pressure Gradients for an Orthobaric-density Ratio of 20.6 at a Quality of 0.11 and a Mass Flow Rate of 0.46×10^6 lb/hr-sq ft

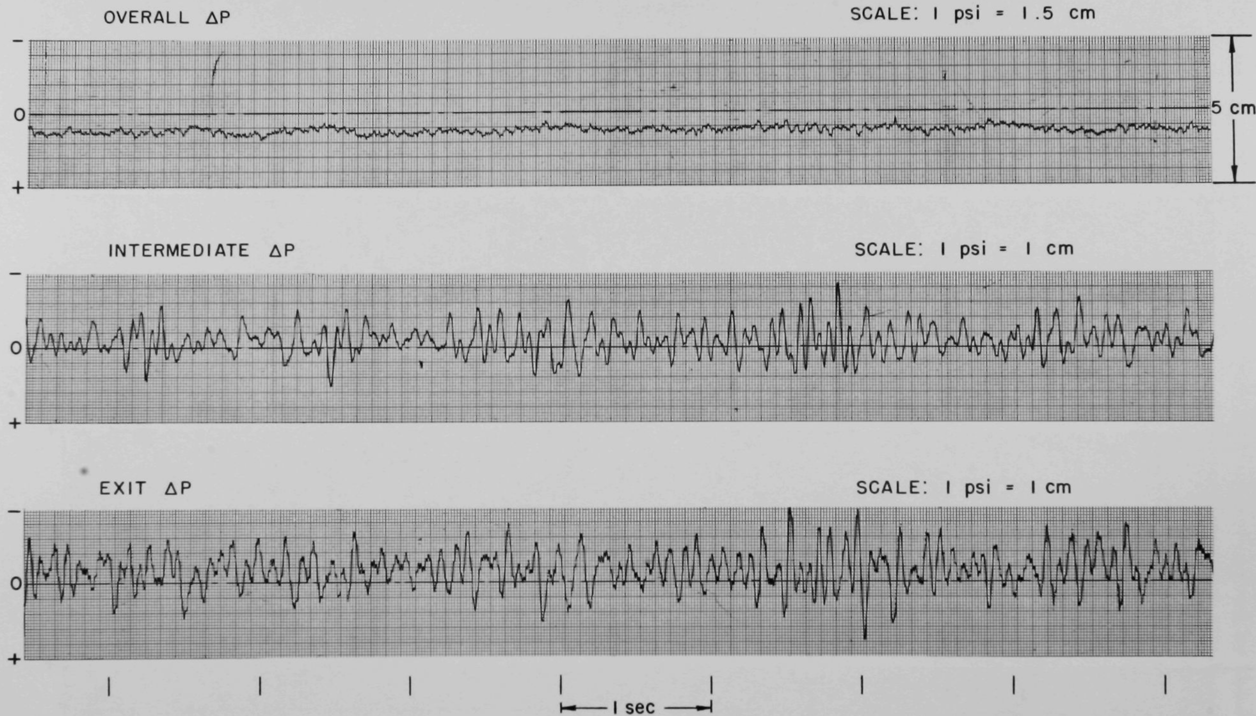

Fig. VI.10. Local Pressure Gradients for an Orthobaric-density Ratio of 20.6 at a Quality of 0.11 and a Mass Flow Rate of 1.04×10^6 lb/hr-sq ft

Fig. VI.11. Local Pressure Gradients for an Orthobaric-density Ratio of 20.6 at a Quality of 0.7 and a Mass Flow Rate of 0.67×10^6 lb/hr-sq ft

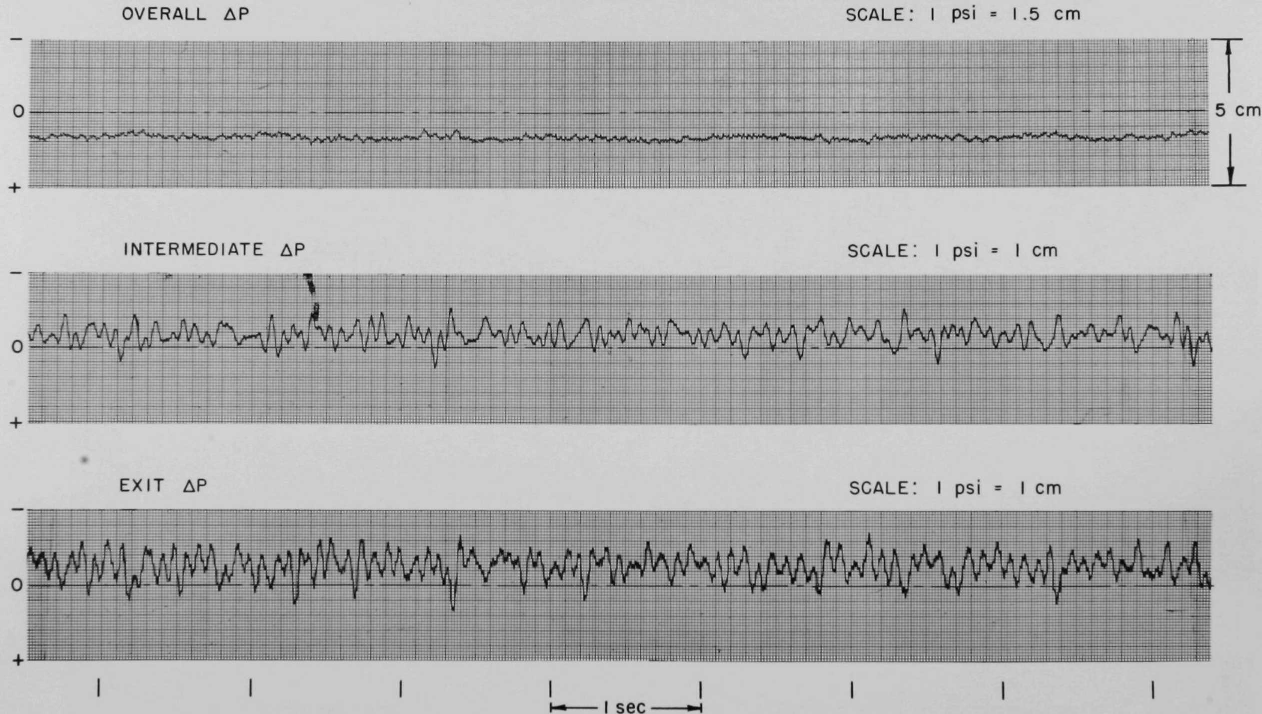

Fig. VI.12. Local Pressure Gradients for an Orthobaric-density Ratio of 20.6 at a Quality of 0.15 and a Mass Flow Rate of 0.72 x 10^6 lb/hr-sq ft

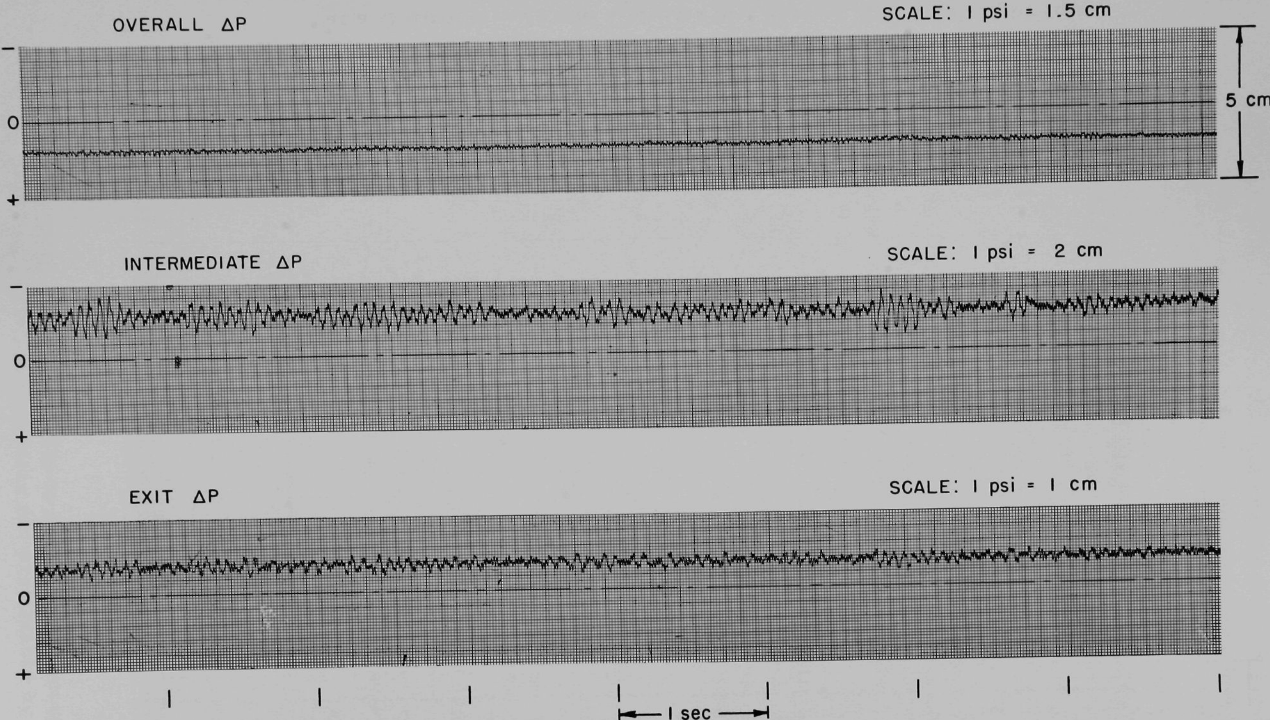

Fig. VI.13. Local Pressure Gradients for an Orthobaric-density Ratio of 20.6 at a Quality of 0.39 and a Mass Flow Rate of 0.54×10^6 lb/hr-sq ft

Fig. VI.14. Local Pressure Gradients for an Orthobaric-density Ratio of 20.6 at a Quality of 0.38 and a Mass Flow Rate of 0.36 x 10^6 lb/hr-sq ft

The local pressure-drop fluctuations ranged to 2 psi in the largest values seen in these plots. The inertia of the recording pen may have accounted for some of the spread. Operation of the chart speed at various values did not appear to produce any great deviations in the spread of the pressure-drop oscillations. The recorder was employed to determine the form of the pressure-drop oscillation for slug flow by operation during nonforced-flow conditions. The characteristic of this type of flow is somewhat different from the churn-type flow encountered during the forced-flow conditions.

The test procedure involved a fixed heat flux with a variation of flow rate. In general, the flow rate was reduced in the test series in order to pass through the various transition regions. The wall temperatures of the heated section remained constant as the system condition passed into the annular regime. A subsequent reduction of flow led to a slight depression of the wall temperature before a rapid rise. At low mass flow rates, the heat flux required for this rise in wall temperature varied, whereas at high flow rates, a nearly constant heat flux value was obtained for the departure of the wall temperatures to high values. At low flow rates, the motion-picture results indicated the existence of spray droplets and a thin, tranquil, liquid film. At high flow rates, the wispy-annular flow regime was in evidence at the increased wall-temperature condition. During several points in the series of tests, the wall temperature was allowed to rise without the burn-out trip in the circuit. It was found that the wall temperature would occasionally rise to a high value and then decrease to nearly the same value before the rise. Since the wall temperature would undergo an excursion to values of approximately 1000°F, the number of attempts to repeat these excursions was limited to prevent the breakdown of the fluid. The wall temperature tended to increase slightly at a given system pressure as the heat flux was increased. The increase was not substantial, and no accurate values were obtained due to the limited precision in reading the indicated values. No "burn-outs" were sustained in the churn-flow region. Although the tests were not designed to search for this result, an occasional random excursion might have been expected.

The observations of the transitions occurring in this study may be summarized as follows:

1. The orthobaric-density ratio is the proper modeling parameter for comparison of refrigerants, such as R-11, with water. Within the refrigerant group, modeling on the reduced pressure or reduced temperature would be sufficient for this group because of the reduced property relationship among the members.

2. The transition from churn to annular flow occurred at low superficial liquid velocities, which were not predictable by the expression

for air-water and steam-water systems without modifications. The transition for R-11 (and R-22 of a different study) occurred at earlier superficial vapor velocities than predicted by Eq. (II.B-2). By consideration of the linearized stability analysis for the Taylor-Helmholtz and the Kelvin-Helmholtz problems, bounds could be obtained on the modification of the transition expression. The ratio of the fluid density (either liquid or vapor) of the refrigerant and water at the same orthobaric-density ratio would modify the expression to yield the correct direction for the expression that was given as Eq. (VI.B-3). The upper limit of this transition appeared to be of the order of 1 to 2 ft/sec for the superficial liquid velocity.

3. The transition from churn to a flow regime described as wispy-annular flow occurred at decreasing superficial vapor velocities for increasing liquid velocities. An expression was obtained for the transition in terms of the square root of the orthobaric-density ratio, and given approximately by Eq. (VI.B-12). The square-root term does not entirely effect a correlation since the comparison of these results with that of water at identical orthobaric-density ratios indicated that the vapor (or liquid) density entered the correlation. The square root of either saturation density would bring the data into agreement.

4. Plug flow did not appear in the net-quality results of these tests for the forced-circulation, high-pressure conditions.

5. The transition from wispy-annular flow to annular flow was initiated at lower superficial vapor velocities for decreasing orthobaric-density ratios. The transition band is very narrow when plotted on superficial-velocity coordinates. In comparison with the available water data, the transition occurred at slightly lower superficial liquid velocities at a given orthobaric-density ratio. No diameter effect was evident. The transition line is one of nearly constant superficial liquid velocity. An approximation of the change with orthobaric-density ratio can be made by one-third-power effect of the above ratio, as given by Eq. (VI.B-13). From the spread in the transition band, a definite transition criterion cannot be made. For a given quality, the R-11 transition takes place at a slightly higher mass flow rate than water at the same orthobaric-density ratio.

6. A comparison of the electrical-resistance-probe results between two different investigations for water revealed that the probe may be inadequate as a quantitative device for the wispy-annular to annular transition. The probe apparently is as subjective as motion pictures in the matter of interpretation.

7. The possible effects of inertial controlled processes and those governed by surface and viscous effects could not be uncoupled, since the

variations in transitions can be effectively termed in either form. A recent study by Shearer and Davidson[83] investigated the initiation of standing-wave formation due to gas blowing upward over a liquid film and employed a combination of a Weber- and Reynolds-number representation of the critical gas velocity at which the standing wave was formed. Their results indicated that the development employed in obtaining Eq. (VI.B-3) was substantiated. Their resultant definition of the Weber number led to a coefficient modification in Eq. (VI.B-3) which was closer in magnitude to the result given in Eq. (VI.B-4) where the ratio of saturation densities was employed. Thus, the proper modification for the churn-to-annular transition is still uncertain.

C. Local Void Fractions

Local void fractions were determined in the unheated rectangular channel, and the reduced values are listed in Appendix C. The channel width was arbitrarily subdivided into 12 sections. Thus, each element represented the width of the collimating window at the photomultiplier tube. The minimum time required to traverse each element, which was approximately 1/32 in. wide, was 20 sec. The temporal and spatial averages were, therefore, assumed to be sufficiently close for a mean value to be assigned to each element.

The void fractions obtained in the unheated section above a heated section should be lower at a fixed quality and mass flow rate than the values that would be obtained in the heated section. A comparison of the average void fraction obtained in a mass-flow-rate range comparable to the R-22 study[47] indicated that at the same quality and mass flow rate, the void fraction was slightly lower than that obtained in the heated section. The difference was approximately 5%. A change in distribution of the vapor toward the core would represent an increase in slip ratio, i.e., a decrease in the void fraction.

Examples of the effect of mass flow rate, quality, and orthobaric density on the void-fraction profile are given in Figs. VI.15, 16, and 17. For a given mass flow rate and quality, increasing the system pressure (i.e., decreasing the orthobaric density) decreases the average void profile. For increasing quality, the void profile becomes flattened. For fixed quality and density ratio, the local void profile becomes flatter with increasing flow rate. The void profile in the semiannular or churn region is somewhat parabolic in nature. The transition into annular and wispy-annular flow flattens the profile.

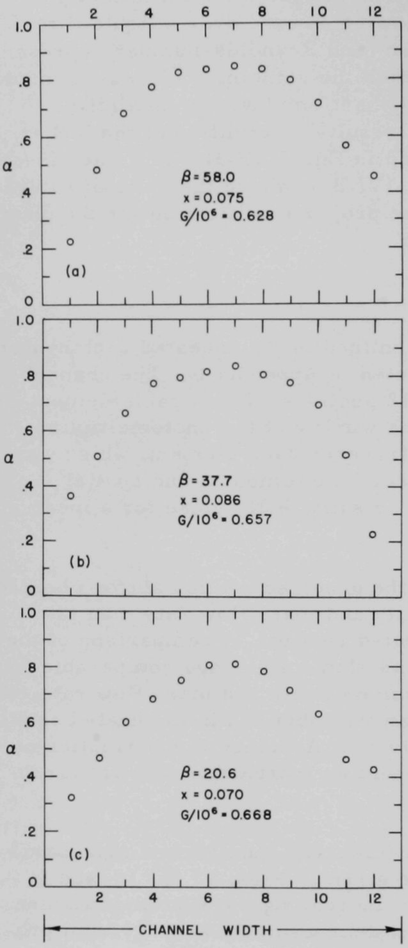

Fig. VI.15. Local Void-fraction Profiles for $x = 0.075$, 0.086, and 0.070, and for $G/10^6 = 0.628$, 0.657, and 0.668

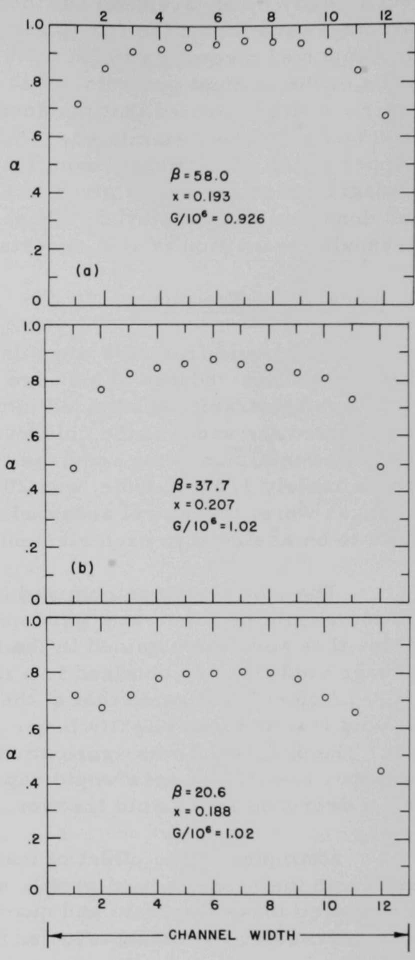

Fig. VI.16. Local Void-fraction Profiles for $x = 0.193$, 0.207, and 0.188, and for $G/10^6 = 0.926$ and 1.02

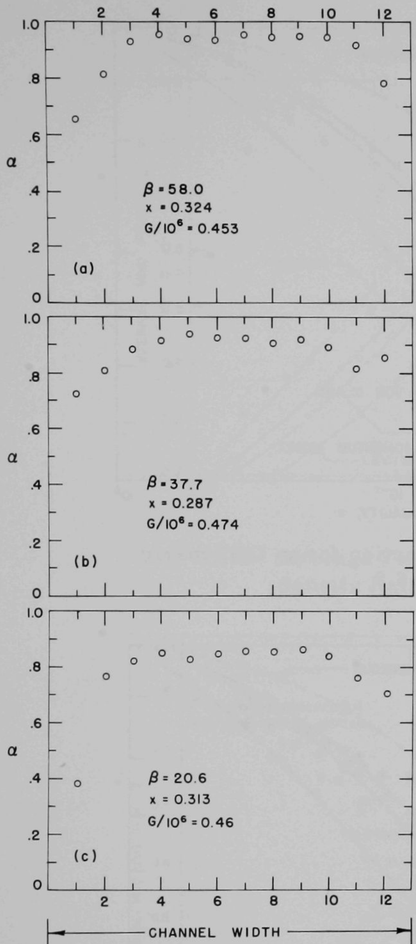

Fig. VI.17. Local Void-fraction Profiles for $x = 0.324, 0.287$, and 0.313, and for $G/10^6 = 0.453, 0.474$, and 0.46

Figures VI.18, 19, 20, 21, and 22 show the average void fraction as a function of the mass quality, based upon thermodynamic equilibrium, with the data separated arbitrarily into the results for mass flow rates above and below 1.0×10^6 lb/hr-sq ft. For comparison, the void-fraction data of Janssen and Kervinen[84] are included in Figs. VI.19 and 21. Their results were obtained for steam-water flow in a vertical, rectangular channel (1/2 by $1\frac{3}{4}$ in.). The mass flow rate for the steam-water data in Fig. VI.19 was approximately 0.5×10^6 lb/hr-sq ft, with a pressure of approximately 600 psia. In Fig. VI.21, the mass flow rates for the steam-water data at 1000 psia were 0.25, 1.0, and 2.0×10^6 lb/hr-sq ft. With the extensive number of void-fraction correlations available in the literature, these three correlations were selected on the basis that the orthobaric-density ratio and quality were the only required quantities for determining the void fraction. Thus, the momentum model of Levy[85] and the correlations of von Glahn[86] and Polomik[87] are included, in addition to the homogeneous-flow model. None of these models contains a mass-flow-rate effect and as such cannot yield a precise representation of the void fraction. Levy's momentum model provided a lower bound on the void fractions obtained in this investigation, but it does not provide a lower bound for flow rates below those utilized in this result. Since Polomik[87] presented several expressions for void fraction, the particular expression employed in Figs. VI.18 through VI.22 was Eq. (24) in his paper.

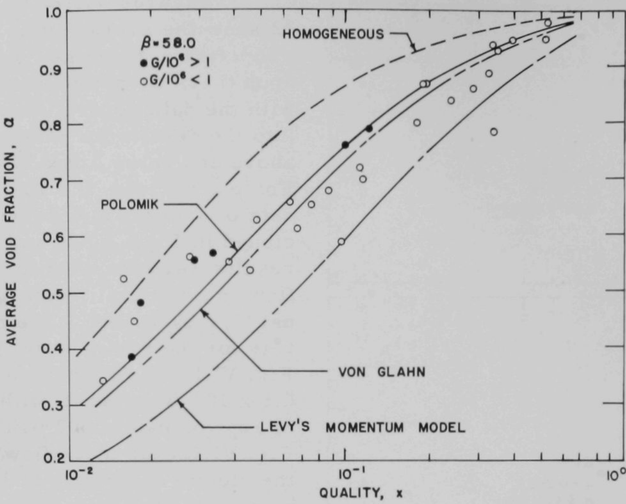

Fig. VI.18. Average Void Fraction for an Orthobaric-density Ratio of 58.0

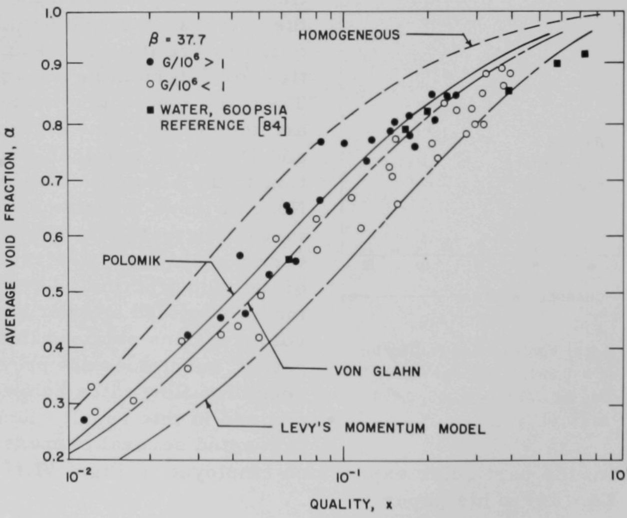

Fig. VI.19. Average Void Fraction for an Orthobaric-density Ratio of 37.7

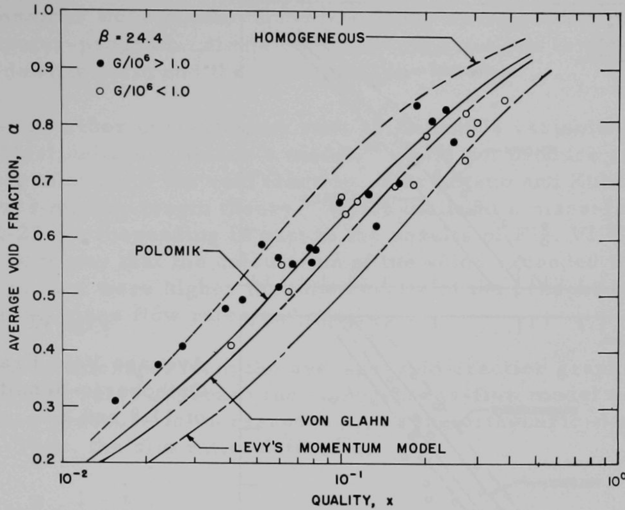

Fig. VI.20. Average Void Fraction for an Orthobaric-density Ratio of 24.4

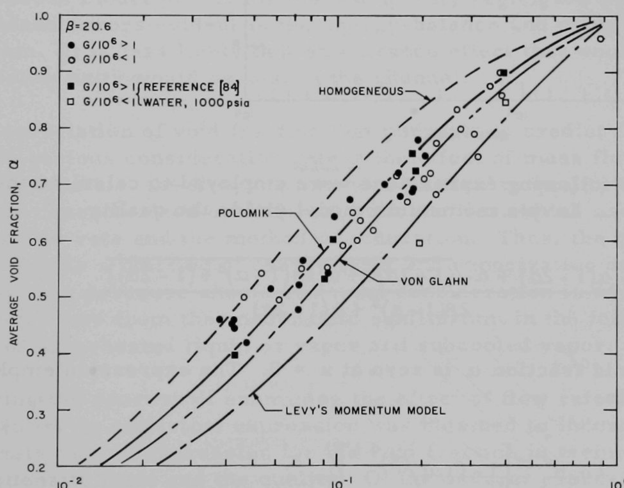

Fig. VI.21. Average Void Fraction for an Orthobaric-density Ratio of 20.6

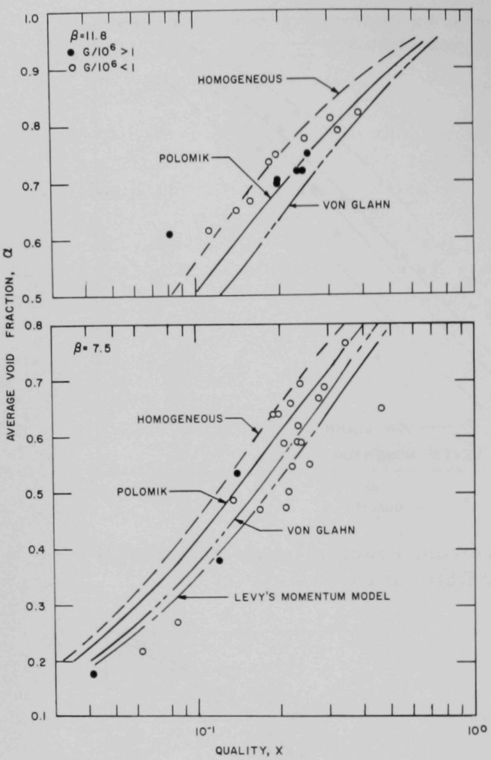

Fig. VI.22

Average Void Fraction for Orthobaric-density Ratios of 11.8 and 7.5

The following expressions were employed to calculate the various void models. Levy's momentum model yields the quality

$$x = \frac{\alpha(1-2\alpha) + \alpha\sqrt{(1-2\alpha)^2 + \alpha[2\beta(1-\alpha)^2 + (1-2\alpha)]}}{2\beta(1-\alpha)^2 + \alpha(1-2\alpha)}, \qquad \text{(VI.C-1)}$$

when the void fraction α is zero at $x = 0$. The expression employed by von Glahn is

$$\frac{1}{x} = 1 - \beta^{0.67}\left[1 - (1/\alpha)^{(\beta)^{0.1}}\right]. \qquad \text{(VI.C-2)}$$

Expression[24] in Polomik's paper was rearranged to obtain

$$\frac{1}{x} = \frac{\beta - (\beta^{2/3} - 1)[\alpha^2(\beta^{1/3} - 1) + \alpha]}{\alpha^2(\beta^{1/3} - 1) + \alpha}. \qquad \text{(VI.C-3)}$$

These expressions were placed in the preceding forms to facilitate a digital-computer-program calculation of the correlations in terms of the orthobaric-density ratio and the void fraction.

To add further correlations, such as Bankoff's variable-density model[21] or Martinelli and Nelson's model,[88] would not produce any better results in correlation of the void fraction. Since Staub and Zuber[47] examined Levy's mixing-length theory,[89] which included a mass-flow-rate effect for R-22 corresponding in part to the results of Fig. VI.20, it should suffice to say that the calculation of the voids exceeded the R-22 data, which in turn were higher than the results of the present investigation at identical mass flow rates and qualities.

It can be inferred, from the average-void-fraction graphs, that the higher mass flow rates approach the homogeneous-flow model as the system saturation pressure is increased, i.e., as the orthobaric-density ratio decreases. Thus, the slip ratio, defined as

$$S = \frac{x}{1 - x} \frac{1 - \alpha}{\alpha}, \tag{VI.C-4}$$

approaches unity. The data points that indicate void fractions in excess of the homogeneous model ($S = 1$) for the low-quality region are probably due to the combined errors evident in the energy-balance and mass-flow-rate determination. It is less likely that an entrance effect that would lower the slip ratio below unity would persist in the channel.

<u>No</u> correlation of void fraction that purports to predict this quantity can be given serious consideration <u>unless</u> the effect of mass flow rate is included. Alternately, the flow regimes at a particular quality and system pressure are characterized by different void profiles, which are a function of the mass flow rate and the method of generation. Thus, the gradient of void generation as a function of energy input and vaporization due to a decrease in system pressure should enter the consideration in addition to the degree of departure from thermodynamic equilibrium in the form of the generation of superheated liquid or vapor and subcooled vapor.

During the process of examining the effect of flow rate upon the void-fraction results, an empirical expression was obtained to incorporate the mass flow rate into an expression for the void fraction in terms of the orthobaric-density ratio and the quality. Of the several expressions contained in Polomik's paper,[87] Eq. (22) was found to have limited agreement with data for steam-water systems. In addition, it contained no mass-flow-rate effect. By chance, it was found that a mass-flow effect could be obtained if the expression were compared with a constant mass-flow-rate line with the orthobaric-density ratio replaced by a variable that contained both the mass flow rate and the orthobaric-density ratio. The following expression is obtained:

$$x = \frac{\alpha^2(Y^{1/3} - 1) + \alpha}{Y - \alpha(Y - Y^{1/3})}, \tag{VI.C-5}$$

where α is the average void fraction, and

$$Y = \beta C(G/10^6)^n. \tag{VI.C-6}$$

An alternate expression is given as

$$\alpha = \frac{\{[x(Y - Y^{1/3}) + 1]^2 + 4xY(Y^{1/3} - 1)\}^{1/2} - [x(Y - Y^{1/3}) + 1]}{2(Y^{1/3} - 1)}. \tag{VI.C-7}$$

The mass flow rate, G, is given in lb/hr-sq ft. For systems with heat addition, the value of C is approximately 2.95, and the exponent, n, is 0.686. The apparent upper bound on the constant, C, given above is the mass flow rate corresponding to the start of wispy-annular flow. The constant mass-flow-rate lines are shown in Fig. VI.23 with Y as the parameter.

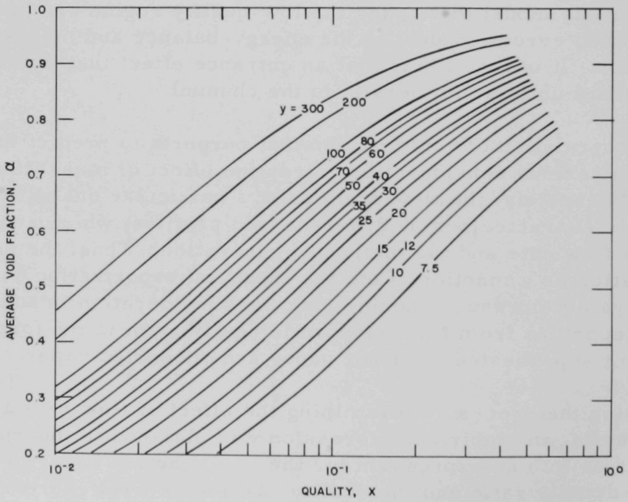

Fig. VI 23. Low-mass-flow-rate Correlation for Average Void Fraction

Figure VI.24 compares the predicted average-void fraction from Eq. (VI.C-7) with the results of three separate investigations. The data presented by Staub and Zuber[47] for R-22 at a reduced pressure of 0.12 and a β of 47.1 were obtained at various degrees of subcooling for vertical flow in a 0.4-in. tube with heat addition. The void fraction appeared to increase as the inlet conditions approached saturation. The steam-water data of Cook[90] for natural circulation in vertical, rectangular, multichannel sections have been included for a saturation pressure of 614 psia (β = 37.1). The two test runs selected were chosen on the basis of the extent of the mass quality. Steam-water void fractions obtained by Egen, Dingee, and Chastain[91] for 2000 psia (β = 7.3) are shown. The mass flow rate was constant at approximately 0.66 x 10^6 lb/hr-sq ft, but the subcooling was varied over a wide range. The greatest range of subcooling occurred in the latter case, which may account for the scatter in the results. The closer a fluid is to the saturation condition at entrance to a boiling section, the better the agreement with Eq. (VI.C-7). The upper limit of the mass flow rate that may be employed in the expression is probably a function of the level of the system pressure. Arbitrarily, the value may be set at approximately 0.7 x 10^6 lb/hr-sq ft. The mass flow rates above 1 x 10^6 lb/hr-sq ft do not follow the suggested trend indicated by the expression. Since subcooling presented a wider band of void fractions at a given quality and mass flow rate, the effect of subcooling (or heat flux level) enters the prediction of the void fraction.

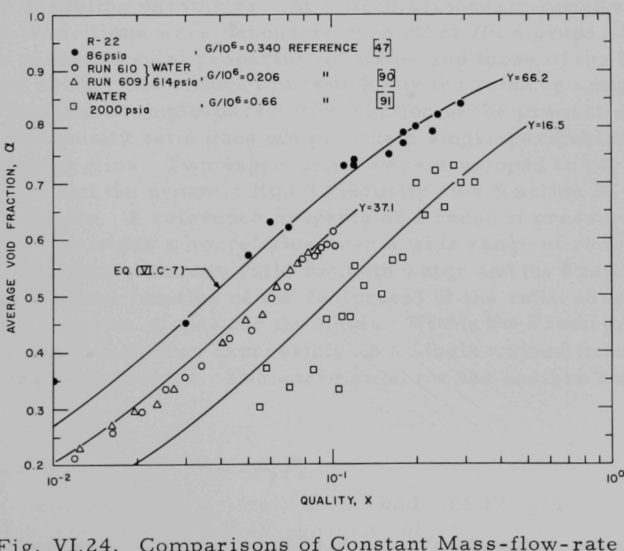

Fig. VI.24. Comparisons of Constant Mass-flow-rate Void-fraction Correlation

In summary, the average void fraction for a given orthobaric-density ratio and quality is a function of the mass flow rate and the degree of subcooling (or heat-flux level). At low mass flow rates and qualities below approximately 40%, the void fraction may be estimated by Eq. (VI.C-7) for inlet-flow conditions approaching saturation. The various graphs of the average void fraction indicate that the prediction of the void from mass quality and orthobaric-density ratio alone is not sufficient to account for the variation of experimental values. Hence, any prediction that does not incorporate a mass-flow-rate effect is at best an approximation.

In general, the higher the mass flow rate at a given quality, the higher the void fraction, or alternately, the lower the slip ratio. As the orthobaric-density ratio decreases (i.e., the system pressure increases), the nearer the void fraction approaches the homogeneous flow model. In addition, the flow regimes that occur due to the mass-flow-rate effect must be taken into account in that the void profile is altered in accordance with the particular flow regime encountered at a fixed quality.

VII. CONCLUSIONS AND RECOMMENDATIONS

The flow regimes and their transitions associated with a single-component fluid were investigated for a range of mass flow rates and qualities at a series of fixed orthobaric-density ratios. The fluid selected for this study was trichloromonofluoromethane, R-11, since it possessed a low critical pressure and temperature, which facilitated the observation of the flow patterns. In addition, the comparison of this fluid with the flow-regime results of water provides a rigorous test of any similarity analysis. The additional information of the local-void-fraction profiles and the average values for this refrigerant at elevated pressures provided data in an area that was lacking in any extensive results for either horizontal or vertical two-phase flow.

The general level of the change in physical properties of this study presented some rather simplifying relationships, which may not hold at either very high orthobaric-density ratios or near the critical point. The range of orthobaric-density ratio was from 60 to 7.5, which is considered as a range of moderate variations in thermodynamic and transport properties.

From the results of this investigation, the selection of the orthobaric-density ratio as a modeling parameter for comparison of fluids as widely divergent in their physical properties as R-11 and water was shown to be the proper basic modeling parameter. At a fixed orthobaric-density ratio, the flow-regime transitions were dependent upon other fluid properties. The examination of the physical properties of water and those of the Freon group indicated that neither the reduced pressure nor the reduced temperature were adequate to express a single-parameter function of the properties. The use of the orthobaric-density ratio does not provide a single-parameter function for the physical properties. Two expressions were developed to correlate the surface tension and the dynamic liquid viscosity as a function of the reduced saturation pressure. A reference property at a reduced pressure of 0.03 was selected, which provided a correlation over a wide range of reduced pressures. The orthobaric-density ratio for both water and the Freons could be expressed as a linear function of the reciprocal of the reduced-saturation pressure with separate slopes for the fluids. Within the Freon group, the orthobaric-density ratio was expressible as a single-valued function of the reduced saturation pressure. The correlation for the surface tension was obtained as

$$\frac{\sigma}{\sigma_{0.03}} = 0.749(P_r)^{-1/10}(1 - P_r)^2, \qquad \text{(IV.A-9)}$$

where the values of $\sigma_{0.03}$ are given in Table I. The dynamic liquid viscosity was expressed as

$$\frac{\mu_f}{\mu_{f_{0.03}}} = 0.4(P_r)^{-0.261}, \qquad \text{(IV.A-16)}$$

and the reference values are listed in Section IV.A-3.

The investigation of μ_f/σ disclosed that at identical orthobaric-density ratios, this ratio had an approximately constant value of 20/3 when R-11 was compared with water. In the examination of the fluid-property group employed by Baker,[34] this group possessed a nearly constant value of 0.25 when this grouping was compared for R-11 and water at identical orthobaric-density ratios. The errors involved in Baker's paper were considered in Section II.B.

The flow regimes observed by the fluoroscope method and in the high-speed, color motion pictures were categorized as bubble, churn (or semi-annular), wispy-annular, and annular flow. The appearance of the distinctive flow regime termed wispy-annular flow agreed with the recent observations of the Harwell group[27] for water. An agglomerated, entrained, liquid phase was transported in the vapor core while there was a slow-moving liquid film on the walls. This entrainment of liquid ligaments probably occurred through the shearing of wave crests and the break-up of liquid bridges. The break-up of these ligaments into droplets leads to the dispersed annular-flow regime. There was an absence of plug flow at elevated pressures. The churn-flow regime was employed as a descriptive term for both churn-slug and churn-annular flow.

The flow-regime data were presented in the form of a graph of superficial vapor and superficial liquid velocity for fixed orthobaric-density ratios. A comparison of the transition zones obtained for the refrigerant, R-11, did not correspond to the values indicated for steam-water systems. The linearized stability analyses, which led to the Taylor-Helmholtz and Kelvin-Helmholtz stability criteria, were examined. Application of these results led to a transition expression for churn to annular flow, which could be represented as either a function of the surface-tension and liquid-saturation-density ratios between R-11 and water, or as a function of the liquid (or vapor) saturation-density ratio alone when the fluids were compared at identical orthobaric-density ratios. The resultant expression for the transition from churn to annular flow was

$$V_{sg} = 0.9(g_c D)^{1/2} (\beta - 1)^{1/2} \left[\frac{\rho_{g_{H_2O}} \sigma}{\sigma_{H_2O} \rho_g}\right]^{1/2} + 0.6\beta^{1/2} V_{s\ell}, \qquad \text{(VI.B-3)}$$

which was a modification of the Haberstroh and Griffith result.[18] The transition could also be expressed as

$$V_{sg} = 0.9(g_c D)^{1/2} (\beta - 1)^{1/2} \frac{\rho_{g_{H_2O}}}{\rho_g} + 0.6 \beta^{1/2} V_{s\ell}, \qquad \text{(VI.B-4)}$$

where the superficial velocities are expressed in ft/sec. It was not possible to distinguish between a purely inertial, controlled system and one in which the interfacial forces are dominant. The values obtained for the modifying factors for the churn-to-annular transition expression are relatively constant over the test range and are approximately 0.49, 0.61, and 0.70 for the Taylor-Helmholtz, vapor-density ratio, and Kelvin-Helmholtz methods, respectively.

The transition from churn to wispy-annular flow occurred at higher values of the superficial vapor velocity for water than for R-11 at identical orthobaric-density ratios. An expression in which no diameter effect is included was obtained for the transition from churn to wispy-annular flow as

$$\frac{V_{sg}}{\beta^{1/2}} + 0.194 V_{s\ell} = 1.6 \left[\frac{\rho_{g_{R-11}}}{\rho_g}\right]^{1/2}, \qquad \text{(VI.B-12)}$$

where the velocities are expressed in ft/sec, and the vapor densities are evaluated at identical orthobaric-density ratios. This expression intersects the churn-to-annular-flow expression. However, physically, there does not appear to be a sharp discontinuity in these transitions. A smoothed transition line was shown in the plot of mass flow rate versus quality in Fig. VI.7 joining the two expressions. The expression given by Eq. (VI.B-12) would result in the vanishing of this regime at a superficial liquid velocity greater than the actual value since the bubble-flow transition was not considered in the limiting value.

The transition from wispy-annular flow to annular flow occurred at nearly constant superficial liquid velocity at a given orthobaric-density ratio. There was not a great spread in the transition zone on the plot of superficial velocity. A nearly cube root of the orthobaric-density-ratio dependency was noted in the data for the transition. An approximate expression was obtained for the wispy-annular to annular flow transition as

$$V_{sg} = 25 V_{s\ell} - 150 D_1/\beta^{1/3}, \qquad \text{(VI.B-13)}$$

where D_1 was unity for R-11. A comparison of the transition for water at identical orthobaric-density ratios indicated that some factor separated the data from the R-11 results. The cube-root dependency appeared to hold for the water results also. The factor D_1 may involve the surface tension and the viscosity of the fluids. However, it was indicated previously that the differentiation between the inertial effects and the interfacial effects was not possible. As an approximation for the variation of D_1 between the water data and R-11, the following expression was given

$$D_1 \sim \rho_{f_{R-11}} / \rho_{f_{H_2O}}, \tag{VI.B-14}$$

which leads to identical transition lines in Fig. VI.7.

In conclusion, the transitions observed at elevated pressures are best correlated in terms of the orthobaric-density ratio. That another fluid-property term is required to translate results from one fluid system to another was expected from thermodynamic considerations. The linear-stability analyses for open systems presented reasonable bounds for the transitions. An extensive examination of the stability relationships is required to determine more precise information for fluid flow in closed systems.

The results of the void-fraction determinations indicate that no present correlation that excludes the mass-flow-rate effect can be considered adequate. It would also appear that subcooling or the heat-flux level must be taken into account for an adequate account of the variables involved. This factor becomes evident when the expression that was obtained for the mass-flow-rate effect was examined in Fig. VI.24. For mass flow rates below approximately 0.7 x 10^6 lb/hr-sq ft, the following expression was determined for the average void fraction

$$\alpha = \frac{\{[x(Y - Y^{1/3}) + 1]^2 + 4xY(Y^{1/3} - 1)\}^{1/2} - [x(Y - Y^{1/3}) + 1]}{2(Y^{1/3} - 1)}, \tag{VI.C-7}$$

where $Y = \beta C(G/10^6)^n$; C is approximately 2.95, and the exponent n is 0.686. This result was compared to steam-water and R-22 systems with good success for fluids that are near saturation at entrance to the heated section. It is concluded, from this investigation, that the flow regime is important in the determination of the void fraction in a given system, since the average void fraction is not uniquely determined from the knowledge of the mass quality and the system-saturation conditions. The increase in mass flow rate, in general, tends to increase the void fraction at a fixed quality and orthobaric-density ratio. The average void fraction approaches the homogeneous flow model as the system pressure approaches the critical point. This was evident in the absence of distinguishing characteristics in the flow patterns at elevated pressures, i.e., at low orthobaric-density ratios.

The following recommendations for continued investigations are made:

1. The findings of the flow-regime transitions obtained in this study should be extended to liquid-metal systems. A cursory look at the available literature of the therodynamic and transport properties of liquid metals

indicates that some of the general property relationships obtained in this investigation can be applied. The use of the fluoroscope and X-ray unit would facilitate an investigation of this type. In addition, it would be recommended that single-plate, X-ray photographs be utilized. This may entail a modification of the present unit, but the results would be beneficial in obtaining results that could not be photographed under the high-speed, color, motion-picture techniques employed in this study. Several orthobaric-density-ratio levels could be investigated to determine the correspondence.

2. The high-speed, color motion pictures of the type obtained in this investigation should be given further study to determine local bubble and liquid velocities as well as wave velocities and amplitudes in annular flow. A more comprehensive photographic study at a low-pressure level can be initiated to determine the zone of entrainment of liquid droplets. The precise causes for the development and termination of the wispy-annular flow regime should be examined, both experimentally and analytically.

3. The effect of diameter has not been established in any of the investigations to a satisfactory degree. It would be beneficial to consider a fixed external loop and to vary the shape, size, and length of the test facility. In particular, the proper equivalent diameter to be employed for non-circular conduits must be established.

4. An extension of the investigation to flow regimes in the subcooled boiling region to determine the effect of heat-flux level and mass flow rate upon the patterns would be a logical extension of the program of employing fluids for simulation of steam-water systems. However, it should be established to what extent both plug and bubble flow exist in fluid systems such as R-11 in comparison with the steam-water systems. The governing factors in these flow regimes are unknown for systems involving single-component fluids at elevated pressures.

5. In an intermediate region along the saturation curve, the viscosity and surface tension undergo a large gradient as the orthobaric-density ratio decreases. This region is between the atmospheric air-water studies and the present investigation. A further examination of the flow patterns and their transitions in this region may present more complicated functional relationships, and this realm should be investigated. This area may present the greatest problems for analysis, since the gradients of the various properties should be taken into account.

6. In the selection of the particular fluorocarbon as a modeling fluid, the fluid must be chosen on the basis of the operating temperature level that will be attained by the system. To reduce the uncertainty in the energy balance, the test fluid should be such that the operating temperature of the equipment is at, or near, room temperature. The order-of-magnitude difference in the latent heat of vaporization between the refrigerants and water is the prime factor in modeling accuracy for heat-transfer results.

APPENDIX A

Void-fraction Correction

During the experimentation, empty and full determinations were carried out with the void-traverse equipment. In general, the empty and full readings did not coincide with the temperature of the particular test run. Therefore, these readings had to be corrected to the test condition. The following derivations were made for the correction factors. A series of test empty-full determinations was instituted to verify the derivations and the assumptions made. Within the accuracy of the equipment involved, the test results verified the correction factors developed in the following paragraphs.

The voltage output for an empty reading is

$$v_E = C_1 \exp(-u_g x_0),$$

where

$$C_1 = v_E C_0 / I_E.$$

The voltage output for a full reading is

$$v_F = C_1 \exp(-u_f x_0).$$

The above relationships hold if the empty and full readings are taken at the same temperatures; otherwise, $C_1 = C_1(T)$, $u_g = u_g(T)$, and $u_f = u_f(T)$. The absorption coefficient can be approximated by

$$u_g = a\rho_g \quad \text{and} \quad u_f = a\rho_f,$$

where a is a proportionality constant.

If the empty reading is taken at a different pressure but at the same temperature as the full reading, it follows that

$$v_E'/v_F = \exp[x_0(u_f - u_g')] = \exp[ax_0(\rho_f - \rho_g')], \tag{A-1}$$

and

$$v_E/v_F = \exp[x_0(u_f - u_g)] = \exp[ax_0(\rho_f - \rho_g)], \tag{A-2}$$

where the prime denotes the saturation condition corresponding to the different pressure for the empty reading. The above expressions may be written as

$$\ln (v'_E/v_F) = ax_0(1 - \rho'_g/\rho_f)\,\rho_f \tag{A-3}$$

$$= ax_0[1 - (1/\beta')(\rho'_f/\rho_f)]\,\rho_f, \tag{A-3a}$$

and

$$\ln (v_E/v_F) = ax_0(1 - \rho_g/\rho_f)\,\rho_f$$

$$= ax_0(1 - 1/\beta)\,\rho_f. \tag{A-4}$$

Thus, the correction is obtained as

$$\frac{\ln (v_E/v_F)}{\ln (v'_E/v_F)} = \frac{(1 - 1/\beta)}{1 - (1/\beta')(\rho'_f/\rho_f)}, \tag{A-5}$$

where the saturation-density ratio, ρ_f/ρ_g, is given as β. Now, consider an empty-full ratio obtained at a different temperature than the desired empty-full ratio. It is seen, from Eq. (A-4), that

$$\frac{\ln \left(v_E/v_F\right)_1}{\ln \left(v_E/v_F\right)_2} = \frac{\left[\rho_f(1 - 1/\beta)\right]_1}{\left[\rho_f(1 - 1/\beta)\right]_2} = k. \tag{A-6}$$

The variation in the empty-full ratios is approximately a function of the liquid-density ratios at the different temperatures when the saturation-density ratio, β, is large. For example, the saturation-density ratio for water at 1000 psia is approximately 20. Thus, $1/\beta$ is 0.05, which represents a rather small factor when the actual empty-full ratio is determined at some value of pressure not far removed from this value. The void fraction, α, can be written as

$$\alpha = \frac{\ln \left(v/v_F\right)_1 + \ln \left(v_F/v_F\right)_2}{\ln \left(v_E/v_F\right)_1}$$

$$= \frac{\ln \left(v_1/v_{F_2}\right) + \ln \left(v_{F_2}/v_{F_1}\right)}{k \ln \left(v_E/v_F\right)_2}. \tag{A-7}$$

Thus, this expression provides a means of correcting the void fraction for empty-full ratios taken at some other condition.

The expression for the full readings taken at different conditions is given by

$$\ln\left(v_{F_2}/v_{F_1}\right) = ax_0\left(\rho_{f_1} - \rho_{f_2}\right) + d_s\left(u_{s_1} - u_{s_2}\right), \tag{A-8}$$

where d_s is the thickness of the structural material and u_s is the absorption coefficient for the structural material. Hence, the additional term in the void-fraction relationship is given by

$$\frac{\ln\left(v_{F_2}/v_{F_1}\right)}{k \ln\left(v_E/v_F\right)_2} = \frac{\left(\rho_{f_1} - \rho_{f_2}\right) + \left(d_s/ax_0\right)\left(u_{s_1} - u_{s_2}\right)}{k\left(\rho_f - \rho_g\right)_2}$$

$$= \frac{\left(\rho_{f_1}/\rho_{f_2}\right) - 1}{k\left(1 - 1/\beta\right)_2} + \frac{\left(d_s/ax_0\right)\left(u_{s_1} - u_{s_2}\right)}{k\rho_{f_2}\left(1 - 1/\beta\right)_2}. \tag{A-9}$$

The evaluation of the second term on the right-hand side of Eq. (A-9) is dependent upon the ratio of the change in absorption coefficient of the structural material to the value of the absorption coefficient of the liquid. The second term may be written as

$$\left[\frac{d_s/x_0}{k(1 - 1/\beta)_2}\right]\left[\frac{u_{s_1} - u_{s_2}}{u_{f_2}}\right],$$

where d_s/x_0 is of the order of $1/8$ and $k(1 - 1/\beta)_2$ is of the order of unity. The change in the absorption coefficient for the structural material is dependent upon the change in the density of steel with temperature. Thus, the change in absorption coefficient for the structural material is negligible for small changes in temperature. Hence, the second term may be neglected. Or, the correction term may be approximated by

$$\frac{\ln\left(v_{F_2}/v_{F_1}\right)}{k \ln\left(v_E/v_F\right)_2} = \frac{\left(\rho_{f_1}/\rho_{f_2}\right) - 1}{k\left(1 - 1/\beta\right)_2}. \tag{A-10}$$

The local void fraction, α_1, is determined by

$$\alpha_1 = \frac{\ln\left(v_1/v_{F_{2_i}}\right)}{k \ln\left(v_E/v_F\right)_2} - \frac{1 - \left(\rho_{f_1}/\rho_{f_2}\right)}{k\left(1 - 1/\beta\right)_2}. \tag{A-11}$$

APPENDIX B

Properties of F-11 at High Temperatures

The orthobaric properties of trichloromonofluoromethane at elevated temperatures were obtained in a preliminary data form as mentioned in Section IV.-A and checked for consistency by the expressions obtained in that section. Table II includes the original information. The orthobaric-liquid enthalpy indicated very little deviation from a smoothed curve and was employed directly without modification in graphical form. The latent heat of vaporization showed slight deviations from a smoothed curve above a saturation temperature of 300°F and was employed in graphical form as shown in Fig. B.1.

TABLE II. Properties of F-11 at High Temperatures*

Liquid and Saturated Vapor
(preliminary)

Temp, °F	Pressure, psia	Volume, cu ft/lb		Heat Content, Btu/lb (-40°F)		
		Liquid	Vapor	Liquid	Latent	Vapor
160	61.04	0.01179	0.7176	41.23	69.89	111.12
170	70	0.01198	0.617	43.8	68.7	112.5
180	80	0.01214	0.534	46.4	67.6	114.0
190	91	0.01226	0.472	48.6	66.5	115.1
200	102	0.01239	0.422	50.8	65.4	116.2
210	117	0.01262	0.380	53.1	63.9	116.0
220	131	0.01275	0.334	55.5	62.7	118.2
230	147	0.01293	0.292	58.0	61.1	119.1
240	164	0.01312	0.263	60.5	59.5	120.0
250	182	0.01331	0.240	62.7	58.1	120.8
260	202	0.01349	0.213	65.0	56.7	121.7
270	226	0.01373	0.189	67.5	55.1	122.6
280	250	0.01396	0.169	70.0	53.5	123.5
290	276	0.0142	0.153	72.5	51.7	124.2
300	302	0.0145	0.140	75.0	50.0	125.0
310	332	0.01485	0.123	77.5	48.0	125.5
320	362	0.01525	0.110	80.0	45.7	125.7
330	395	0.0157	0.0979	83.5	42.4	125.9
340	430	0.01622	0.0868	87.0	38.7	125.7
350	468	0.01683	0.0782	90.5	34.9	125.4
360	507	0.0177	0.0667	94.0	30.8	124.8
370	545	0.01875	0.0584	98.0	25.6	123.6
380	590	0.02083	0.0458	103.0	19.3	122.3
388.4	635	0.0290	0.0290	113.4	0	113.4

*This table is through the courtesy of R. C. Downing, E.I. du Pont de Nemours & Company, Wilmington, Delaware.

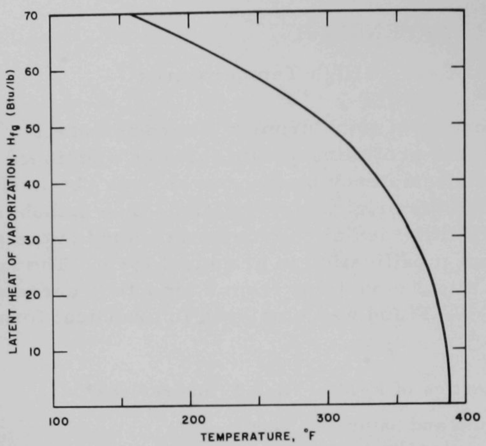

Fig. B.1

Latent Heat of Vaporization for Freon-11

The orthobaric-density ratio is shown in Figs. B.2 and B.3. This ratio had the largest deviations since it was formed from the saturated-liquid and -vapor densities that exhibited deviations individually. The saturated-liquid density is shown in Figs. B.4 and B.5.

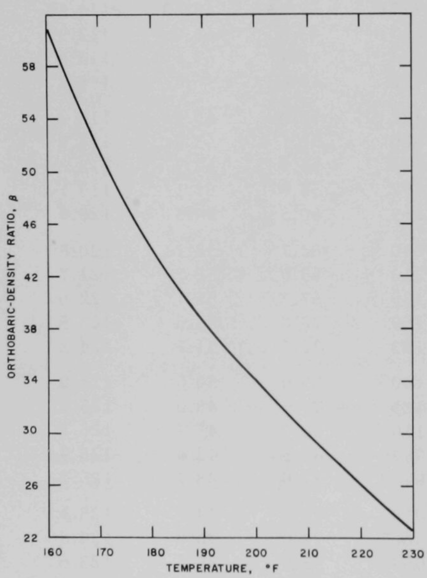

Fig. B.2. Orthobaric-density Ratio for Freon-11 at 160-230°F

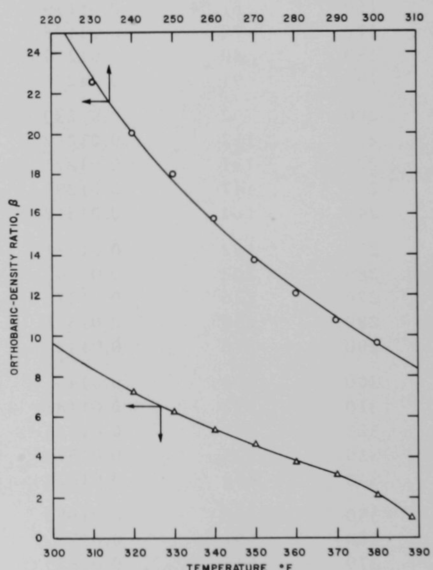

Fig. B.3. Orthobaric-density Ratio for Freon-11 at 220-390°F

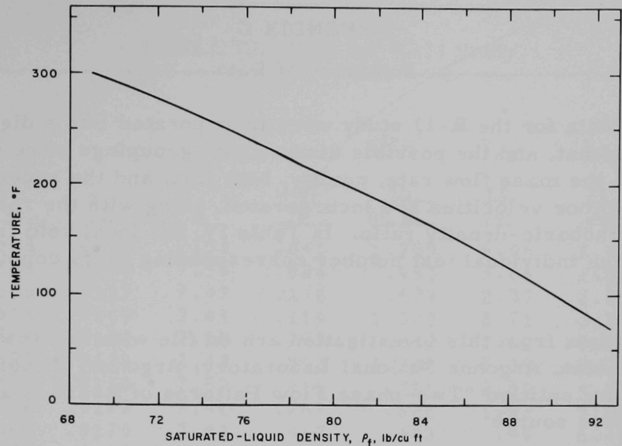

Fig. B.4. Saturated-liquid Density for Freon-11 below 300°F

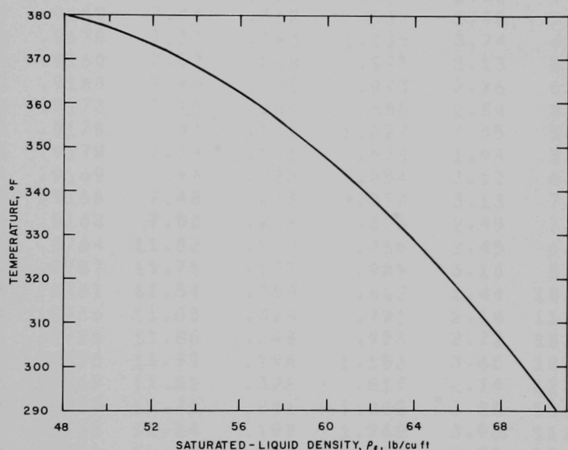

Fig. B.5. Saturated-liquid Density for Freon-11 at 290-380°F

The saturated-vapor density is not shown since it can be obtained from the included figures. The saturation line as a function of pressure and temperature is also omitted.

APPENDIX C

Summary of Data

The data for the R-11 study were incorporated into a digital-computer format, and the possible dimensional groupings were evaluated. In Table III, the mass flow rate, quality, heat flux, and the superficial liquid and vapor velocities are incorporated, along with the reduced pressure and orthobaric-density ratio. In Table IV, the local void fractions are listed with the individual test number corresponding to its counterpart in Table III.

The data from this investigation are on file with the Reactor Engineering Division, Argonne National Laboratory, Argonne, Illinois. The motion picture entitled "Two-phase Flow Patterns of R-11" is available from the above source.

TABLE III. Data for R-11 Study

Run No.	P_r	T_r	β	Qual. x	$G/10^6$, $\frac{lb}{hr\ ft^2}$	$V_{s\ell}$, $\frac{ft}{sec}$	V_{sg}, $\frac{ft}{sec}$	Heat Flux x 10^3, $\frac{Btu}{hr\ ft^2}$
1	.5568	.9159	7.54	.040	1.255	5.06	1.62	25.999
2	.5568	.9159	7.54	.084	.953	3.66	2.56	25.872
3	.5600	.9167	7.47	.170	.679	2.37	3.64	26.510
4	.5615	.9169	7.44	.119	1.000	3.71	3.75	31.574
5	.5584	.9162	7.50	.257	.682	2.12	5.55	31.574
6	.5623	.9170	7.43	.063	1.366	5.39	2.71	24.085
7	.5571	.9160	7.52	.211	.721	2.39	4.81	36.425
8	.5626	.9172	7.41	.267	.626	1.93	5.22	36.638
9	.5618	.9170	7.43	.467	.443	.99	6.48	35.702
10	.5677	.9183	7.32	.236	.519	1.67	3.79	27.744
11	.5582	.9162	7.50	.198	.996	3.36	6.22	45.574
12	.5590	.9166	7.48	.219	.724	2.38	5.01	34.851
13	.5614	.9169	7.44	.342	.537	1.48	5.78	34.978
14	.5644	.9178	7.37	.143	1.035	3.74	4.61	42.170
15	.5573	.9160	7.52	.208	.941	3.13	6.20	44.553
16	.5612	.9168	7.46	.238	.893	2.86	6.71	45.191
17	.5628	.9173	7.40	.289	.680	2.04	6.14	37.063
18	.5620	.9170	7.43	.139	1.227	4.45	5.37	42.765
19	.5653	.9179	7.34	.191	.570	1.94	3.39	21.574
20	.5614	.9169	7.44	.223	.954	3.12	6.67	39.872
21	.5588	.9166	7.48	.233	.970	3.13	7.13	39.744
22	.5582	.9162	7.50	.276	.806	2.45	7.03	38.127
23	.4086	.8764	11.82	.179	.766	2.45	6.36	28.510
24	.4099	.8767	11.78	.197	.989	3.10	8.98	40.297
25	.4078	.8761	11.84	.384	.602	1.44	10.70	44.042
26	.4094	.8766	11.80	.304	.791	2.14	11.10	46.680
27	.4078	.8760	11.86	.248	.928	2.72	10.67	46.170
28	.4070	.8758	11.90	.198	1.153	3.60	10.63	45.872
29	.4088	.8765	11.81	.326	.817	2.14	12.30	50.978
30	.4096	.8767	11.78	.241	1.082	3.20	12.04	51.872
31	.4080	.8761	11.84	.197	1.268	3.96	11.57	51.872
32	.4100	.8768	11.77	.234	1.253	3.74	13.52	59.106
33	.4103	.8768	11.77	.254	1.191	3.46	13.95	60.255
34	.4110	.8770	11.75	.081	1.022	3.67	3.80	19.191
35	.4086	.8764	11.82	.110	.814	2.82	4.15	18.978
36	.4086	.8764	11.82	.147	.678	2.25	4.61	20.808
37	.4086	.8764	11.82	.156	.917	3.01	6.63	29.787

TABLE III (Contd.)

Run No.	P_r	T_r	β	Qual. x	$G/10^6$, $\frac{lb}{hr\ ft^2}$	$V_{s\ell}$, $\frac{ft}{sec}$	V_{sg}, $\frac{ft}{sec}$	Heat Flux $\times 10^3$, $\frac{Btu}{hr\ ft^2}$
38	.2527	.8221	20.69	.187	1.015	2.99	14.33	44.723
39	.2527	.8221	20.69	.318	.679	1.68	16.25	47.276
40	.2535	.8226	20.60	.168	.789	2.38	9.98	31.787
41	.2511	.8214	20.85	.133	.947	2.97	9.58	31.489
42	.2527	.8221	20.69	.225	.598	1.68	10.14	31.319
43	.2503	.8211	20.92	.313	.459	1.14	10.93	31.531
44	.2521	.8216	20.82	.047	1.944	6.72	6.91	33.063
45	.2505	.8212	20.92	.058	1.673	5.72	7.38	33.276
46	.2537	.8227	20.56	.073	1.369	4.61	7.48	33.021
47	.2513	.8215	20.84	.092	1.179	3.88	8.21	33.021
48	.2521	.8216	20.84	.125	.925	2.93	8.81	33.148
49	.2505	.8212	20.92	.181	.925	2.74	12.73	46.085
50	.2535	.8226	20.60	.072	1.912	6.45	10.31	45.999
51	.2535	.8226	20.60	.093	1.642	5.41	11.47	46.510
52	.2511	.8214	20.85	.107	1.497	4.85	12.15	47.361
53	.2511	.8214	20.85	.119	1.403	4.48	12.64	48.042
54	.2496	.8206	21.06	.155	1.161	3.56	13.85	48.297
55	.2543	.8228	20.56	.182	.948	2.81	12.96	46.638
56	.2519	.8215	20.82	.268	.741	1.96	15.08	48.085
57	.2525	.8220	20.70	.042	1.866	6.49	5.92	23.361
58	.2541	.8227	20.56	.041	1.668	5.81	5.21	23.361
59	.2541	.8227	20.56	.057	1.481	5.07	6.35	23.361
60	.2518	.8214	20.85	.075	1.321	4.43	7.50	23.531
61	.2518	.8214	20.85	.096	1.139	3.73	8.35	23.531
62	.2518	.8214	20.85	.091	.964	3.17	6.69	24.042
63	.2518	.8214	20.85	.126	.700	2.22	6.68	23.914
64	.2532	.8224	20.60	.147	1.946	6.02	21.42	61.702
65	.2492	.8206	21.06	.164	1.679	5.08	21.10	61.617
66	.2516	.8214	20.85	.193	1.452	4.25	21.21	61.702
67	.2532	.8224	20.60	.205	1.370	3.95	21.06	61.787

TABLE III (Contd.)

Run No.	P_r	T_r	β	Qual. x	$G/10^6$, $\frac{lb}{hr\ ft^2}$	$V_{s\ell}$, $\frac{ft}{sec}$	V_{sg}, $\frac{ft}{sec}$	Heat Flux $\times 10^3$, $\frac{Btu}{hr\ ft^2}$
68	.2518	.8214	20.85	.166	1.126	3.40	14.15	43.999
69	.2533	.8225	20.60	.184	1.030	3.05	14.26	43.744
70	.2518	.8214	20.85	.223	.886	2.49	14.95	44.340
71	.2510	.8213	20.85	.277	.728	1.91	15.29	44.595
72	.2510	.8213	20.85	.388	.544	1.20	15.99	44.553
73	.2502	.8208	21.00	.874	.251	.11	16.77	44.170
74	.2502	.8208	21.00	.120	.888	2.83	8.16	24.553
75	.2518	.8214	20.85	.151	.723	2.22	8.27	24.382
76	.2510	.8213	20.85	.202	.556	1.60	8.50	24.212
77	.2494	.8206	21.06	.307	.388	.97	9.13	24.893
78	.2525	.8220	20.70	.042	1.200	4.17	3.84	15.148
79	.2525	.8220	20.70	.061	.943	3.21	4.35	15.063
80	.2533	.8225	20.60	.074	.843	2.83	4.68	15.148
81	.2518	.8214	20.85	.104	.640	2.08	5.06	15.106
82	.2510	.8213	20.85	.177	.405	1.20	5.44	15.574
83	.2486	.8202	21.15	.213	.342	.97	5.60	15.574
84	.2525	.8220	20.75	.146	1.054	3.26	11.65	34.680
85	.2494	.8206	21.06	.175	.854	2.55	11.42	34.382
86	.2533	.8225	20.60	.350	.469	1.10	12.29	34.212
87	.2510	.8213	20.85	.265	.489	1.30	9.85	28.297
88	.2510	.8213	20.85	.380	.357	.80	10.29	28.553
89	.2510	.8213	20.85	.873	.160	.07	10.58	28.553
90	.2525	.8220	20.75	.110	1.039	3.35	8.61	27.872
91	.2494	.8206	21.06	.162	.749	2.27	9.31	27.999
92	.2533	.8225	20.60	.037	1.065	3.72	3.00	11.617
93	.2518	.8214	20.85	.045	.947	3.27	3.29	11.659
94	.2510	.8213	20.85	.053	.827	2.84	3.33	11.574
95	.2525	.8220	20.75	.070	.667	2.25	3.53	11.531
96	.2502	.8208	21.00	.113	.463	1.49	3.99	11.531
97	.2502	.8208	21.00	.162	.324	.98	4.01	11.659

TABLE III (Contd.)

Run No.	P_r	T_r	β	Qual. x	$G/10^6$, $\frac{lb}{hr\ ft^2}$	$V_{s\ell}$, $\frac{ft}{sec}$	V_{sg}, $\frac{ft}{sec}$	Heat Flux x 10^3, $\frac{Btu}{hr\ ft^2}$
98	.2196	.8073	24.37	.213	1.273	3.57	23.67	59.999
99	.2212	.8079	24.19	.162	1.049	3.14	14.75	40.425
100	.2192	.8070	24.40	.240	1.047	2.83	21.93	60.212
101	.2200	.8074	24.36	.295	.576	1.45	14.82	40.170
102	.2212	.8079	24.19	.134	1.274	3.94	14.83	40.680
103	.2189	.8068	24.50	.015	1.269	4.46	1.73	12.893
104	.2174	.8061	24.72	.022	1.060	3.69	2.06	12.978
105	.2182	.8063	24.69	.040	.848	2.90	3.02	13.106
106	.2174	.8061	24.72	.065	.614	2.04	3.57	13.319
107	.2218	.8083	24.00	.027	1.290	4.48	3.05	20.297
108	.2195	.8071	24.39	.044	1.056	3.60	4.09	20.468
109	.2203	.8074	24.36	.078	.792	2.60	5.38	20.765
110	.2187	.8077	24.18	.183	.419	1.22	6.64	20.297
111	.2211	.8077	24.18	.060	1.244	4.17	6.51	29.702
112	.2179	.8062	24.67	.038	1.151	3.94	3.92	20.170
113	.2179	.8062	24.67	.061	.918	3.07	4.98	20.468
114	.2187	.8077	24.18	.105	.587	1.87	5.34	20.297
115	.2199	.8073	24.37	.280	.325	.83	7.95	20.468
116	.2171	.8060	24.65	.078	1.049	3.44	7.20	29.617
117	.2190	.8070	24.40	.101	.847	2.71	7.46	27.872
118	.2182	.8063	24.69	.310	.422	1.03	11.54	29.787
119	.2182	.8063	24.69	.203	.544	1.54	9.76	29.489
120	.2182	.8063	24.69	.188	1.058	3.06	17.57	55.872
121	.2196	.8073	24.37	.258	1.134	3.00	25.51	58.212
122	.2196	.8073	24.37	.282	.938	2.40	23.02	57.787
123	.2196	.8073	24.37	.388	.705	1.53	23.86	57.531
124	.2192	.8071	24.39	.052	1.624	5.49	7.41	32.255
125	.2200	.8074	24.36	.060	1.408	4.72	7.42	32.212
126	.2215	.8081	24.10	.077	1.212	3.99	8.12	32.978
127	.2215	.8081	24.10	.116	.935	2.95	9.37	32.595
128	.2200	.8073	24.37	.067	1.889	6.28	11.10	45.702
129	.2184	.8064	24.68	.081	1.683	5.51	12.05	45.617
130	.2181	.8063	24.69	.099	1.403	4.50	12.31	45.872
131	.2181	.8063	24.69	.125	1.186	3.70	13.11	45.957
132	.2181	.8063	24.69	.157	.970	2.91	13.48	45.999

TABLE III (Contd.)

Run No.	P_r	T_r	β	Qual. x	$G/10^6$, $\frac{lb}{hr\ ft^2}$	$V_{s\ell}$, $\frac{ft}{sec}$	V_{sg}, $\frac{ft}{sec}$	Heat Flux $\times 10^3$, $\frac{Btu}{hr\ ft^2}$
163	.1496	.7701	36.80	.057	.880	2.82	6.29	21.914
164	.1502	.7705	36.65	.107	.553	1.68	7.38	22.042
165	.1518	.7714	36.35	.012	.505	1.71	.76	10.425
166	.1486	.7694	37.08	.114	.858	2.60	12.49	28.638
167	.1464	.7682	37.52	.156	.669	1.92	13.42	27.957
168	.1455	.7676	37.78	.316	.400	.93	16.33	28.978
169	.1472	.7686	37.45	.212	1.325	3.56	35.97	66.936
170	.1456	.7678	37.78	.251	1.147	2.92	37.25	67.319
171	.1467	.7683	37.50	.012	.997	3.36	1.62	4.978
172	.1459	.7680	37.65	.017	.750	2.51	1.68	4.893
173	.1451	.7674	37.96	.027	.550	1.82	1.95	4.978
174	.1462	.7681	37.57	.044	.340	1.11	1.92	4.893
175	.1444	.7668	38.10	.049	.271	.88	1.75	4.978
176	.1395	.7639	39.42	.173	1.214	3.40	28.24	45.361
177	.1442	.7668	38.10	.323	.623	1.44	26.21	45.404
178	.1447	.7670	38.08	.287	.683	1.66	25.56	45.148
179	.1439	.7665	38.19	.180	1.117	3.12	26.30	45.787
180	.1434	.7663	38.25	.206	.966	2.61	26.06	46.042
181	.1450	.7673	37.95	.027	2.029	6.73	7.20	18.723
182	.1447	.7670	38.08	.035	1.753	5.76	8.19	18.723
183	.1447	.7670	38.08	.044	1.579	5.15	9.10	18.723
184	.1447	.7670	38.08	.053	1.342	4.33	9.41	18.723
185	.1447	.7670	38.08	.067	1.123	3.57	9.83	18.893
186	.1439	.7665	38.19	.082	1.614	5.05	17.33	32.553
187	.1447	.7670	38.08	.100	1.381	4.24	17.96	32.723
188	.1447	.7670	38.08	.125	1.167	3.48	19.04	34.297
189	.1455	.7676	37.78	.153	.926	2.67	18.30	33.234
190	.1451	.7674	37.96	.062	2.026	6.48	16.38	33.744
191	.1451	.7674	37.96	.071	1.844	5.84	17.10	33.319
192	.1447	.7670	38.08	.122	1.957	5.86	31.04	61.319
193	.1448	.7672	38.00	.153	1.813	5.23	36.12	62.212
194	.1448	.7672	38.00	.171	1.624	4.59	36.11	61.702
195	.1433	.7663	38.25	.207	1.340	3.62	36.19	61.191
196	.1440	.7667	38.18	.234	1.200	3.13	36.68	61.191

TABLE III (Contd.)

Run No.	P_r	T_r	β	Qual. x	$G/10^6$, $\frac{lb}{hr\ ft^2}$	$V_{s\ell}$, $\frac{ft}{sec}$	V_{sg}, $\frac{ft}{sec}$	Heat Flux $\times 10^3$, $\frac{Btu}{hr\ ft^2}$
197	.0980	.7332	58.70	.237	.203	.51	9.36	12.851
198	.0966	.7319	59.80	.048	.830	2.59	7.85	12.978
199	.0966	.7319	59.80	.048	.830	2.59	7.85	12.978
200	.0980	.7332	58.70	.045	.209	.65	1.82	4.093
201	.0980	.7332	58.70	.086	.271	.81	4.55	8.510
202	.0948	.7306	60.75	.027	.618	1.97	3.35	8.765
203	.0964	.7318	59.80	.180	.273	.73	9.67	12.851
204	.0980	.7332	58.70	.115	.430	1.25	9.56	13.021
205	.0984	.7336	58.30	.075	.627	1.90	9.06	13.148
206	.0972	.7326	59.10	.017	.357	1.15	1.20	4.012
207	.0984	.7336	58.30	.096	.108	.32	2.00	4.093
208	.0972	.7326	59.10	.334	.090	.19	5.87	8.595
209	.0933	.7294	61.75	.015	.954	3.07	3.02	8.723
210	.0966	.7319	59.80	.350	.319	.68	21.99	27.829
211	.0958	.7316	60.00	.334	.340	.74	22.44	28.638
212	.0958	.7316	60.00	.515	.395	.62	40.19	51.191
213	.1005	.7353	57.00	.099	1.002	3.02	19.11	38.595
214	.0970	.7321	59.05	.189	.565	1.50	20.81	28.042
215	.0942	.7297	61.60	.525	.219	.34	23.29	28.255
216	.0942	.7297	61.60	.394	.522	1.03	41.57	51.659
217	.0966	.7319	59.80	.192	.925	2.45	34.94	50.893
218	.0974	.7327	59.00	.323	.452	1.00	28.43	39.574
219	.0974	.7327	59.00	.121	1.056	3.04	24.86	39.574
220	.0990	.7340	58.00	.028	1.236	3.95	6.75	11.744
221	.0971	.7325	59.10	.018	1.218	3.93	4.33	8.468
222	.0982	.7334	58.50	.013	.892	2.89	2.29	6.085

TABLE III (Contd.)

Run No.	P_r	T_r	β	Qual. x	$G/10^6$, $\frac{lb}{hr\ ft^2}$	$V_{s\ell}$, $\frac{ft}{sec}$	V_{sg}, $\frac{ft}{sec}$	Heat Flux $\times 10^3$, $\frac{Btu}{hr\ ft^2}$
223	.1146	.7463	48.90	.146	1.329	3.77	31.71	53.148
224	.1096	.7424	51.60	.495	.533	.89	45.26	62.893
225	.1020	.7366	56.00	.525	.427	.66	41.53	52.638
226	.1036	.7377	55.10	.062	.756	2.34	8.60	12.936
227	.1058	.7399	53.40	.111	.433	1.27	8.59	13.021
228	.1081	.7413	52.40	.075	.632	1.93	8.25	12.936
229	.1007	.7354	57.00	.033	1.316	4.19	8.26	12.808
230	.0998	.7346	57.60	.016	1.071	3.46	3.43	6.097
231	.0968	.7325	59.50	.038	.544	1.72	4.04	6.170
232	.0976	.7327	59.20	.066	.309	.94	4.02	6.170
233	.1039	.7383	54.70	.282	.308	.73	15.73	21.872
234	.1036	.7377	55.10	.062	.756	2.34	8.60	12.936
235	.1088	.7420	51.90	.217	.227	.58	8.51	13.234
236	.0995	.7344	57.80	.044	1.080	3.39	9.20	12.765
237	.1023	.7372	55.50	.005	1.316	4.32	1.27	6.097
238	.0985	.7337	58.40	.020	.875	2.82	3.52	6.170
239	.0976	.7327	59.20	.066	.309	.94	4.02	6.170
240	.0946	.7305	60.90	.040	.306	.96	2.49	4.059
241	.1039	.7383	54.70	.005	2.143	7.04	2.27	28.808
242	.1192	.7498	46.60	.253	.910	2.27	35.98	72.851
243	.1018	.7364	56.20	.000	2.420	7.98	.08	28.595
244	.1058	.7398	53.50	.073	.887	2.72	11.55	29.234
245	.1102	.7432	51.00	.291	1.022	2.40	50.48	74.042
246	.1118	.7445	50.10	.139	1.866	5.34	43.36	74.510
247	.1118	.7445	50.10	.139	1.866	5.34	43.36	74.510

TABLE IV. Void Data for R-11 Study

Run No.	Local Void Values										
1	.3200	.2559	.1378	.1278	.1405	.1486	.1559	.1540	.1344	.1483	.1508	.1452
2	.2534	.3238	.2690	.2579	.2865	.2968	.3099	.3257	.3063	.3000	.2119	.2757
3	.4156	.4754	.4554	.4765	.5170	.5374	.5400	.5285	.4782	.4383	.3780	.3584
4	.3992	.4299	.3756	.3539	.3902	.4186	.4024	.4054	.3666	.3954	.3279	.3160
5	.4563	.5714	.5424	.5468	.5938	.6153	.5771	.5751	.5467	.5098	.4974	.5778
6	.2087	.2738	.2089	.2355	.2399	.2250	.2232	.2356	.1988	.2071	.1731	.1869
7	.3770	.4583	.4601	.4903	.5309	.5639	.5567	.5515	.4705	.4464	.3947	.3932
8	.4150	.4747	.5317	.5213	.5591	.5924	.5934	.5795	.5299	.4891	.3999	.3577
9	.7123	.7167	.6213	.6099	.6280	.6470	.6581	.6333	.6141	.6318	.6303	.6770
10	.7067	.6770	.7147	.6763	.6419	.6416	.6332	.6438	.6487	.6701	.7252	.8505
11	.3642	.5341	.6199	.6325	.6366	.6456	.6154	.6097	.6047	.5897	.6767	.8546
12	.3232	.5971	.6726	.6799	.6640	.6668	.6244	.6316	.6300	.5962	.6763	.7702
13	.4429	.7609	.7497	.7415	.7120	.7359	.6912	.6935	.6924	.6961	.7835	.9594
14	.2221	.4474	.5465	.5515	.5644	.5768	.5916	.5616	.5444	.5171	.5778	.6657
15	.4995	.5835	.6146	.6101	.6230	.6129	.6086	.6119	.6036	.5721	.5964	.7338
16	.4063	.5927	.6474	.6247	.6240	.6456	.6323	.6293	.6185	.5914	.5942	.6782
17	.7933	.7285	.7322	.6935	.6828	.6762	.6729	.6704	.6914	.6787	.6655	.6773
18	.5992	.5812	.6122	.6313	.6302	.5977	.6224	.6226	.6183	.5625	.4446	.3417
19	.7542	.7383	.7547	.7444	.6911	.6845	.6909	.6854	.7101	.7053	.6597	.4893
20	.3563	.5199	.5876	.5875	.5726	.5688	.6064	.5899	.5843	.5445	.5203	.5248
21	.7100	.6323	.5945	.6152	.6272	.6305	.6044	.6228	.6083	.5904	.6552	.6786
22	.7438	.6789	.6333	.6293	.6310	.6375	.6285	.6435	.6257	.6396	.6769	.5607
23	.5751	.7203	.7980	.8273	.8342	.8640	.8461	.8324	.8136	.7860	.7135	.4955
24	.7838	.7861	.7802	.7973	.8018	.8164	.8054	.7997	.7961	.7845	.7346	.6794
25	.8191	.9073	.9063	.8926	.8948	.8943	.8670	.8724	.8827	.9027	.8251	.5894
26	.8176	.8415	.8512	.8353	.8327	.8534	.8446	.8617	.8437	.8518	.8236	.7242
27	.6818	.8258	.8367	.8147	.8249	.8487	.8220	.8324	.8358	.8299	.7809	.6354
28	.5758	.6994	.7229	.7319	.7508	.7401	.7368	.7385	.7072	.7352	.7369	.5901
29	.7853	.8327	.7882	.8052	.8095	.8272	.8069	.8075	.8072	.8366	.8163	.6809
30	.5372	.7331	.7539	.7621	.7769	.7790	.7532	.7586	.7542	.7674	.7346	.6339
31	.5751	.6915	.7288	.7475	.7469	.7805	.7609	.7601	.7492	.7517	.6906	.5894
32	.6095	.7260	.7605	.7814	.7769	.7601	.7594	.7681	.7639	.7674	.7436	.7242
33	.6451	.7544	.7605	.7942	.7800	.7790	.7748	.7840	.7801	.7845	.7571	.6339
34	.3723	.5875	.6638	.7334	.7511	.7623	.7529	.7236	.6954	.6428	.5130	.3910
35	.4919	.6236	.7005	.7516	.7786	.7638	.7769	.7641	.7510	.6514	.4915	.2750
36	.5771	.7027	.7422	.7914	.8013	.7896	.7866	.7641	.7409	.7049	.6178	.4497
37	.5490	.6653	.7249	.7649	.7786	.7799	.7866	.7641	.7510	.6943	.5372	.4686

TABLE IV (Contd.)

Run No.	Local Void Values											
38	.7197	.6702	.7169	.7750	.7917	.7974	.7988	.7960	.7749	.7024	.6540	.4435
39	.6561	.7322	.8130	.8381	.8274	.8498	.8518	.8491	.8476	.8079	.7070	.4785
40	.0603	.6016	.6919	.7464	.7450	.7874	.7993	.7915	.7559	.7031	.6064	.5718
41	.1253	.5212	.6464	.7020	.7218	.7527	.7670	.7603	.7119	.6722	.5952	.5630
42	-.0934	.5621	.7165	.7659	.7927	.7915	.8083	.8103	.7811	.7308	.6562	.6304
43	.3807	.7635	.8133	.8466	.8265	.8414	.8548	.8551	.8568	.8340	.7596	.7064
44	.5483	.5298	.4658	.4977	.4944	.5191	.5282	.5056	.4945	.4746	.3761	.1407
45	.5932	.5464	.5036	.5757	.6035	.6232	.6256	.6159	.6031	.5416	.4475	.3466
46	.5014	.5325	.5256	.5841	.6293	.6688	.6493	.6332	.6202	.5597	.4644	.4727
47	.4875	.5298	.5538	.6414	.7014	.7167	.7099	.6784	.6524	.6066	.4176	.1314
48	.4798	.5871	.6324	.6864	.7278	.7471	.7737	.7664	.7188	.6353	.4658	.2674
49	.5635	.7099	.7213	.7650	.8023	.8188	.8243	.8080	.7689	.7410	.5913	.4068
50	.5433	.5732	.6291	.6915	.7231	.7299	.7358	.7170	.6779	.6745	.5621	.5240
51	.6408	.6315	.6458	.7228	.7523	.7723	.7748	.7369	.6952	.6804	.5913	.5051
52	.3950	.5972	.6277	.7310	.7716	.7771	.7712	.7614	.7313	.6794	.5568	.5071
53	.6618	.6226	.6841	.7495	.7745	.7993	.7987	.7809	.7369	.6705	.6078	.4102
54	.5433	.6315	.6854	.7841	.8010	.8056	.8104	.7872	.7518	.7129	.6238	.4409
55	.6912	.6743	.7757	.8292	.8432	.8521	.8508	.8365	.8125	.7907	1.0115	.5984
56	.6738	.7455	.8335	.8749	.8807	.8804	.8683	.8702	.8626	.8564	.8347	.5065
57	.3994	.4759	.5437	.5657	.6157	.6782	.6860	.6239	.5346	.5022	.4879	.4201
58	.0556	.3819	.4980	.5543	.5784	.5905	.5789	.5693	.5463	.4765	.3992	.4188
59	.3513	.4626	.5625	.6919	.6402	.6737	.6549	.6318	.5723	.5249	.4472	.3286
60	.4001	.4567	.5812	.6424	.7458	.7713	.7595	.7335	.6753	.6111	.4964	.4651
61	.3533	.5621	.6468	.7320	.7612	.8074	.8021	.8005	.7304	.6374	.5273	.4913
62	.2088	.4527	.5812	.6619	.7149	.7501	.7306	.7186	.6815	.5643	.4173	.4208
63	.3533	.4845	.6468	.7507	.7975	.8223	.7936	.7716	.7364	.6276	.4807	.5087
64	.7930	.7562	.7936	.8385	.8413	.8566	.8291	.8253	.8098	.7641	.6392	.5509
65	.7363	.7472	.7800	.8160	.8311	.8436	.8224	.8127	.7820	.7658	.7313	.8403
66	.7104	.7536	.7670	.7940	.8185	.8311	.8161	.8063	.7990	.7526	.6695	.5260
67	.6668	.7668	.7783	.8144	.8205	.8302	.8067	.8139	.7862	.7548	.6576	.5251

TABLE IV (Contd.)

Run No.	Local Void Values											
68	.7490	.7184	.7793	.7982	.8163	.8063	.8118	.7992	.7814	.7199	.5904	.4441
69	.6861	.7226	.7912	.8072	.8198	.8203	.8177	.8187	.8125	.7578	.6056	.3331
70	.7490	.7679	.8179	.8419	.8519	.8382	.8330	.8394	.8418	.8185	.7310	.6576
71	.7787	.8253	.8744	.8741	.8707	.8538	.8695	.8918	.8953	.8676	.7728	.5834
72	.8663	.8697	.9009	.9006	.9001	.9081	.9081	.9254	.9425	.9052	.7632	-.2249
73	-.0177	-.0177	-.0177	-.0177	-.0177	.9790	.9741	.9840	1.0020	.9868	.9434	.9671
74	.5229	.5900	.6977	.7567	.7861	.7905	.7691	.7668	.7312	.6412	.4600	.2981
75	.1551	.6095	.7232	.7732	.7886	.7903	.7904	.7748	.7675	.6881	.4922	.2978
76	.5617	.6708	.7709	.8063	.8162	.8115	.8196	.8340	.8226	.7625	.5730	.3717
77	.6826	.7409	.8484	.8668	.8769	.8650	.8832	.8848	.8854	.8412	.6923	.5842
78	.3938	.4530	.4867	.5504	.5719	.6079	.6112	.5985	.5689	.4454	.2904	.2212
79	.2588	.3638	.5055	.5899	.6531	.6710	.6600	.6451	.6229	.5152	.3554	.1826
80	.3576	.4517	.5656	.6451	.6840	.7034	.7092	.7091	.6831	.5233	.4027	.2199
81	.4829	.5565	.6481	.7196	.7605	.7659	.7715	.7720	.7450	.6020	.4121	.2372
82	.4961	.6419	.7625	.8118	.8354	.8380	.8302	.8206	.8034	.7053	.5487	.3717
83	.4096	.6787	.7945	.8460	.8586	.8553	.8735	.8619	.8404	.7865	.6429	.6389
84	.5746	.6969	.8198	.8640	.8690	.8961	.9178	.9145	.8555	.7966	.7167	.6085
85	.5760	.6722	.7996	.8714	.8704	.9033	.9020	.8784	.8482	.7891	.6476	.5603
86	.9125	.8954	.9240	.9337	.9336	.9665	.9644	.9529	.9537	.9312	.8649	.7243
87	.6950	.7813	.9111	.9443	.9468	.9741	.9636	.9549	.9106	.8589	.7173	.5379
88	.7604	.8973	.9612	.9819	.9692	1.0217	1.0025	.9969	.9834	.9612	.8876	.7464
89	.9349	.9986	1.0132	1.0217	1.0025	1.0272	1.0326	1.0381	1.0299	1.0190	.9954	.9412
90	.5898	.6332	.7258	.8002	.8221	.8282	.8219	.8152	.7819	.7150	.5892	.5445
91	.4669	.6346	.7652	.8261	.8412	.8623	.8818	.8697	.8307	.7530	.6059	.5388
92	.4162	.4270	.4803	.5671	.6139	.6631	.6680	.6381	.5492	.4616	.3003	.1355
93	.1661	.3878	.5345	.6192	.6607	.6906	.7322	.7032	.6319	.5439	.3782	.2825
94	.2439	.4330	.5446	.6290	.6826	.7374	.7716	.7432	.6601	.5635	.4029	.3136
95	.3276	.4690	.5949	.6838	.7500	.8012	.8100	.7852	.7184	.6338	.4634	.4273
96	.4586	.5533	.6947	.7796	.8171	.8589	.8523	.8340	.8037	.6757	.4884	.3526
97	.4665	.6303	.7554	.8348	.8671	.8942	.8843	.8751	.8361	.7526	.6055	.4875

TABLE IV (Contd.)

Run No.	Local Void Values											
98	.6662	.7414	.8083	.8656	.8568	.9070	.8176	.8657	.8750	.8268	.8040	.8237
99	.5935	.6350	.7189	.7425	.7788	.8051	.7653	.7892	.7681	.7139	.6438	.5566
100	.7371	.7978	.8496	.8651	.8885	.8857	.8867	.9046	.8518	.8242	.7843	.7084
101	.5330	.7551	.8171	.8505	.8570	.8939	.8865	.8835	.8662	.8009	.7246	.6099
102	.3257	.5499	.6520	.7260	.7337	.7783	.7375	.7444	.7004	.6050	.6322	.5270
103	.1554	.1990	.3264	.4551	.4490	.4056	.3821	.3651	.3203	.2787	.2663	.1510
104	.1496	.2729	.3480	.4275	.4818	.5312	.5210	.5386	.4901	.2934	.3052	.2552
105	.1280	.2687	.4307	.5002	.5525	.5801	.6032	.5536	.4991	.4169	.3419	.3087
106	.2806	.4050	.5367	.6047	.6484	.7112	.6542	.6470	.5793	.4985	.4572	.2784
107	.3952	.3931	.4320	.4750	.5283	.5606	.5489	.5319	.4716	.4154	.3225	.2953
108	.3738	.4254	.5038	.5689	.6160	.5813	.6646	.6256	.5680	.5025	.3582	.2973
109	.4738	.4994	.5743	.6570	.7375	.7542	.7277	.7367	.7000	.6142	.4312	.3601
110	.3020	.5715	.7585	.8382	.8733	.8558	.8635	.8350	.8117	.7521	.5545	.4822
111	.3810	.4734	.5280	.5892	.6309	.6717	.6698	.6399	.6133	.5296	.4309	.3285
112	.2301	.3664	.5049	.5770	.5993	.6366	.6194	.6199	.5626	.4801	.3699	.3785
113	.3377	.4308	.6248	.6426	.6931	.7166	.7383	.7071	.6204	.5530	.4079	.4162
114	.3803	.5115	.6668	.7336	.7765	.7926	.7799	.7871	.7307	.6741	.5066	.4147
115	.4875	.6745	.8121	.8478	.8643	.8735	.8618	.8950	.8710	.7939	.6521	.6325
116	.4094	.5297	.6077	.6695	.6792	.7255	.7096	.7046	.6568	.5921	.4645	.4909
117	.7268	.6436	.7501	.7832	.8053	.8352	.8330	.8139	.7786	.6912	.4618	.3314
118	.8312	.8033	.8854	.9230	.9289	.9461	.9381	.9382	.9118	.8782	.7104	.4839
119	.5822	.6872	.8500	.8905	.9119	.9107	.8919	.9085	.8757	.8124	.6213	.5922
120	.5488	.7071	.7721	.8034	.8072	.8066	.8148	.8198	.7841	.7405	.6491	.4673
121	.7985	.7659	.7778	.7979	.7994	.8141	.8071	.7901	.7917	.7649	.7412	.6645
122	.8290	.8326	.8383	.8400	.8441	.8492	.8464	.8464	.8385	.8069	.7927	.7360
123	.9185	.8879	.8722	.8785	.8735	.8666	.8686	.8575	.8787	.8540	.8332	.7037
124	.4772	.5405	.5777	.6508	.6879	.7013	.6878	.6724	.6145	.5464	.4269	.2986
125	.6472	.5599	.5842	.6669	.7069	.7403	.7268	.6908	.6399	.5728	.4440	.3089
126	.5584	.5515	.5870	.6761	.7095	.7308	.7262	.7118	.6457	.5623	.3911	.1900
127	.5132	.6055	.6842	.7773	.8120	.8131	.8255	.7958	.7543	.6627	.4879	.2874
128	.4763	.5563	.5852	.6451	.6850	.6848	.7029	.6545	.6241	.5388	.4312	.2373
129	.5264	.5731	.6350	.6786	.7302	.7604	.7484	.7158	.6748	.6207	.4646	.1352
130	.3768	.5889	.6988	.7677	.7952	.8538	.8268	.7924	.7566	.6735	.5363	.3206
131	.6229	.6923	.7362	.7863	.8256	.8331	.8297	.8068	.7537	.7026	.5519	.1637
132	.7625	.7147	.7669	.8141	.8496	.8627	.8608	.6859	.8155	.7536	.5907	.2568

TABLE IV (Contd.)

Run No.	Local Void Values											
133	.5511	.6205	.7375	.7986	.8201	.8490	.8577	.8352	.8056	.7419	.6286	.6167
134	.7252	.8053	.8868	.9124	.9399	.9294	.9269	.9079	.9209	.8980	.8190	.7566
135	.5188	.6249	.7420	.8088	.8498	.8727	.8676	.8535	.8411	.7662	.6506	.5509
136	.6992	.7694	.8775	.9085	.9091	.9122	.9231	.9229	.9252	.8727	.7878	.6227
137	.6267	.5595	.6532	.7264	.7725	.7911	.8031	.7912	.7518	.6584	.5501	.3287
138	.2059	.2790	.3887	.4808	.5626	.6005	.6054	.5762	.5274	.4162	.2828	.0058
139	.2883	.4156	.5945	.6682	.7248	.7644	.7625	.7560	.7125	.5911	.4781	.3837
140	.6056	.6729	.7939	.8163	.8486	.8585	.8574	.8446	.8070	.7806	.6918	.5726
141	.8366	.8888	.9515	.9411	.9302	.9334	.9404	.9566	.9484	.9254	.8659	.6677
142	.6068	.7270	.8850	.8943	.9181	.9347	.9199	.9442	.9193	.8866	.7817	.5899
143	.2812	.5412	.7135	.7780	.8247	.8324	.8073	.8169	.7640	.7043	.6197	.5086
144	.0893	.1986	.3081	.3408	.3903	.3993	.3807	.3790	.3130	.2673	.1258	-.0338
145	.2159	.3145	.4477	.5244	.5713	.6020	.6039	.5827	.4984	.4067	.3037	.0945
146	.5345	.7548	.8182	.8759	.8865	.8973	.8768	.8614	.8325	.8237	.5804	.7486
147	.6900	.8142	.8757	.8989	.9017	.9051	.8792	.8876	.8877	.8603	.5904	.7075
148	.7539	.8977	.9296	.9372	.9272	.9184	.9074	.9137	.9215	.9422	.6769	.8952
149	.6253	.8261	.8734	.8992	.9019	.9080	.8769	.8930	.8775	.8735	.6032	.7077
150	.1674	.4829	.6167	.6938	.7360	.7381	.7264	.7234	.6702	.5709	.3636	.4504
151	.3150	.6290	.7888	.8472	.8631	.8603	.8508	.8534	.8270	.7540	.4868	.4668
152	.9259	.9169	.9171	.9002	.8986	.9025	.9100	.9100	.9219	.9190	.8446	.5354
153	.9265	.8795	.8582	.8549	.8835	.8980	.9029	.8851	.8863	.8725	.7838	.4601
154	1.0604	.9800	.9273	.9078	.9037	.8974	.9276	.9276	.9398	.9164	.8747	.6464
155	.3203	.4573	.5412	.6041	.6522	.6847	.6953	.6730	.6216	.5316	.3973	.0534
156	.4187	.5637	.6777	.7404	.7810	.8011	.8034	.7954	.7734	.6847	.4860	.0530
157	.6375	.7668	.8494	.8591	.8982	.9097	.9071	.9045	.8906	.8450	.7038	.2210
158	.2946	.4423	.5875	.6674	.7279	.7476	.7244	.6995	.6464	.8174	.4150	.3129
159	.2284	.5125	.6945	.7714	.8028	.8382	.8104	.7973	.7710	.6659	.5044	.3647
160	.4835	.6577	.8084	.8449	.8786	.8918	.8885	.8617	.8492	.7569	.6171	.4669
161	.1070	.2240	.3651	.4414	.4970	.5125	.5110	.4782	.4092	.2988	.2157	.1465
162	.2898	.3613	.3594	.5983	.6543	.6890	.6872	.6411	.6055	.4874	.4022	.3601

TABLE IV (Contd.)

Run No.	Local Void Values											
163	.3494	.4734	.6152	.6949	.7713	.7883	.7992	.7661	.7229	.6379	.8107	.3910
164	.3220	.5389	.6877	.7808	.8162	.8440	.8343	.8154	.7884	.7109	.5710	.3385
165	.2400	.2332	.3084	.3918	.4471	.4706	.4944	.4788	.3905	.3292	.2045	.1598
166	.5397	.5912	.6398	.6846	.7153	.7307	.7222	.7172	.7012	.6494	.5345	.3686
167	.5406	.6260	.7068	.7292	.7664	.7831	.7624	.7620	.7588	.6901	.5641	.4389
168	.9011	.8046	.7989	.7997	.8298	.8538	.8358	.8273	.8278	.8085	.7381	.5948
169	.6301	.7936	.8348	.8485	.8618	.8690	.8697	.8583	.8593	.8306	.7813	.6609
170	.7940	.8666	.8630	.8739	.8898	.8885	.8838	.8773	.8760	.8773	.8348	.7603
171	.0597	.2278	.1967	.2412	.3313	.3108	.3264	.2913	.2394	.1743	.0866	.1217
172	.1343	.2406	.3048	.3489	.4188	.4536	.4378	.4159	.3436	.2761	.1935	.0893
173	.2744	.3119	.3626	.4127	.4956	.5224	.5311	.4892	.4296	.3563	.2237	.0550
174	.0231	.3412	.4371	.5230	.5579	.5775	.5910	.5461	.4948	.4029	.2976	.1885
175	.1984	.3559	.4313	.4992	.5699	.5575	.5723	.5407	.5038	.4031	.2906	.2210
176	.6100	.7248	.8226	.8580	.8633	.8541	.8527	.8629	.8223	.7972	.7488	.5669
177	.8358	.9046	.9250	.9450	.9530	.9503	.9338	.9349	.9293	.9137	.8584	.7398
178	.5595	.8270	.8870	.9313	.9228	.9002	.8924	.8847	.8779	.8564	.8132	.7051
179	.4435	.7031	.7784	.8250	.8331	.8442	.8509	.8557	.8497	.8251	.7611	.6705
180	.4829	.7678	.8210	.8422	.8588	.8767	.8536	.8422	.8259	.8063	.7276	.4882
181	.1162	.3790	.4431	.5440	.5554	.5841	.5625	.5436	.4968	.4122	.3446	.2121
182	.1162	.3355	.4823	.5666	.6096	.6473	.6334	.5742	.5029	.4535	.3524	.1956
183	.1338	.3554	.5017	.5825	.6410	.6591	.6276	.6044	.5544	.4691	.3248	.0773
184	.0895	.4063	.5368	.6297	.6903	.7232	.6995	.6813	.6453	.5490	.4335	.2934
185	.1775	.4295	.5683	.6700	.7055	.7404	.7276	.7102	.6597	.5968	.4600	.3332
186	.6460	.7599	.8397	.8646	.8993	.9084	.9048	.8961	.8711	.8041	.6885	.4719
187	.4950	.6919	.8023	.8640	.9014	.9052	.9118	.8955	.8652	.7979	.6557	.5102
188	.5097	.7417	.8222	.8613	.8799	.9000	.8914	.8850	.8759	.8090	.6847	.5940
189	.3593	.7136	.8533	.8697	.8963	.9002	.9095	.9009	.8841	.8314	.6946	.5412
190	.5095	.6041	.6852	.7386	.7635	.7867	.7939	.7777	.7242	.6595	.5796	.4555
191	.4050	.5779	.7002	.7443	.7635	.7701	.7993	.7695	.7441	.6595	.5560	.3998
192	.5316	.7488	.8390	.8694	.8880	.8868	.8836	.8772	.8625	.8173	.7417	.5940
193	.6033	.7523	.8586	.8694	.8745	.8868	.8914	.8955	.8812	.8421	.7727	.6682
194	.7075	.8009	.8586	.8694	.8691	.8921	.8965	.8955	.8812	.8366	.7850	.7901
195	.8090	.8733	.8792	.8841	.8838	.8933	.9054	.8967	.8930	.8786	.8347	.8948
196	.7413	.8754	.8835	.8829	.8907	.8656	.8939	.9033	.8971	.8882	.8543	.7405

TABLE IV (Contd.)

Run No.	Local Void Values											
197	.7364	.7738	.8395	.9178	.9363	.9393	.9654	.9461	.9376	.8856	.7436	.6155
198	.3012	.4744	.6463	.7471	.7967	.8217	.8266	.8113	.7781	.6795	.4662	.2644
199	.3992	.4585	.5357	.6192	.6848	.7023	.6956	.6790	.6338	.5400	.4317	.2794
200	.3428	.4317	.5423	.6407	.6937	.7321	.7105	.7085	.6507	.5504	.3963	.3246
201	.4394	.5745	.6897	.8064	.8336	.8534	.8595	.8478	.8055	.7326	.5283	.4128
202	.3718	.4222	.5724	.6730	.7289	.7689	.7552	.7309	.7001	.5935	.4091	.2525
203	.5700	.7196	.8436	.8915	.9191	.9321	.9160	.9015	.8857	.8475	.7261	.6465
204	.1658	.5466	.7726	.7759	.7933	.8459	.9280	.9426	.8753	.7805	.7244	.8337
205	.4682	.5651	.7189	.7988	.8389	.8456	.8324	.8232	.7720	.6818	.4886	.2241
206	.2536	.3671	.4753	.5439	.5922	.6219	.6144	.5637	.5088	.3907	.3609	.3587
207	.4903	.5010	.6053	.6760	.7403	.7607	.7573	.7397	.7235	.5893	.5091	.4172
208	.6191	.7328	.8242	.8707	.9029	.9100	.9080	.9143	.8790	.8059	.6546	.5063
209	.2919	.3956	.5698	.6602	.7083	.7175	.7214	.6906	.6377	.5311	.3754	.2293
210	1.0780	.9865	.9847	1.0088	1.0161	.9879	.9662	.9821	1.0005	.9848	.8943	.7549
211	1.3153	.9540	.9689	.9876	.9967	.9836	.9716	.9902	1.0059	.9822	.9390	.7807
212	1.3828	.9704	.9502	.9661	.9684	.9791	.9609	.9636	.9663	.9689	.8944	.6761
213	.6676	.7370	.8018	.8368	.8570	.8882	.8636	.8660	.8581	.8126	.6721	.4449
214	.6131	.8389	.9596	.9894	.9977	1.0034	.9785	.9702	.9703	.9292	.8059	.6520
215	1.0893	1.0321	1.0232	1.0271	1.0302	1.0334	1.0203	1.0139	1.0212	1.0159	.9684	.8451
216	.8920	.9417	.9836	.9838	1.0057	.9838	.9811	.9727	.9674	.9701	.9185	.8315
217	.6770	.8358	.9054	.9399	.9480	.9478	.9331	.9256	.9154	.9072	.8410	.7171
218	.7879	.9141	.9404	.9478	.9476	.9558	.9326	.9336	.9563	.9289	.8126	.6517
219	.6765	.7704	.8521	.8860	.8910	.9133	.8979	.8853	.8926	.8360	.7233	.5016
220	.3191	.4459	.5553	.6549	.7007	.7386	.7305	.6962	.6551	.5451	.4081	.3779
221	.4067	.3963	.5018	.5995	.6426	.6674	.6548	.6059	.5633	.4441	.3356	.3274
222	.0749	.2087	.3496	.4370	.4845	.5283	.5180	.4838	.4171	.3213	.1870	.0985

TABLE IV (Contd.)

Run No.	Local Void Values											
223	.5560	.6410	.7826	.8555	.8665	.8685	.8712	.8864	.8809	.7971	.6363	.2348
224	1.0379	.9269	.9078	.9115	.9092	.9106	.9414	.9451	.8980	.9212	.8807	.7377
225	.5038	.8238	.8806	.8954	.9029	.9056	.9217	.9229	.9229	.8779	.8503	1.0160
226	.1355	.5262	.7002	.8387	.9053	.8674	.7897	.8047	.7039	.6233	.4427	.3670
227	.4189	.6063	.8096	.9420	.9676	.9298	.8534	.8585	.7847	.7297	.5301	.2727
228	.2421	.5394	.7392	.8620	.8886	.8770	.7861	.8294	.7144	.6336	.4754	.2245
229	.0621	.3905	.5547	.6586	.8003	.7896	.7102	.7349	.6492	.5260	.4451	.3694
230	-.0142	.2070	.3976	.4931	.5551	.6651	.5683	.5217	.4701	.3920	.2166	.1840
231	.1402	.4106	.5570	.6900	.8163	.8190	.7402	.7519	.6370	.5137	.3732	.3261
232	.2141	.4281	.6024	.7044	.8026	.8722	.7944	.8236	.7367	.6280	.4837	.2798
233	.7443	.8093	.9174	.9302	.9815	.9690	.8934	.9550	.9052	.8846	.8142	.5420
234	.2591	.4569	.6172	.6871	.7804	.7490	.8142	.8336	.8207	.7462	.5124	.2809
235	.3073	.6734	.8160	.8289	.8725	.7313	.9278	.9421	.9298	.8444	.7300	.6568
236	.0428	.3697	.5633	.6630	.7556	.7396	.8043	.8113	.7850	.6693	.7251	.2611
237	-.1346	.1129	.2646	.3620	.4474	.4432	.4817	.5007	.3936	.3106	.1969	-.0178
238	-.0722	.1973	.4128	.4893	.5837	.6462	.6789	.6350	.5487	.4541	.3164	.1651
239	.0440	.4617	.5790	.7056	.7567	.7796	.8591	.8124	.7056	.6568	.4578	.2387
240	-.0686	.3547	.5079	.6101	.6718	.7300	.7668	.7216	.6385	.5607	.4298	.1190
241	.2107	.3510	.5068	.5963	.6252	.6684	.6397	.6054	.5368	.4663	.3677	.4226
242	.8916	.9061	.9000	.9254	.9126	.9126	.9126	.9099	.8999	.9118	.8987	.9631
243	.6135	.4188	.3940	.4847	.5140	.5615	.5759	.5302	.4902	.3767	.2792	.2179
244	.4578	.6992	.7715	.8298	.8660	.8831	.8828	.8828	.8811	.7711	.6579	.4632
245	1.0818	.9169	.9228	.9107	.9358	.9486	.9489	.9491	.9241	.9363	.9892	.8883
246	.8344	.8081	.8150	.8177	.8286	.8686	.8834	.8849	.8591	.8311	.8313	.7860
247	.6680	.7443	.8286	.8443	.8422	.8819	.8703	.8591	.8461	.8575	.8313	.7860

APPENDIX D

Installation of Glass Section

The installation of the rectangular glass section ($1\frac{1}{4}$ by 36 by 7/8 in. thick) proved to be very difficult and resulted in many broken sections. Primarily, the major difficulty occurred when the bolts at either end of the longest dimension were employed. A shearing failure took place at a point approximately 3 to 4 in. from the end. The final procedure involved tightening the nuts along the length of the section in a preferential order and eliminating the end bolts. The glass itself should be free from stress-concentrating chips or cracks, either in the face or along the edge. Stress-relieving of the glass is highly recommended. Inclusions or voids inside the glass did not present any difficulties in the present installation. The prime consideration is to place the glass in compression and to avoid any tension-producing situations. If improperly carried out, the tightening sequence is one source of tension production. The following procedure was successfully employed:

1. All nuts were hand-tightened.

2. A calibrated torque wrench was used to apply 50 in.-lb to the nuts nearest the center of the section. This torque was applied alternately above and below the center working toward the ends.

3. The torque was to be uniform; therefore the same procedure was followed for reapplying the 50-in.-lb torque. The center nuts did not have the initially applied torque after the tightening sequence was completed. Therefore the tightening was repeated several times.

4. The torque was increased in 25- to 50-in.-lb increments.

It was found that 100 in.-lb of torque were sufficient for sealing the glass section for pressures of 200 psia. It is recommended that systems should be undertorqued in a cold condition and pressure-tested to determine the pressure required for leakage. In the hot-test condition, the seal will generally be more efficient than in the cold test. Since the expansion of the particular system is not easily predictable, the trial-and-error method of sealing is to be expected.

When the glass section is removed after the system has been heated, particular care should be exercised in removing the torque load. Reversing the tightening procedure was successful. Stress concentrations are normally found upon rapid cooling and are to be avoided. The glass may fail when the bolt torque is removed, especially when rapid cooling of the glass has occurred.

ACKNOWLEDGMENTS

The author wishes to express his sincere appreciation to Professor B. T. Chao for the assistance and encouragement throughout his graduate program at the University of Illinois.

This research was made possible by the joint graduate research program of the U. S. Atomic Energy Commission and the Associated Midwest Universities at the Argonne National Laboratory, Argonne, Illinois. The author is indebted to Dr. Michael Petrick for his guidance during the experimental investigation carried out in the Heat Engineering Section of the Reactor Engineering Division at Argonne.

As in any experimental program, the assistance rendered by the technical personnel contributed greatly to the results. Mr. M. P. Gats provided many valuable suggestions and the following technical support: Messrs. L. Bova, E. R. Gunchin, L. M. Indykiewicz, J. R. Kemp, G. A. Lambert, J. E. Norco, J. P. O'Grady, and A. M. Stogsdill. Mr. E. A. Spleha contributed to the design of the optical glass test section. Through the efforts of these men, the periods of continuous operation of the equipment were made possible. The quality of the high-speed, color motion pictures was due to the fine assistance of Mr. D. S. Giroux of the Motion Picture Production group.

REFERENCES

1. S. W. Gouse, Jr., An Index to the Two-phase Gas-Liquid Flow Literature, Part I, M.I.T. Engineering Projects Laboratory Report DSR 8734-1, Mechanical Engineering Department (May 1963).
2. R. R. Kepple and T. V. Tung, Two-phase (Gas-Liquid) System: Heat Transfer and Hydraulics, An Annotated Bibliography, ANL-6734 (1963).
3. J. D. van der Waals, thesis, University of Leiden (1873).
4. E. R. Hosler and J. W. Westwater, Film Boiling on a Horizontal Plate, A.R.S. J. 32, 553-558 (1962).
5. J. Kestin, Forced Convection Heat Transfer from an Isothermal Sphere to Water, J. Heat Transfer, Trans. ASME, Series C, 83, 172-174 (1961).
6. F.E. Tippets, Critical Heat Flux and Flow Pattern Characteristics of High Pressure Boiling Water in Forced Convection, GEAP-3766, Office of Tech. Services, Dept. of Commerce, Washington, D. C. (April 1962).
7. A. J. Martenson, Transient Boiling in Small Rectangular Channels, Ph.D. thesis, University of Pittsburgh (1962).
8. E. R. Hosler, Visual Study of Boiling at High Pressure, WAPD-T-1566, Presented at the Sixth National Heat Transfer Conference, Boston (Aug 1963).
9. J. G. Collier, A Review of Two-phase Heat Transfer (1935-1957), UKAEA Report, AERE CE/R 2496, Harwell, England (1958).
10. N. Hall-Taylor, G. F. Hewitt, and P. M. C. Lacey, The Motion and Frequency of Large Disturbance Waves in Annular Two-phase Flow of Air-Water Mixtures, Chem. Eng. Sci. 18, 537-552 (1963).
11. J. H. Vohr, Flow Patterns of Two-phase Flow - A Survey of Literature, TID-11514, Office of Tech. Services, Dept. of Commerce, Washington, D. C. (1960).
12. F. W. Staub and N. Zuber, A Program of Two-phase Flow Investigation, Second Quarterly Report, July-Sept, GEAP-4367 (1963).
13. J. H. Vohr, A Photographic Study of Boiling Flow, NYO-9650 (TID-4500) Office of Tech. Services, Dept. of Commerce, Washington, D. C. (1963).
14. S. Calvert and B. Williams, Upward Cocurrent Annular Flow of Air and Water in Smooth Tubes, AIChE J. 1, 78-86 (1955).
15. G. F. Hewitt, Analysis of Annular Two-phase Flow: Application of the Dukler Analysis to Vertical Upward Flow in a Tube, UKAEA Report, AERE-R 3680, Harwell, England (1961).

16. G. H. Anderson, G. G. Haselden, and B. G. Mantzouranis, Two-phase (Gas-Liquid) Flow Phenomena-III, Chem. Eng. Sci. 16, 222-230 (1961).

17. S. Ostrach and A. Koestel, Film Instabilities in Two-phase Flows, AIChE J. 11, 294-303 (1965).

18. R. D. Haberstroh and P. Griffith, The Transition from the Annular to the Slug Flow Regime in Two-phase Flow, Tech. Report 5003-28, Dept. of Mech. Eng., M.I.T. (1964). Also, The Slug-annular Two-phase Flow Regime Transition, ASME Paper, 65-HT-52 (Aug 1965).

19. G. B. Wallis, J. M. Turner, I. Bemberis, and D. Kaufman, Two-phase Flow and Boiling Heat Transfer, Quarterly Progress Report No. NYO-3114-4, Thayer School of Engineering, Dartmouth College (July-Sept 1964).

20. J. O. Hinze, Momentum and Mechanical-energy Balance Equations for a Flowing Homogeneous Suspension with Slip Between the Phases, Appl. Sci. Res. 11, Section A, 33-46 (1962).

21. S. G. Bankoff, A Variable Density Single-fluid Model for Two-phase Flow with Particular Reference to Steam-Water Flow, J. Heat Transfer, Trans. ASME, Series C, 82, 265-272 (1960).

22. G. W. Govier, Developments in the Understanding of the Vertical Flow of Two-fluid Phases, Canadian J. of Chem. Eng. 43, No. 1, 3-10 (1965).

23. D. J. Nicklin and J. F. Davidson, The Onset of Instability in Two-phase Slug Flow, Proc. Symposium on Two-phase Fluid Flow, Paper 4, Inst. Mech. Engr. (London), (Feb 1962).

24. J. G. Collier, Burn-out in Liquid Cooled Reactors-1, Nuclear Power, 61-66 (June 1961).

25. J. G. Knudsen and D. L. Katz, Fluid Dynamics and Heat Transfer, McGraw-Hill Book Co., New York (1958).

26. J. J. Jicha and S. Frank, An Experimental Local Boiling Heat Transfer and Pressure-drop Study of a Round Tube, ASME Preprint 62-HT-48 (1962).

27. A. W. Bennett, G. F. Hewitt, H. A. Kearsey, R. K. F. Keeys, and P. M. C. Lacey, Flow Visualization Studies of Boiling at High Pressure, UKAEA Report, AERE-R 4874, Harwell, England (March 1965).

28. J. J. Bikerman, Surface Chemistry, Theory and Applications, Academic Press Inc., New York (1958).

29. F. A. Jeglic and T. M. Grace, Onset of Flow Oscillations in Forced-Flow Subcooled Boiling, NASA TN D-2821 (May 1965).

30. S. S. Kutateladze and M. A. Styrikovich, Hydraulics of Gas-Liquid Systems, (Translation), F-TS-9814/V, Liason Office, TIC, Wright-Patterson Air Force Base, Ohio (Sept 1960).

31. R. Moissis, The Transition from Slug to Homogeneous Two-phase Flows, J. Heat Transfer, Trans. ASME, Series C, 85, 366-370 (1963).

32. M. Suo, A. E. Bergles, E. F. Doyle, L. Clawson, and P. Goldberg, Investigation of Boiling Flow Regimes and Critical Heat Flux, Dynatech Report No. 517, NYO-3304-3 (March 1965).

33. G. B. Wallis, D. A. Steen, and J. M. Turner, Joint U. S.-Euratom Research and Development Program, Contract No. AT(30-1)-3114, Quarterly Progress Report, Dartmouth College (March 1964).

34. O. Baker, Simulatneous Flow of Oil and Gas, The Oil and Gas Journal 53, 185-195 (July 1954).

35. J. J. van Rossum, Experimental Investigation of Horizontal Liquid Films, Wave Formation, Atomization, Film Thickness, Chem. Eng. Sci. 11, 35-52 (1959).

36. D. A. Steen and G. B. Wallis, The Transition from Annular to Annular-mist Cocurrent Two-phase Downflow, Report No. NYO-3114-2, Dartmouth College (June 1964).

37. N. Zuber, On the Atomication and Entrainment of Liquid Films in Shear Flow, General Electric Co. T.I.S. Report No. 62GL153 (Sept 1962).

38. L. Cravarolo and A. Hassid, Liquid Volume Fraction in Two-phase Adiabatic Systems, Presented at the Symposium on Two-phase Flow, University of Exeter, England (June 1965).

39. P. Griffith and G. B. Wallis, Two-phase Slug Flow, J. Heat Transfer, Trans. ASME, Series C, 83, 307-320 (1961).

40. B. K. Kozlov, Forms of Flow of Gas-Liquid Mixtures and Their Stability Limits in Vertical Tubes, Zhur. Tekh. Fiz., 24, No. 12, 2285-2288 (1954). Trans. RJ-418, Associated Technical Services, Inc., East Orange, N. J.

41. S. I. Kosterin, Study of Influence of Tube Diameter and Position upon Flow Structures of Gas-Liquid Mixtures, Izvest. Akad. Nauk SSSR, Otdel. Teckl. Nauk 12, 1824-1831 (1949), Trans. RT-1355.

42. C. J. Hoogendoorn and A. A. Buitelaar, The Effect of Gas Density and Gradual Vaporization on Gas-Liquid Flow in Horizontal Pipes, Chem. Eng. Sci. 16, 208-221 (1961).

43. R. A. S. Brown, G. A. Sullivan, and G. W. Govier, The Upward Vertical Flow of Air-Water Mixtures; III. Effect of Gas Phase Density on Flow Pattern, Holdup and Pressure Drop, Canadian J. of Chem. Eng. 38, 62-66 (April 1960).

44. K. Goldman, H. Firstenberg, and C. Lombardi, Burnout in Turbulent Flow - A Droplet Diffusion Model, J. Heat Transfer, Trans. ASME, Series C, 83, 158-162 (1961).

45. G. B. Wallis, The Onset of Droplet Entrainment in Annular Gas-Liquid Flow, Report No. 62GL127, General Engineering Laboratory, General Electric Co. (Aug 1962).

46. P. Griffith, The Slug-annular Flow Regime Transition at Elevated Pressure, ANL-6796 (Nov 1963).

47. F. W. Staub and N. Zuber, A Program of Two-phase Flow Investigation, Sixth Quarterly Progress Report, July-Sept, GEAP-4733 (1964).

48. E. A. Guggenheim, Thermodynamics, North-Holland Publishing Co., Amsterdam (1959).

49. P. S. Epstein, Textbook of Thermodynamics, John Wiley & Sons, Inc., New York (1937).

50. H. S. Green, The Molecular Theory of Fluids, North-Holland Publishing Co., Amsterdam (1952).

51. J. B. Roll, Ph.D. thesis, Purdue University, Lafayette, Indiana (1962).

52. S. G. Bankoff, A Note on Latent Heat Transport in Nucleate Boiling, AIChE J. 8, 63-65 (1962).

53. J. H. Lienhard and V. E. Schrock, The Effect of Pressure, Geometry, and the Equation of State Upon the Peak and Minimum Boiling Heat Flux, J. Heat Transfer, Trans. ASME, Series C, 85, 261-272 (1963).

54. J. J. Martin, Correlations and Equations Used in Calculating the Thermodynamic Properties of Freon Refrigerants, Symposium on Thermal Properties, Purdue University (Feb 1959), published by ASME in Thermodynamic and Transport Properties of Gases, Liquids and Solids, 110-122.

55. R. C. Downing, E. I. DuPont de Nemours and Company, Personal Communication (1963).

56. A. F. Scott and R. Dillon, Reduced Temperatures for the Liquid State. General Equations for the Orthobaric Densities as Functions of the Reduced Temperature, J. Chem. Phys. 17, 1179-1181 (1949).

57. B. J. Eiseman, Jr., Pressure-Volume-Temperature Properties of the Freon Compounds, Refrigerating Engineering 60, 496-503 (1952).

58. A. Ferguson and J. T. Miller, On the Temperature Variation of the Orthobaric Density of Unassociated Liquids, Proc. Phys. Soc. (London) 46, 140-147 (1934).

59. S. H. Fishtine, Estimates of Saturated Fluid Densities and Critical Constants, I. & E.C. Fundamentals 2, 149-155 (1963).

60. N. K. Adam, The Physics and Chemistry of Surfaces, Chapter IV, Oxford University Press, London, 3rd Ed. (1946).

61. V. M. Borishansky, I. I. Novikov, and S. S. Kutateladze, Use of Thermodynamic Similarity in Generalizing Experimental Data of Heat Transfer, International Dev. in Heat Transfer, Part II, University of Colorado, 475-482 (1961).

62. H. Steinle, The Surface Tension of Refrigerants, of Lubricants, and of Their Mixtures, Kaltetechnik, 12, 334-339 (1960), in German; translated by Dr. E. K. Wilip, Argonne National Laboratory (Nov 1963).

63. A. Ferguson, Relations Between Thermo-physical Properties, Proc. Phys. Soc. (London) 52, 759-763 (1940).

64. S. Sugden, The Parachor and Valency, George Routledge & Sons, Ltd. London (1930).

65. D. B. Macleod, On a Relation Between Surface Tension and Density, Trans. Faraday Soc. 19, 38-42 (1923-1924).

66. A. Bondi, Viscosity of Nonassociating Liquids, I. & E.C. Fundamentals 2, 95-102 (1963).

67. J. A. Jossi, L. I. Stiel, and G. Thodos, The Viscosity of Pure Substances in the Dense Gaseous and Liquid Phases, AIChE J. 8, 59-63 (1962).

68. L. I. Stiel and G. Thodos, The Viscosity of Polar Gases at Normal Pressures, AIChE J. 8, 229-232 (1962).

69. L. I. Stiel and G. Thodos, The Viscosity of Polar Substances in the Dense Gaseous and Liquid Regions, AIChE J. 10, 275-277 (1964).

70. K. E. Starling, B. E. Eakin, J. P. Dolan, and R. T. Ellington, Critical Region Viscosity Behavoir of Ethane, Propane and n-Butane, Progress in International Research on Thermodynamic and Transport Properties, Princeton University, 530-540 (1962).

71. G. Birkhoff, Hydrodynamics, A Study in Logic, Fact and Similitude, Princeton University Press, Princeton, N. J. (1960).

72. S. Chandrasekhar, Hydrodynamic and Hydromagnetic Stability, Oxford at the Clarendon Press, Oxford University Press, London (1961).

73. G. Taylor, The Instability of Liquid Surfaces When Accelerated in a Direction Perpendicular to Their Planes. I., Proc. Roy. Society (London), Series A, 201, 192-196 (1950).

74. D. J. Lewis, The Instability of Liquid Surfaces When Accelerated in a Direction Perpendicular to Their Planes. II., Proc. Roy. Society (London), Series A, 202, 81-102 (1950).

75. L. M. Milne-Thomson, Theoretical Hydrodynamics, Chapter 14, The MacMillan Company, New York, Third Edition (1955).

76. S. G. Bankoff, On Taylor Instability of Plane Surfaces, The Physics of Fluids 2, No. 5, 576-577 (1959).

77. R. Bellman and R. H. Pennington, Effects of Surface Tension and Viscosity on Taylor Instability, Quart. Appl. Math. 12, 151-162 (1954).

78. J. N. Hunt, A Note on Instability at a Viscous Interface, Quart. J. Mech. and Appl. Math. 14, Part 3, 359-362 (1961).

79. F. Van der Walle and H. J. Lamein, On the Hydrodynamic Aspects of Two-phase Flows in Vertical Boilers, Part 1, Theory, Technological University of Eindhoven, Report WW-16-R50 (Oct 1963).

80. J. Johanns, Development of a Fluoroscope for Studying Two-phase Flow Patterns, ANL-6958 (Oct 1964).

81. K. D. Cooper, G. F. Hewitt, and B. Pinchin, Photography of Two-phase Flow, UKAEA Report, AERE-R 4301, Harwell, England (1963).

82. H. H. Hooker and G. F. Popper, A Gamma-ray Attenuation Method for Void Fraction Determinations in Experimental Boiling Heat Transfer Test Facilities, ANL-5766 (Nov 1958).

83. C. J. Shearer and J. F. Davidson, The Investigation of a Standing Wave Due to Gas Flowing Upwards Over a Liquid Film; Its Relation to Flooding in Wetted-Wall Columns, J. Fluid Mech. 22, 321-335 (1965).

84. E. Janssen and J. A. Kervinen, Two-phase Pressure Drop in Straight Pipes and Channels; Water-Steam Mixtures at 600 to 1400 psia, GEAP-4616 (May 1964).

85. S. Levy, Steam Slip Theoretical Prediction from Momentum Model, J. Heat Transfer, Trans. ASME, Series C, 82, 113-124 (1960).

86. U. H. von Glahn, An Empirical Relation for Predicting Void Fraction with Two-phase, Steam-Water Flow, NASA TN D-1189 (Jan 1962).

87. E. E. Polomik, Phase Velocities in Boiling Flow Systems by Total Energy and by Diffusion, ASME Paper, 65-HT-34 (Aug 1965).

88. R. C. Martinelli and D. B. Nelson, Prediction of Pressure Drop During Forced-Circulation Boiling of Water, Trans. ASME 70, 695-702 (1948).

89. S. Levy, Prediction of Two-phase Pressure Drop and Density Distribution from Mixing Length Theory, J. Heat Transfer, Trans. ASME, Series C, 85, 137-152 (Feb 1963).

90. W. H. Cook, Boiling Density in Vertical Rectangular Multichannel Sections with Natural Circulation, ANL-5621 (Nov 1956).

91. R. A. Egen, D. A. Dingee, and J. W. Chastain, Vapor Formation and Behavior in Boiling Heat Transfer, Battelle Memorial Institute, BMI 1163 (1957).